INTRATRACHEAL LIPOPOLYSACCHARIDE EXPOSURE INDUCED ATHEROSCLEROTIC PLAQUE DESTABILIZATION: A NOVEL MURINE PLAQUE VULNERABILITY MODEL

by

Jen Erh Jaw

B.Sc., Simon Fraser University, 2008

A THESIS SUBMITTED IN PARTIAL FULFILLMENT OF

THE REQUIREMENTS FOR THE DEGREE OF

DOCTOR OF PHILOSOPHY

in

THE FACULTY OF GRADUATE AND POSTDOCTORAL STUDIES

(Experimental Medicine)

THE UNIVERSITY OF BRITISH COLUMBIA

(Vancouver)

June 2016

Abstract

Rationale: Literature has implicated lung inflammation as a risk factor for acute cardiovascular (CV) diseases (CVD), but the underlying mechanisms linking lung injury with CVD are largely unknown. Plasma neutrophilic myeloperoxidase (MPO) is an inflammatory biomarker for acute CVD, but its pathological role in CVD is unclear.

Hypothesis: A murine model of atheromatous plaque vulnerability can be established by intratracheal Lipopolysaccharide (LPS) exposure. Neutrophils and MPO may contribute to this process.

Approaches: LPS (3 mg/kg) or saline (control) was instilled directly into the lungs of male apolipoprotein E-knockout ($ApoE^{-/-}$) C57BL/6J mice following 8 weeks of a Western-type diet. 24 hours later, atheromas in the right brachiocephalic trunk (BCT) were assessed for stability *ex vivo* using high-resolution optical projection tomography (OPT) and histology. Circulating neutrophils were depleted *in vivo* using neutrophil-specific antibodies to investigate the role of neutrophils in this model and determine the source of MPO. 4-aminobenzoic acid hydrazide (4-ABAH) was injected intraperitoneally to inhibit MPO.

Results: LPS-exposed mice developed vulnerable plaques, characterized by intraplaque hemorrhage and thrombus compared to saline-exposed mice ($p=0.0004$). Plaque vulnerability was detectable as early as 8 hours post-intratracheal LPS instillation but not with intraperitoneal instillation. Depletion of circulating neutrophils attenuated plaque destabilization ($P=0.027$). MPO was found acutely localized in the vulnerable plaques and attached thrombi of LPS-exposed mice but not in the stable plaques of saline-exposed mice. Enzymatic inhibition of MPO in LPS-exposed mice decreased plaque vulnerability ($P=0.038$) and MPO/HOCl mediated

oxidation (P=0.0076) Depletion of circulating neutrophils in LPS-exposed mice prevented intraplaque MPO accumulation, confirming that they were the major source of MPO in this model.

Conclusion: We have established a novel plaque vulnerability model related to lung inflammation induced by intratracheal exposure to LPS. In this model, neutrophils play an important role in both lung inflammation and plaque destabilization. 3D OPT analysis revealed that during LPS-induced lung inflammation, MPO localizes acutely in atherosclerotic plaques and contributes to plaque vulnerability. MPO could be an important therapeutic target for prevention of acute CV events related to lung injury. This model could be useful for screening therapeutic targets to prevent acute vascular events related to lung inflammation.

Preface

This research was approved by the Animal Care Committee of the University of British Columbia under protocol numbers A06-1494, A10-0257, and A15-0167.

The content of Chapter 1 is based on an unpublished review article written by Jen Erh Jaw. Figure 3 was obtained from Nature Publishing Group, and reprinted by permission from Macmillan Publishers Ltd: [Nature] (Sanz J, Fayad ZA. Imaging of atherosclerotic cardiovascular disease. Nature. 2008; 451(7181): 953-7.), copyright (2008). Figure 5 was obtained from Wolters Kluwer Health, Inc. with permission to reprint (Soehnlein O. Multiple roles for neutrophils in atherosclerosis. Circ Res. 2012; 110(6):875-88.)

The entire contents of Chapters 3 and 4 were previously published in the European Respiratory Journal. (Jen Erh Jaw, Masashi Tsuruta, Yeni Oh, John Schipilow, Yuki Hirano, David A. Ngan, Koichi Suda, Yuexin Li, Jin Young Oh, Konosuke Moritani, Sheena Tam, Nancy Ford, Stephan van Eeden, Joanne L. Wright, S.F. Paul Man, and Don D. Sin. Lung exposure to Lipopolysaccharide causes atherosclerotic plaque destabilisation. Eur Respir J 2016; 0: 1–11. doi: 10.1183/13993003.00972-2015). I designed, scheduled, and performed all the experiments, collected and analyzed the data, and wrote first draft of the manuscript. Subsequent editing and modification was done by Dr. Don Sin and the manuscript was submitted with approval of all authors. Drs. Masashi Tsuruta, Yuki Hirano, Konosuke Moritani, and Koichi Suda were responsible for intratracheal LPS instillation and animal sacrifice procedures. Yeni Oh, Jin Young Oh, and David Ngan were responsible for blood and tissue processing, and assistance in data collection. John Schipilow and Nancy Ford were responsible for scheduling, optimization,

and operation of optical projection tomography equipment in the Centre for High-Throughput Phenogenomics at UBC. Lung and plaque histology stains and the method of histological quantification were recommended by Dr. Joanne L. Wright. Drs. Stephan van Eeden and S.F. Paul Man made significant intellectual contributions to the design of the study and provided useful recommendations for manuscript preparation. Dr. Yuexin Li and Sheena Tam were responsible for ordering and organization of reagents related to this study.

Some of the content of Chapter 5 about the effect of myeloperoxidase inhibition on plaque vulnerability is published as an abstract in the American Journal of Respiratory and Critical Care Medicine. (Jen Erh(David) Jaw, Masashi Tsuruta, Koichi Suda, Yeni Oh, JinYoung Oh, Yuki Hirano, Yuexin Li, David Ngan, Sheena Tam, Stephan Van Eeden, S F Paul Man, Joanne L. Wright, Don Sin. Myeloperoxidase inhibition prevents atherosclerotic plaque rupture related to lung inflammation. B33. GRANULOCYTE ACTIVATION IN LUNG DISEASE : pp. A2759-A2759 doi:10.1164/ajrccm-conference.2014.189.1_MeetingAbstracts.A2759). I performed all the experiments and data analysis and wrote the abstract for submission with the approval of Dr. Don Sin. Drs. Masashi Tsuruta and Yuki Hirano were responsible for intratracheal LPS instillation and animal sacrifices. Drs. Joanne L. Wright, Stephan van Eeden, and S.F. Paul Man made significant intellectual contributions to the design of the study. Dr. Yuexin Li and Sheena Tam were responsible for ordering and organization of reagents related to this study. The rest of the content in Chapter 5 is based on work conducted in the Centre for High-Throughput Phenogenomics at UBC by John Schipilow and Jen Erh Jaw. I designed and performed all the experiments and analyzed the data; John Schipilow was responsible for specimen preparation and optical projection tomography.

Table of Contents

List of Tables

List of Figures

List of Abbreviations

2D: Two Dimensional

3D: Three Dimensional

4-ABAH: 4-Aminobenzic Acid Hydride

μm: micrometer

mm: millimeter

$ApoE^{-/-}$: Apolipoprotein E-deficient

ApoE KO: Apolipoprotein Knockout

ACS: Acute Coronary Syndrome

ADAM17: ADAM Metallopeptidase Domain 17

AHA: American Heart Association

AMI: Acute Myocardial Infarction

BAL: Bronchoalveolar Lavage

BCT: Brachiocephalic Trunk

CAD: Coronary Artery Disease

CHD: Coronary Heart Disease

CMV: Cytomegalovirus

COPD: Chronic Obstructive Pulmonary Disease

CV: Cardiovascular

CVD: Cardiovascular Disease

Ctrl: Control

ER: Endoplasmic Reticulum

H&E: Hematoxylin and Eosin

ICAM: Intercellular Adhesion Molecule

IHD: Ischemic Heart Disease

IL: Interleukin

IP: Intraperitoneal Administration

IT: Intratracheal Administration

IVC: Inferior Vena Cava

IVUS: Intravascular Ultrasound

KC: Keratinocyte chemoattractant

LDL: Low-Density Lipoprotein

LPS: Lipopolysaccharide

MAP: Mitogen-activated Protein

MCP: Monocyte Chemoattractant Protein

MI: Myocardial Infarction

MMP: Matrix Metalloproteinase

MPO: Myeloperoxidase

NC: Necrotic Core

NCD: Non-communicable Diseases

ND: Neutrophil Depletion

OCT: Optical Coherence Tomography

OPT: Optical Projection Tomography

PMN: Polymorphonuclear Cell

SAP: Stable Angina Pectoris

SMC: Smooth Muscle Cells

SE: Standard Error

TCFA: Thin Cap Fibroatheroma

TF: Tissue Factor

TLR4: Toll-like receptor 4

TNF: Tumor Necrosis Factor

UAP: Unstable Angina Pectoris

UBC: University of British Columbia

US: United States

VCAM: Vascular Cell Adhesion Molecule

VSMC: Vascular Smooth Muscle Cells

WD: Western-type Diet

WHO: World Health Organization

Acknowledgements

First, I offer my enduring gratitude to my supervisor, Dr. Don Sin, for his generous full tuition support and financial support throughout my entire PhD studies. He has offered me various learning opportunities and connections, and he has shown enormous patience, trust, and understanding in the design and execution of this project. He also worked intensely with me in editing and modifying manuscripts for publication. His advice and inspiration has kept me focused and helped me leap forward in a good direction. Without him I would not have completed this thesis.

Second, I would like to extend my gratitude to all the members of my supervisory committee, Dr. Paul Man, Dr. Joanne Wright, and Dr. David Granville, who have always attended committee meetings and have provided very useful comments and methodology for this project to progress. Their support helped me reach my goals and finish this study.

Third, I would like to thank Dr. Yuexin Li, the former lab manager in Dr. Sin's laboratory. Without her support and understanding, I would never have the animal experiments scheduled and performed in a manageable way. Her support was essential to the completion of this project.

Fourth, I would like to thank Dr. Koichi Suda, Dr. Masashi Tsuruta, Dr. Yuki Hirano, and Dr. Konosuke Moritani for all their technical assistance in the animal experiments throughout the studies. Without their consistent and precise surgical techniques, the animal model could not be established as it is.

Fifth, I would like to thank all the members from Dr. Sin's laboratory, especially Yeni Oh and Dr. Jin Young Oh, who had worked extensively with me in blood processing, tissue processing, histology, and image capturing. They were very consistent in the processing procedure and technique throughout the studies to minimize variations in data collection. Without their efforts, the enormous amount of data would not be collected in a consistent way. I also offer much thanks to the staff at the Centre for Heart Lung Innovation, St. Paul's Hospital, UBC, who have encouraged me to continue my work in this field. I owe particular thanks to Claire Smits and her GEM staff for the animal husbandry and assistance in animal ethics applications.

This thesis was also the result of an extensive collaboration with the Centre for High-Throughput Phenogenomics at UBC. I would like to express special thanks to John Schipilow and his supervisor Dr. Nancy Ford, who have helped me extensively in evolving new immunofluorescence staining and optical projection tomography techniques. Their work and collaboration were invaluable and essential for the establishment of this model and thesis completion.

Special thanks are owed to my parents, Hsiao-Chun Meng and Bih-Shiaw Jaw who have supported me throughout my years of education. Much thanks to my wife, Rongrong He, as she showed understanding in my long working hours and took good care of my daughter Allison Jaw independently. Also much thanks to my brother, Chu-I Jaw, and my sister, Ling-Ying Jaw, who provided their apartments for me to live in Vancouver and Richmond during this study.

Dedication

To My Beloved Father, Mother, Wife, and Daughter

Chapter 1: Introduction

1.1 Current Global Burden of Cardiovascular Diseases

In 2014, the World Health Organization (WHO) reported a total of 56 million deaths around the world in 2012. Of these, cardiovascular (CV) diseases (CVD) were the primary leading cause of deaths, accounting for 17.5 million deaths (31.25%) worldwide (1). Among global premature deaths (deaths before the age of 70 years) caused by non-communicable diseases (NCD), CVD were responsible for the largest proportion (37%) [Figure 1]. According to the WHO's estimation, if we fail to prevent and treat CVD in this decade, the annual CVD mortality will increase to 22.2 million by 2030 and will cost $1,044 billion annually. Therefore, the WHO has now set a 10-year target of a 25% relative reduction in the overall CV mortality rate by the year 2025 (1). Geographical analyses showed that 80% of CVD deaths occurred in low- and middle-income countries and occur almost equally in men and women. Therefore, one of the key strategies to reduce global CV burden is to develop cost-effective drug therapies or interventions that are also high-impact and feasible for implementation in resource-constrained settings (1). Identifying and consulting with those high CV risk patients who have acute CV history and who have high risk (≥ 30%) of a CV event in the next 10 years using a total risk approach would be important in reducing CV mortality. Regardless, increasing investments in CVD prevention and control in all countries will be necessary to attain this outcome (1).

Studies have shown that reducing the mortality rate for acute CV events (ischemic heart disease (IHD) and stroke) by 10% with the implementation of proper multidrug therapy would avert about 17.9 million deaths over a 10-year period, and approximately 56% of deaths averted would

be in those younger than 70 years (2). Beyond saving countless lives, it would reduce economic losses in low- and middle-income countries by an estimated US$25 billion per year. It is estimated that on average, this would cost just over US$1 per day per person annually by using a proper cost-effective drug therapy. Therefore, implementation of a proper drug therapy (singly or in combination with multiple drugs) would be a concrete investment for saving and lengthening lives (3).

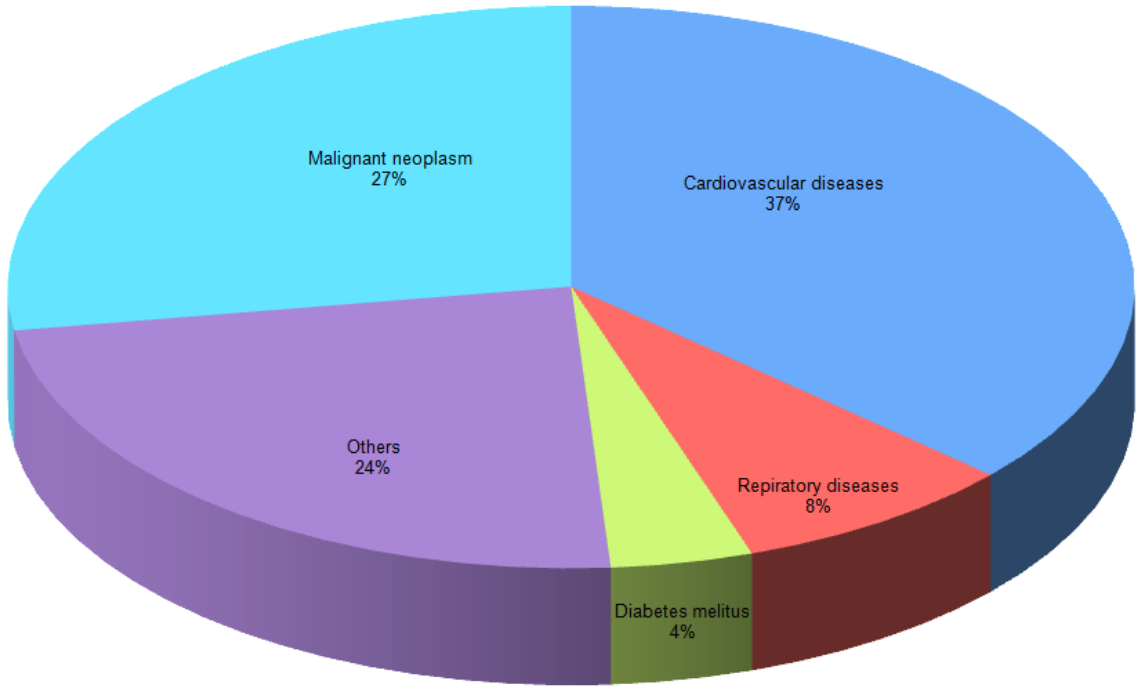

Figure 1: Proportion of Global Premature Death Caused by Non- Communicable Diseases in 2012 (1).

This graph was plotted based on the reported data.

Even in the United States (US), one of the most developed countries, according to the latest 2015 statistical update of the American Heart Association, an estimated 85.6 million (more than one-third) of American adults have suffered CVD (4). By 2030, 43.9% of the US population is projected to have CVD (4). CVD, on average, caused more than 2,150 American deaths per day in 2011, which means 1 death every 40 seconds on average (4). Overall, CVD caused 1.6 million deaths per year in the Americas, accounting for 30% of total mortality and 38% of deaths due to NCDs (5). Among the causes of CV deaths, coronary heart diseases (CHD) and strokes were the primary leading causes of CV deaths, accounting for 47.7% and 16.4% of CV deaths respectively in 2011 [Figure 2]. The high mortality rates are due to the unpredictable and lethal disease manifestation. In fact, one of the major limitations for CVD prevention and therapeutic development is the poor understanding of the molecular mechanisms of acute atherosclerotic plaque destabilization that leads to plaque erosion and rupture in the blood vessels.

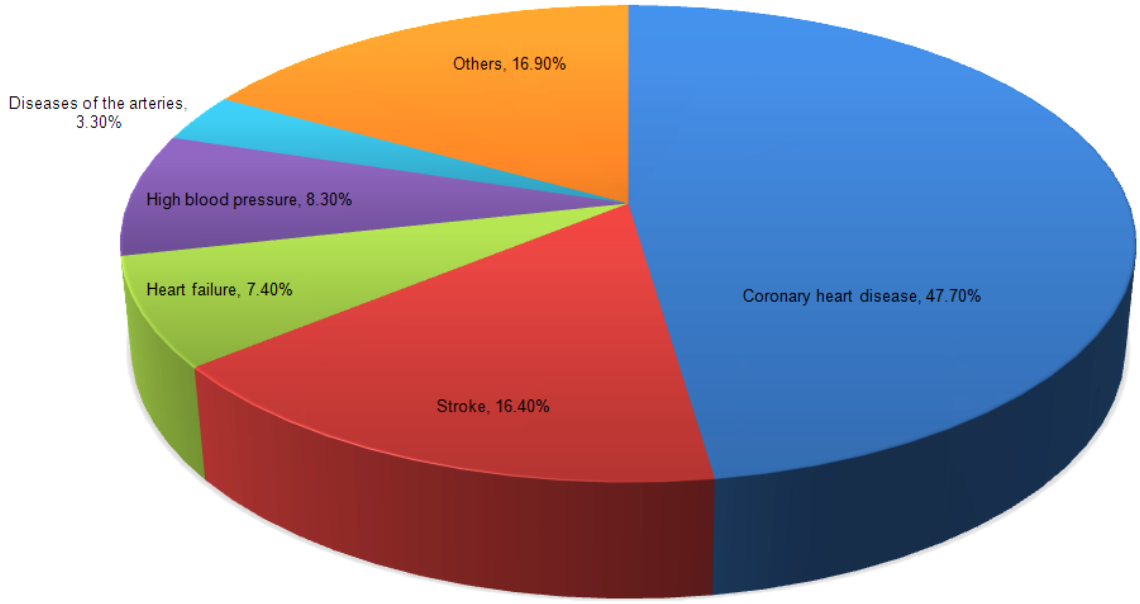

Figure 2: Proportion of Deaths in the United States Caused by Cardiovascular Diseases in 2011.

This figure was plot based on the reported statics from Dariush Mozaffarian et al. Circulation. 2015;131:e29-e322 (4).

1.2 Underling Pathogenesis of Major CVD: Atherosclerosis

The overarching term "CVD" includes IHD, strokes, acute coronary syndrome (ACS), and myocardial infarction (MI). All these CV events are the clinical manifestation of a long-term chronic inflammatory process called atherosclerosis, a progressive inflammatory disease characterized by the accumulation of lipids and fibrous elements in the blood vessel wall. This leads to formation of atherosclerotic plaques in the major arteries, which most frequently develop in the coronary, carotid, peripheral, and renal arteries and cause CHD, angina (chest pain),

carotid artery disease, peripheral artery disease (PAD), and chronic kidney disease, respectively. There are also non-atherosclerotic types of CVD, such as aneurysm, aortic dissection, etc.

Scientific views of atherosclerosis have evolved substantially over the past 5 decades. The concepts of hyperlipidemia and atherosclerosis dominated in the research field based on strong evidence between hypercholesterolaemia and atherosclerosis before the 1970s (6). However, progress and advancement of knowledge of vascular biology in the 1980s led the research field to a new focus on the control of growth factors and the proliferation of vascular smooth muscle cells in atherosclerotic plaques. In the 1990s, researchers started to realize the prominent role inflammation played in atherosclerosis and CVD. The atherosclerotic plaques in blood vessels were no longer considered as bland lesions of lipids enrobed by a capsule of proliferated smooth muscle cells; instead, the cellular immune response and inflammation in the plaques became of great interest and were considered key determinants of the clinical manifestation (7).

Since then, atherosclerosis has been considered an ongoing inflammatory disease initiated by endothelial injury mostly due to blood flow turbulence and continually progressed by deposition of oxidized and modified lipoproteins in the vessel wall. This leads to persistent vascular inflammation predominantly characterized by macrophages, activated smooth muscle cells, and T cells infiltrating into the inflamed region (intima) due to upregulation of vascular cell adhesion molecule-1 (VCAM-1), intercellular adhesion molecule-1 (ICAM-1), and selectins on vascular endothelium. Recruited monocytes differentiate into macrophages, which internalize oxidized low-density lipoprotein (ox-LDL) by their scavenger receptors and became foam cells with overloaded lipids. Continuation of this process causes intimal thickening and formation of fatty

acid streaks. Eventually, in these plaques, the intracellular cholesterol, resulting from ox-LDL decomposition, precipitates as microcrystals that activate the inflammasome and results in interleukin (IL)-1β secretion (8). IL-1β can induce production of various pro-inflammatory molecules by vascular smooth muscle cells, including IL-6 and eicosanoids (PGE_2) (9, 10). Upregulation of leukocyte adhesion molecules and matrix metalloproteinase (MMP) by stimulation of IL-1β and TNF-α (secreted through Toll-like receptor 4 (TLR4) pathway activation) results in collagen degradation, inflammation, and tissue remodeling (11).

At the same time, T cells can be activated by the presentation of LDL fragments on dendritic cells and differentiate into pro-inflammatory Th1 effector cells under the context of IL-12 stimulation (12-15). These Th1 effector T cells in atherosclerotic plaques also produce excessive amounts of TNF-α and interferon-γ that stimulate macrophages, vascular smooth muscle cells, and endothelial cells to express leukocyte adhesion molecules and MMPs, and down-regulate fibrillar collagen formation (16, 17). In contrast, regulatory T cells can also play a role in counterbalancing the inflammation in atherosclerotic plaques (18, 19). Furthermore, mast cells are also known to infiltrate into advanced atherosclerotic plaques and contribute to plaque inflammation. (20) This complicated inflammatory crosstalk eventually leads to proteolysis, cell death, and the formation of the necrotic core (also known as the lipid core).

The necrotic core is the result of cell death (apoptosis) and necrosis in the atherosclerotic plaques. Excessive inflammation, oxidized lipids and cholesterol, and intracellular endoplasmic reticulum (ER) stress effector CHOP are known triggers of macrophage apoptosis (21). In general, At least two known mechanisms can lead to necrosis. One mechanism is apoptosis

followed by defective efferocytosis (phagocytic clearance) of apoptotic cells. The apoptotic bodies, if not phagocytosed, become secondarily necrotic due to loss of membrane integrity. This mechanism is also called secondary necrosis. The other mechanism is called primary necrosis (22). In advanced plaques, efferocytosis is defective due to impaired phagocytosis associated with impaired resolution of inflammation (23-26). The release of pro-inflammatory damage associated molecular patterns (DAMPs) is believed to be important in this process (27). However, the exact mechanism is not known. ADAM metallopeptidase domain 17 (ADAM17)-mediated cleavage of a macrophage efferocytosis receptor, MerTK, has been shown to be an important contributor in this process (23-26). The process of primary necrosis is mediated by another signaling cascade involved in receptor-interacting protein kinase 1 and 3 (RIPK1 and RIPK3), which has also shown significant contribution to necrotic core formation (28).

Computational analysis suggests that lipid core accumulation and necrotic core enlargement can reduce the mechanical stability of plaques (29). In advanced plaques, activated smooth muscle cells proliferate and secrete matrix materials such as collagen and elastin to facilitate fibrous cap formation overlaying the necrotic core. The collagen in the plaque is believed to contribute to the tensile strength and increase plaque stability. When an atherosclerotic plaque features a fibrous cap overlaying the necrotic core, it is categorized as a fibrous atheroma. The stages of plaque progression are defined by the presence of these morphological characteristics and shown in the simplified diagram Figure 3 (30-33). Figure 3 was obtained from a review article written by Sanz et al. (33), reused with permission from Nature Publishing Group.

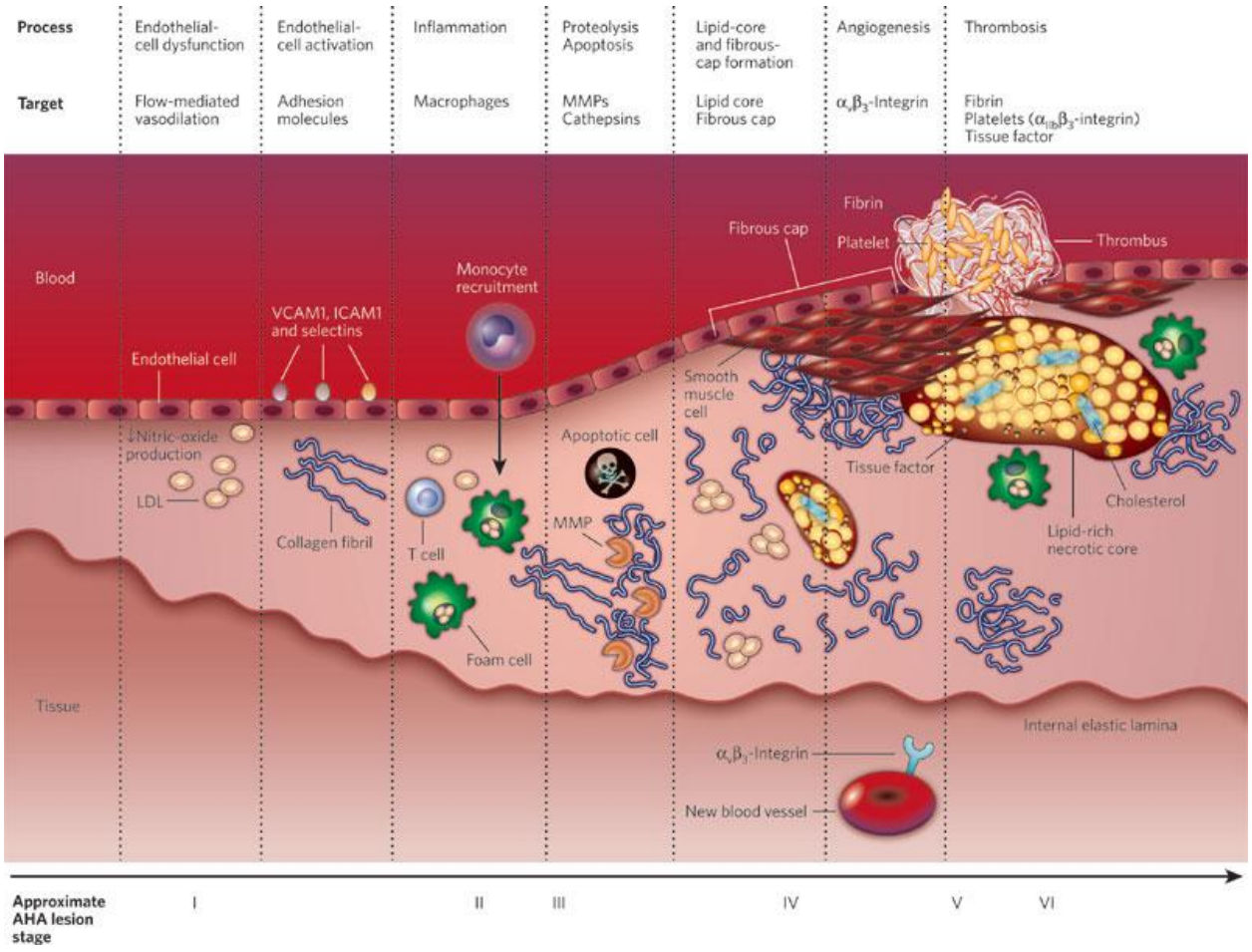

Figure 3: Simplified Illustration of the Progression and Developmental Stage of an Atherosclerotic Plaque.

Figure from Sanz et al. (34), reused with permission from Nature Publishing Group. The simplified progression of an atherosclerotic plaque is shown from a stage of normal blood vessel (left) to a stage of vessel with an atherosclerotic plaque disrupted and eroded with a superimposed thrombus (right). The AHA defied stages corresponding to the development were listed in the bottom. Potential targets for molecular imaging at each stage are listed on the top. AHA, American Heart Association; ICAM1, intercellular adhesion molecule 1; LDL, low-density lipoprotein; MMP, matrix metalloproteinase; VCAM1, vascular cell-adhesion molecule 1.

1.3 Manifestation of Acute CVD: Atherosclerotic Plaque Rupture and Erosion

The atherosclerotic process is usually unnoticed for years or even decades, and may never result in any clinical manifestation. However, when a plaque is destabilized, loses integrity, and

ruptures, thrombotic occlusion of the artery may occur and result in clinical manifestation of an acute CV event, such as ACS. Most death-causing CV events, including acute myocardial infarction (AMI), strokes and sudden death, are now known to be caused by vulnerable plaques, which are those that have a high risk of rupture or erosion (35). When a vulnerable plaque fissures or ruptures, it may trigger a secondary thrombosis event due to exposure to tissue factor (TF) and result in blockage of blood flow and organ failure, as illustrated in Figure 3. The term "rupture" has been frequently used in the literature to describe an acute process of plaque destabilization that results in the fissure or breakage of the plaque and thrombus formation due to contact with plaque content (lipid crystal and tissue factor) (35, 36). Studies have shown that these disease-causing atherosclerotic plaques are vulnerable, as characterized by a larger necrotic core, a thinner cap (less than 65 μm thick), increased inflammatory cells at the lateral margins (shoulder regions), presence of intraplaque hemorrhage, and thrombus formation in the lumen. In contrast, patients without symptoms contain stable plaques characterized by a thicker cap, a smaller lipid core, no intraplaque hemorrhage, and no thrombus formation in the lumen (35, 36). Importantly, there are two phenotypes of vulnerable plaques that lead to clinical manifestation, categorized by their histological features. The first type is the ruptured plaque, with attached thrombi, that contains intraplaque hemorrhage in the necrotic core. Intraplaque hemorrhage is believed to be caused by microvascular leakage and plaque fissure. The second type is called an eroded plaque and features endothelial surface erosion and thrombi formation without detectable loss of plaque integrity or intraplaque hemorrhage. Plaque rupture is dominant in ACS. This phenotype can be observed in ~70% of cases of ACS. (32, 37) The surface erosion is minor and can be found in ~30% of cases with coronary thrombosis (especially in women and young adults of sudden coronary death) (38-40). It is generally believed that a vulnerable atherosclerotic

plaque could be transited from a stable atheroma (41), but the triggers and mechanisms by which this could occur remain largely unknown. These heterogeneous phenotypes of vulnerable plaques suggest that there might be different molecular mechanisms leading to plaque destabilization.

1.4 Concept of Plaque Vulnerability

The concepts of plaque vulnerability and plaque rupture were mainly derived from case studies of sudden coronary death and AMI using postmortem pathological methods. Based on the histomorphological evidence of autopsy, the predominant characteristics of death-causing plaques in human appear to be the presence of a larger necrotic core covered by a thin fibrous cap. Plaques with this phenotype are characterized as thin-cap fibroatheromas (TCFA), which are believed to be vulnerable and prone to plaque rupture (36). The highest frequency of rupture is at the shoulders of the plaque where infiltration of inflammatory cells often occurs (38, 42, 43). Mostly, vulnerable plaques were found to be infiltrated by macrophages and lymphocytes. The smooth muscle cell content within the fibrous cap at the rupture site is frequently sparse. These ruptured plaques also demonstrate intraplaque hemorrhage and blood clots in most cases. The result of plaque rupture has been shown in histology of autopsy as an atherosclerotic plaque with cap disruption and a luminal thrombus in contact with the underlying necrotic core. These kinds of ruptured plaques are found in 60% of sudden coronary death cases, suggesting that plaque destabilization, plaque rupture, and subsequent thrombotic occlusion are a central mechanism of AMI that results in sudden death (32, 37). These vulnerable plaques are often not highly stenotic. This phenomenon indicates that the cellular and molecular compositions of the plaque, rather than the size of the plaque, determine plaque vulnerability. However, these postmortem pathological studies are limited by its nature and are fundamentally retrospective. The

observations can be affected by selection bias and background pathophysiology. Differences in clinical assessments and the lack of medical history of these patients before coronary death limit interpretation of the results. The tissue processing and sectioning may also disrupt the plaques and cause artifacts. Therefore, the underlying mechanisms and cause-effect relationship cannot be directly established.

The use of intracoronary imaging modalities, such as intravascular ultrasound (IVUS) and optical coherence tomography (OCT), have provided some prospective evidence regarding atherosclerotic plaque vulnerability leading to CVD. IVUS has been used to determine vessel geometry, and it can also be used to detect the presence of a vulnerable plaque that contains high lipid content, a cavity in contact with the lumen, and an overlying residual fibrous cap fragment. One IVUS study has shown that ruptured plaques are more frequently observed in patients with ACS (49%) than in those with stable angina (25%) (44). Another prospective IVUS study has demonstrated that vulnerable plaques characterized as TCFAs are indeed a risk factor for coronary events. These findings support the concept of plaque destabilization and vulnerability as the precursor to CVD. While IVUS was limited by its low spatial resolution (100–200 μm), OCT (using near-infrared light with a shorter wavelength and higher frequency than ultrasound) possesses 10 times higher spatial resolution (10–20 μm). Therefore, OCT enables fibrous cap thickness to be measured *in vivo* more precisely and accurately. The cap disruption can be detected with better sensitivity than IVUS (45). Furthermore, a later OCT study has reported detection of plaque rupture in 73% of 30 AMI cases while IVUS could only detect plaque rupture in 40% of the same AMI population. (46). This result indicates that OCT is more sensitive than IVUS. The development of various *in vivo* and *ex vivo* high resolution imaging

modalities allow clinicians and researchers to identify the presence of vulnerable plaques more accurately and with less concern of histological artifact or sample selection bias compared to traditional histological approaches.

1.5 Mechanisms of Plaque Destabilization

Although the triggers and mechanisms by which a stable plaque transforms to a vulnerable plaque remains unclear, previous literature has described some possible physical and molecular mechanisms that could lead to plaque vulnerability. It is believed that inflammation, local shear stress, and protease activation can destabilize atherosclerotic plaques (22, 47, 48). During the process of plaque destabilization, there is leukocytic infiltration accompanied by necrotic core enlargement, which could be caused by enhanced plaque inflammation followed by macrophage and vascular smooth muscle cell apoptosis. Vascular smooth muscle cell apoptosis and degradation of extracellular matrix may be induced by activation of various proteases that result in the thinning and loss of the fibrous cap. The loss of cap integrity can lead to exposure of the blood to highly thrombogenic materials in the necrotic core, resulting in thrombus formation, occlusion of the coronary artery, and associated ACS (22, 47, 48). Despite the various possible chronic mechanisms that might lead to plaque destabilization, the triggers and molecular mechanisms leading to the transition from a stable plaque to a vulnerable one remain unclear due to the lack of proper animal models of acute plaque rupture and erosion.

1.6 Animal Model of Atherosclerosis Lacking Plaque Rupture and Erosion

Small animals, especially rodents and rabbits, have been used extensively for studying atherosclerosis. There are many advantages of using small animals in atherosclerosis research,

such as 1) affordability, 2) fast breeding, 3) completed genetic characterization and available genetically modified animals, 4) antibody and assay compatibility, 5) fewer ethical concerns compared to using large animals (especially non-human primates), 6) available qualified husbandry facility, 7) easy administration and low drug dosage requirement for *in vivo* screening, 8) rapid development of atherosclerotic plaque in major arteries. These characteristics have permitted the researchers to experimentally validate their hypotheses within reasonable timeframe with sufficiently large number of animals to perform meaningful statistical analyses (49). The various genetically modified animals and compatible research tools (commercial antibodies, assays, etc) allow the experimental results to be interpreted and analyzed more easily. Thus, the major progress in the understanding atherosclerosis has been achieved predominantly by using the small, genetically modified hypercholesterolaemic animals including 1) Watanabe heritable hyperlipidaemic rabbit, which has a low-density lipoprotein receptor (LDLR) gene defect (50), 2) LDLR-deficient (or $LDLR^{-/-}$) mice (51), and 3) apolipoprotein E (ApoE)-deficient ($ApoE^{-/-}$) mice (52); especially in discovering the role of inflammation and innate immune system as the central drivers of this process. These genetically modified animals develop hyperlipidemia and atherosclerotic plaques in their aortas and aortic roots. The atherosclerotic plaque generated in these models present similar basic morphological features of human plaques, including intima lipid deposition, foam cells accumulation, necrotic core formation, and cap formation. Western-type diets (WD) containing high cholesterol and high lipid content are usually used to further accelerate the development of atherosclerotic plaques in these genetically modified animals. These hyperlipidemic and hypercholesterolaemic animals are very useful and have been used extensively to understand the mechanisms controlling initiation and progression of atherosclerosis, but the atherosclerotic plaques present in the aorta and aortic

root of the small animals are usually very stable and rarely spontaneously demonstrate plaque vulnerability including intraplaque hemorrhage and thrombus that observed in susceptible human individuals. This results in very limited investigations of the mechanisms leading to atherosclerotic plaque destabilization. The discovery of therapeutic strategies requires the use of the proper animal models that mimics the pathological process of plaque rupture. Therefore, there is an urgent need for the proper animal models that mimicking this process to be established (53-55).

1.7 Development of Animal Model of Plaque Rupture

Since the atherosclerotic plaques developed in small animals are usually very stable and rarely exhibit plaque vulnerability, various modifications had been applied on the traditional animal model of atherosclerosis to induce the development of vulnerable plaque in these animals [Figure 4] (54).

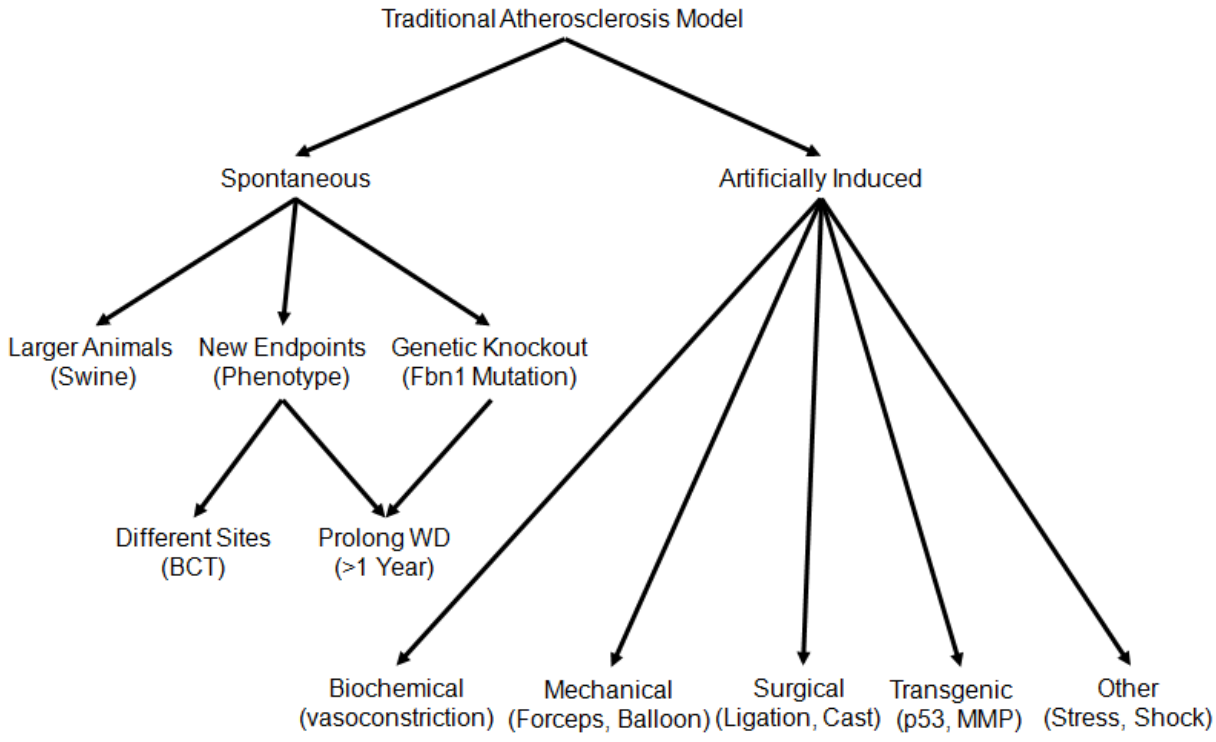

Figure 4: Schematic Diagram for the General Developmental Approaches of Animal Model of Plaque Vulnerability.

One example was to change a different plaque site for evaluation. For instances, Rosenfeld et al. found that 42-54 weeks old ApoE knockout (ApoE KO) mice developed atherosclerotic plaque with intraplaque hemorrhage, loss of fibrous cap in the brachiocephalic artery (56). Brachiocephalic artery (trunk) or BCT is a ~ 2 mm long vessel segment connecting aortic arch to the right carotid artery and the right brachial artery. It also called the innominate artery. Similar to the above study, Johnson and Jackson reported that ApoE KO mice fed a prolong high-fat diet (≥1 year) exhibited development of vulnerable plaques with occlusive thrombus formation in the BCT (57). These plaques were characterized by thin caps, less smooth muscle cells, and intraplaque hemorrhage. However, this model rarely demonstrated platelet-rich fibrin clots

demonstrated in human plaque rupture (58). Reddick et al. (59) showed that mechanical injury (gently squeezing the plaque-bearing segment of abdominal aorta in situ with blunt forceps) disrupted the target plaques and led to rapid formation of platelet aggregates and platelet-rich fibrin clots. Sasaki et al. (60) showed that surgical ligation of the carotid artery in ApoE KO mice for 4 weeks could induce intimal hyperplasia and formation of a lipid-rich and collagen-rich plaque that contains inflammatory cells (macrophages and T lymphocytes), and smooth muscle cells. The subsequent cuff placement proximal to the ligation site caused intraplaque hemorrhage, neutrophil infiltrations, formation of fibrin-positive luminal thrombus, a decrease in collagen content, and an increase in the apoptotic cells in the targeted plaques 2 to 4 days after cuff placement (60). However, in these artificially-intervened animal models, the results were descriptive and the possible contributors of plaque destabilization were not investigated. The systemic, mechanical, or biological effects (induced by vessel ligation or cuff placement) on plaque vulnerability were not identified or experimentally validated. Therefore these animal models had limited use in understanding the molecular process of plaque destabilization.

Instead of using unidentified triggers, Rekhter et al. (53, 61) developed a rabbit model in which an endothelial injury induced atherosclerotic plaque that resembles human plaque compositions can be ruptured by an inflatable intraplaque balloon. The pressure needed to inflate the intraplaque balloon can be determined to be a plaque mechanical strength index. This embedded balloon could be inflated in both *ex vivo* setting and *in vivo* context, leading to plaque disruption. The *ex vivo* setting is designed to measure the mechanical strength of the plaque; the *in vivo* setting allows the investigation of the thrombosis event. This model also allows local delivery of various substances into the plaque for studying determinants of plaque stability (53, 61). It is

probably a suitable model for studying the systemic response of the host to the molecules delivered before and after plaque rupture. However, this model is very labor-intensive and not widely adapted. Importantly, von der Thüsen et al. (62) showed that atherosclerosis could be accelerated by placing a restrictive silastic collar around the target artery (common carotid artery) of ApoE KO mice. These collar-induced plaques in ApoE KO mice demonstrated a necrotic core and a fibrocellular cap after 6 weeks of collar placement. The authors then induced plaque vulnerability by introducing adenoviral vectors expressing human p53 under a cytomegalovirus (CMV) promoter (Ad5-CMV.p53) or a β-galactosidase-expressing reporter gene LacZ under the same CMV promoter. The activation of p53 gene was known to cause smooth muscle apoptosis. They found over-expression of wild-type p53, but not lacZ, reduced cell proliferation and increased the fibrous cap cell apoptosis (62). This application resulted in the reductions of cap thickness 14 days after Ad5-CMV.p53 infection (characterized by a reduction in collagen content and a loss of cap smooth muscle cells). These infected lesions resembled structural features of the vulnerable plaques, but the spontaneous rupture was rarely found (only 12%) (62). These results indicated that smooth muscles apoptosis through activation of p53 pathway would alter the plaque structure and destabilize the plaques. Importantly, in the infected plaques, the incidence of plaque rupture can be increased to 40% after intravenous injection of phenylephrine. Phenylephrine is a vasopressor compound used to raise the arterial pressure. This phenomenon suggested that not only plaque structure and composition determined plaque vulnerability, but also the vascular hemodynamic factors, such as high blood pressure may contribute to mechanical plaque destabilization and rupture.

Instead of specific activation of apoptosis, that did not induce plaque rupture and thrombosis, Eitzman et al. (63) simply applied a photochemical reaction to cause thrombus formation overlaying the atherosclerotic plaque in ApoE KO mice. The time for thrombus formation and occlusion was taken as the endpoint (63). Similarly, intraperitonal injections of Russel's viper venom (a procoagulant and endothelial toxin) combined with intravenous injection of histamine, angiotension II, or serotonin was used in an atherogenic rabbit model to induce thrombosis and AMI (64-66). However, thrombosis and myocardial pathology was not associated with plaque rupture. Regardless, it showed that combination of hypercoagulation, endothelial injury, and vasoconstriction could be sufficient to cause plaque erosion and cardiac ischemia induction. Caligiuri et al. (67) demonstrated that mice with coronary atherosclerosis develop acute ischemia and MI by exposure to mental stress or hypoxia, which is mediated by endothelin type A receptor and independent of plaque rupture and thrombus formation. This model suggested that over heart-workload and hypoxia induced by mental stress might be another pathway leading to CVD independent of plaque vulnerability. Regardless, literature has shown that chronic intermittent mental stress and stress mediated by the sympathetic nervous system slightly promote plaque instability, MI, and mortality in mice (68, 69). It was also shown in a pilot study by Rekhter et al. (54) that stress-hormone injected into the brain of mice was associated with plaque disruption and thrombosis in an unknown pathway.

Larger mammals, for instance, swine with inherited hyper-LDL cholesterolemia, developed complicated phenotypes with spontaneous hemorrhage and rupture in the coronary arteries (70). Swine have blood vessels which closely match humans in size and they have similar hemodynamic factors including blood pressure and heart rates compared to those in humans.

These physiological similarities enable the researchers to study atherosclerosis in them and generalize the experimental results to human patients. Swine had been used predominately in investigating the endovascular therapeutic strategies and novel devices for stent placement. Shi et al. (71) have recently created a new swine model of carotid atherosclerosis based on combined dietary hyperlipidemia and partial surgical ligation (up to 80% stenosis) at the carotid artery of Yucatan mini-pigs. This artificial induction of blood flow turbulence combined with high cholesterol diet results in vulnerable plaque development within the targeted carotid artery. These plaques developed similar morphologic features of advanced human atherosclerosis, such as necrosis, ulceration, calcification, and intraplaque hemorrhage. More importantly, their model was also the first animal model to report the distal embolism. Artery to artery embolism is known to be the cause of stroke. Therefore this model could be a useful tool for studying the mechanisms of stroke and relevant therapeutic strategy after plaque ruptured. However, the authors in this model induced the artificial plaque vulnerability by evasive surgical procedures of ligation directly on the site where plaque formation took place. This artificial intervention by ligation over time resulted in the development of plaque phenotype which is similar to that in human diseases, but the underlying mechanisms that trigger vulnerability might not be corresponding to human disease. Therefore it may not be a proper tool for investigating the physiological transition of plaque vulnerability and underlying mechanisms that lead to plaque rupture.

Both in human and animals, atherosclerotic plaques are mostly observed at bifurcations and in curved arteries, where alteration of shear stress occurs (72). Cheng et al. (73) investigated the effect of shear stress alteration in relation with plaque phenotype development and plaque

cellular composition by instilling a perivascular shear stress modifier (cast) that induces regions of lowered, increased, and oscillatory shear stresses in upstream, middle, and downstream regions of mouse carotid arteries (73). They found that the region of increased shear stress is protected from atherosclerosis. Only the regions with lowered and oscillatory shear stress demonstrated atherosclerotic plaque development (73). Although lowered shear stress and oscillatory shear stress are both essential conditions for plaque formation, lowered shear stress induces significantly larger lesions with more vulnerable plaque phenotype (fewer smooth muscle cells, less collagen, more lipid and more outward vascular remodeling), whereas oscillatory shear stress induces more stable plaque phenotype (73). The exact mechanisms by which lowered shear stress induced different cell composition and morphology of plaque was unknown. But it is noted that matrix metalloproteinases (MMP) activity, adhesion molecules, growth factors and inflammatory cytokine interleukin-6 (IL-6) gene expression were more highly associated with vulnerable plaque formation. Importantly, the vulnerable plaques in the lowered shear stress region demonstrated more intraplaque hemorrhage (75%) when the blood pressure was elevated (from 95±3 to 127±3 mm Hg) by chronic administration of angiotensin II using osmotic minipump delivery (400 ng · kg−1 · min−1) (73). In contrast, no intraplaque hemorrhage was observed in the stable plaques in the region of oscillatory shear stress region (73). Later, in a separate study, they reported that the development of atherosclerotic plaques induced by low shear stress was characterized by a specific expression of cytokines KC, IP-10, and fractalkine. Plaque vulnerability in their model is determined by these chemokines and especially fractalkine (74).

Although the plaque rupture frequencies in most mouse models are lower than optimal and the inflammatory and molecular triggers of plaque vulnerability are somewhat undefined, the majority of plaque vulnerability models almost always described the detection of MMP in the vulnerable plaques (48, 60, 73-76). In contrast, low or no localization of MMP was observed or detected in the stable plaques (48, 60, 73-76). Consistently, Cheng et al. (75) reported that angiotensin II administration not only increased blood pressure, but also increased the incidence of intraplaque hemorrhages from 30% to 73% in the atherosclerotic plaques in the low shear stress region. The area of intraplaque hemorrhages was increased by 5-fold (75). These plaques had a 3-fold reduction in collagen content, contained 2-fold higher MMP8 and MMP13 levels, and had a 2- and 3-fold increase in collagen type I degradation by MMP8 and MMP13, compared to the control group (75). Similarly, Gough et al. (76) hypothesized that macrophage-mediated matrix degradation could induce plaque rupture. They tested this hypothesis by retro-virally overexpressing the MMP-9 in the donor macrophages and repopulated these macrophages in the advanced atherosclerotic lesions of ApoE KO mice (76). They found that while there was a greater than 10-fold increase in the expression of MMP-9 by macrophages, there was only a minor increase in the incidence of plaque fissuring 4 days after macrophage transplantation. However, they discovered that macrophages secreted MMP-9 predominantly as a proform (inactive), and this form was unable to degrade the matrix elastic component (elastin) (76). Importantly, retro-virally induced overexpression of an auto-active form of MMP-9 in the donor macrophages with enhanced elastin-degradation ability significantly increased the incident of plaque disruption in the advanced atherosclerotic lesions of ApoE KO mice *in vivo* (76). These data showed that matrix and protein structure in the plaque are important for plaque stability. The activated proteolysis through macrophage MMP-9 could induce plaque vulnerability and MMPs

might be important contributors to plaque vulnerability. This sophisticated animal model might be an appropriate tool for investigating the role of macrophage related enzymes and molecules in causing plaque rupture.

Along with this concept that van Herck et al. (77), found that a mutation ($C1039G^{+/-}$) in the elastic fibrillin-1(Fbn1) gene promoted arterial stiffness, accelerated atherosclerotic plaque progression (larger plaque size) and developed plaques with multiple vulnerable features (increased apoptosis of smooth muscle cells, decreased in collagen content, enlargement of necrotic core, and increased in macrophages content) in ApoE KO mice after 10 weeks of a WD. They observed more buried fibrous caps in the plaques at aortic valves, BCT and in the upper, middle, and lower thoracic aorta after 20 weeks of a WD (77). However, there was no occlusive thrombus at the site of plaque disruption and no direct evidence that the buried fibrous caps in the plaques were caused by acute plaque ruptures; therefore they failed to demonstrate the potential of this model for studying plaque rupture. Recently, van der Donckt et al. (78) modified the above model by prolonging the WD up to 35 weeks, and they successfully demonstrated plaque disruption and intraplaque hemorrhage in 70% of ascending aorta and 50% of BCT of $ApoE^{-/-}$ $Fbn1^{C1039G+/-}$ mice. Importantly, they found 70% of $ApoE^{-/-}$ $Fbn1^{C1039G+/-}$ mice died suddenly whereas all ApoE KO control mice survived (78). This study suggested that the mice with dysfunction and fragmented elastin would develop plaque vulnerability chronically and eventually lead to intraplaque neovascularization, plaque rupture, MI, stroke, and sudden death progressively after time (78). However, this model addresses the importance of fibrillin-1 in long-term plaque development (atherosclerosis) instead of the transition process of plaque destabilization. How this fibrillin-1 defective state and elastin defragmentation occur or whether

they are the causes of the cardiovascular events in human are still not clear. Interestingly, van der Donckt et al. (78) observed mouse head tilt, disorientation and motor disturbances, disturbed cerebral blood flow and brain hypoxia in this model as indication of stroke. This model may have potential to be a monitorable model for screening therapeutic strategies for strokes after plaque complications occurred (78).

Altogether, these selected animal studies are summarized in Table 1. The results from these various animal studies suggest that the triggers of plaque vulnerability (rupture and erosion) are likely to be multifactoral. Nevertheless, plaque phonotypical changes (size of necrotic core, thickness of cap) and intensified inflammation precedes the loss of plaque integrity, intraplaque hemorrhage, and thrombus formations in the process atherosclerotic plaque destabilization.

Table 1: Summary of Selected Animal Models of Plaque Vulnerability

Method	Animal	Site	Reference
Prolong age > 42-54 weeks	ApoE KO mice	BCT	Rosenfeld et al. (56)
Prolong WD > 1 year	ApoE KO mice	BCT	Jackson et al. (57)
Mechanical injury by forceps	ApoE KO mice	Abdominal aorta	Reddick et al. (59)
Surgical ligation + cuff	ApoE KO mice	Carotid artery	Sasaki et al. (60)
Inflatable intraplaque balloon	New Zealand white rabbits	Thoracic aorta	Rekhter et al. (53, 61)
P53 induction + pheylephrine	ApoE KO mice	Carotid artery	von der Thüsen et al. (62)

Method	Animal	Site	Reference
Photochemical reaction + WD	ApoE KO mice	Carotid artery	Eitzman et al. (63)
Russel's viper venom + histamine, serotonin, angiotensin II	Hypercholesterolemic rabbits	Bilateral femoral arteries or Coronary arteries,	Sun, Constantinides, Nakamura et al. (64-66)
mental stress	ApoE KO mice, ApoE($^{-/-}$) Fbn1(C1039G$^{+/-}$) mice	Coronary arteries, proximal ascending aorta, and carotid artery	Roth, Ni et al. (68, 69)
Stress hormone	ApoE KO mice	N.A.	Rekhter et al. (54)
Combined WD and partial surgical ligation	Yucatan mini-pigs	Carotid artery	Shi et al. (71)
Mutation of apolipoprotein B.	Inherited hyper-LDL cholesterolemia (IHLC) pigs	Coronary artery, and aorta	Prescott et al. (70)
Shear stress alteration by cast	ApoE KO mice	Carotid arteries	Cheng et al. (73)

Method	Animal	Site	Reference
Shear stress + long-term angiotensin II administration by minipump	ApoE KO	Carotid arteries	Cheng et al. (73)
Retro-virally overexpressing active MMP-9	ApoE KO	BCT	Gough et al. (76)
A mutation ($C1039G^{+/-}$) in the elastic fibrillin-1(Fbn1) gene + 20 weeks of a WD	ApoE KO mice	Aortic valves, BCT, and thoracic aorta	van Herck et al. (77)
A mutation ($C1039G^{+/-}$) in the elastic fibrillin-1(Fbn1) gene + 35 weeks of a WD	ApoE KO mice	Ascending aorta, BCT	van der Donckt et al. (78)

1.8 Practical Considerations for Establishing Animal Model of Plaque Vulnerability

In order to establish a physiological model of plaque vulnerability, there are several practical points needed to be addressed carefully besides the induction of plaque vulnerability itself. First, previous literature has shown that atherosclerosis progresses episodically, and may be modified by physiological events (multiple stresses, infections, and inflammation episodes). However, in the most of experimental models, attempts are made to eliminate and exclude all types of stress, infection and inflammation episodes within animal colonies prior to induction of lesions. Secondly, the most researched target sites are often the sites most accessible (such as abdominal

aorta and aortic root), but not the most physiological sites where the physiological parameters are similar to human coronary arteries. Thirdly, the analysis of plaque rupture mostly relies on the two-dimensional (2D) analyses on limited numbers of immunochemical or histological tissue sections with various sectioning intervals, which sacrifices the structure and overall integrity of the plaque. The rupture signal may vary in size and dimension, and the 2D assessments might be too subjective and limited. The sectioning procedure may also eliminate the rupture signal or cause artifact, thus complicate the result evaluation. The change of plaque vulnerability should be determined by presence of proper vulnerability signal along with meaningful structural parameters (% size of necrotic core, thickness of cap) instead of using buried fibrous cap, or break of elastic lamella along with the size of plaque, or vessel stenosis. Fourthly, species-related differences between animals and humans should be considered when testing therapeutic agents and interpreting the experimental data. For instance, on average, the number of platelets in mouse circulation is four times higher than those in humans while the mouse platelet sizes are approximately one half of human platelets (79). Therefore, for testing possible antithrombotic agents or studying thrombosis events following plaque destabilization, larger animals that have similar haemo-states would be more adequate. In fact, nonhuman primates, pigs, and dogs are very useful for testing the antithrombotic efficacy and translational safety of new compounds before human clinical trials. For instance, the pig is a very good model because it develops spontaneous atherosclerotic lesions, has similar cardiovascular anatomy to humans, and even may develop sudden death under stress (70). Both anatomy and function of the pig coronary system as well as the histological anatomy of the aorta are comparable to humans. However, the large animal models present some disadvantages, such as 1) high cost, 2) slow breeding, 3) more ethical concerns, 4) fewer compatible research tools fewer commercial assay available

(antibodies), 5) incomplete genetic characterization, and a scarcity of transgenic models, 6) less qualified facility, and 7) difficulties in husbandry and handling (49). Their human-resemblance in hemodynamic conditions makes them a valuable tool to study atherothrombosis and to investigate the potential and promising therapeutic strategies (49). Surprisingly, however, there are also important similarities between mice and human. Mouse blood pressures (125 mmHg systolic pressure and 90 mmHg diastolic pressures respectively) are similar to those found in the human coronary arteries. Doppler ultrasound studies show that the average peak aortic root blood velocities are 1.04 m/s in mice which is almost equal to what's found in humans (1.03 m/s) (80). Lastly, the differences in gene regulations in different species need to be considered, especially when studying the gene that is selectively expressed. Overall, it is very unlikely that one animal model will meet all the criteria, but one appropriate plaque vulnerability model should have at least reasonable considerations on these aspects.

1.9 New Insight: Lung Inflammation and CVD

In order to establish a physiological plaque vulnerability model, and find out important molecular contributors of plaque vulnerability, detailed clinical observation and new insight are needed. Traditionally, heart and lung were considered to be two distinct and separate entities. Therefore, the CV events were generally considered to be independent events from the pathogenesis of lung diseases. However, the association between the two diseases could be under-recognized due to lack of proper combined examinations for these two groups of patients (81). In the past twenty years, emerging evidence has shown a strong association between these two entities. Lung inflammation is now considered an important risk factor of CVD (81-99). For an example, in the Lung Health Study, nearly 50% lung inflammatory disease patients who had

mild and moderate chronic obstructive pulmonary disease (COPD) were hospitalized due to their CV events (100). On the contrary, ischemic heart disease (IHD) patients who suffered coronary artery disease (CAD) had double the prevalence of airflow limitation compared to the middle aged healthy individuals (86). In the animal models, atherosclerotic burden and plaque vulnerability were found to be increased by chronic lung exposed to small particles that induced small airway inflammation. The lung and consequent systemic inflammatory response were found to be positively associated with the atherosclerotic burden and features of vulnerability in the animals (89). These clinical and experimental findings in the past two decades recently lead to new mechanistic hypotheses made by van Eeden, Man, and Sin et al. concerning the pathological links between lung inflammation and CVD (81, 83, 84). It was postulated that lung inflammation could be an important trigger in acute plaque destabilization.

Review of the literature has revealed many respiratory risk factors of CVD, including cigarette smoke, secondhand smoking, air pollution, particulate matters, diesel exhaust fumes, reduced lung functions, exacerbation of COPD, respiratory infections, and pneumonia. Humans or animals who suffered with these respiratory inflammatory conditions demonstrated high risk in CVD and CVD morbidity and mortality (81, 83, 85, 89-94, 96, 97, 101-110). Among all the risk factors of CVD and CVD related mortality, cigarette smoking is known to be the primary risk factor, especially for IHD patients. It is observed that cigarette smoking and exposure to small particulate matters increased the burden of atherosclerosis (100, 103, 107, 108, 110, 111). Regardless, all these risk factors are small in their particle size, and are capable of causing inflammations in the deep lung tissues (small airway and alveolus) and demonstrating acute or chronic effects on CVD morbidity and mortality. In contrast, larger particles that would mainly

be trapped in the upper and central airways (cause upper and central airway inflammation) usually have weak association with CVD (81, 83, 85). Along with this concept, not surprisingly, reduced lung function that was usually due to small airway inflammation and emphysema was responsible for one in every four deaths in IHD patients independent of the smoking effect. Even in lifetime non-smokers, reduced lung function exerts dose-response relationship with IHD and stroke mortality (85).

Although the exact mechanism by which lung inflammation could trigger acute cardiovascular event is unknown, several longitudinal studies of COPD patients have revealed some possible clues. Although COPD is a chronic lung disease, COPD patients usually show mild and moderate systemic inflammation. This systemic inflammation always becomes intensified during the period of acute exacerbations, most likely caused by acute respiratory infections (often triggered by viral infection, bacterial infection, or both). It was found that in COPD patients, the risk of MI and stroke are transiently elevated within the first five days following the acute exacerbation of COPD (97). This lung-heart association was not only observed in patients with COPD exacerbation. In general, symptoms of respiratory infection often preceding MI and symptoms of chronic bronchitis can predict the risk of coronary disease independently of other major CV risk factors. Similarly, many other studies revealed that the risk of MI and ACS in a person is transiently elevated in the first several days following respiratory tract infection, or pneumonia compared to the individual's baseline risk [Table 2].

Table 2: Selected Studies of Respiratory Infection Transiently Increased the Short-Term Risk of Acute Cardiovascular Events.

Study Method	AMI or ACS Risk (95% CI)	Risk of Stroke (95% CI)	Onset Time	Reference
Case-control	3.6 (2.2-5.7)	N.A.	1-5 days	Meier et al., 1998 (119)
1922 cases (1st MI)	2.3 (1.3-4.2)	N.A.	6-10 days	
7649 controls	1.8 (1.0-3.3)	N.A.	11-15 days	
Odds ratios	1.0 (0.7-1.6)	N.A.	16-30 days	
Case-series	4.95 (4.43-5.53)	3.19 (2.81-3.62)	1-3 days	Smeeth et al., 2004 (97)
relative to baseline	3.20 (2.84-3.60)	2.34 (2.05-2.66)	4-7 days	
risk within-person	2.81 (2.54-3.09)	2.09 (1.89-2.32)	8-14 days	
20,486 (1st MI)	1.95 (1.79-2.12)	1.68 (1.54-1.82)	15-28 days	
19,063 (1st Stroke)	1.40 (1.33-1.48)	1.33(1.26-1.40)	28-91 days	
Case-control	10.2 (3.4-30.7)	N.A.	1-2 weeks	Clayton et al., 2005 (90)
119 MI cases	8.2 (2.3-29.5)	N.A.	3-4 weeks	
214 controls	0.9 (0.4-2.1)	N.A.	≥1 months	
Case-series	132.0 (69.2-255.6)	N.A.	1-3 days	Corrales-Medina et al., 2009 (91)
self-controlled	3.1 (0.7-13.0)	N.A.	5-15 days	

Interestingly, levels of antibodies to the infectious agents, such as *Chlamydia pneumonia*, were also found to be elevated in coronary disease and stroke patients.(112, 113) Therefore, the systemic inflammation responding to lung infections may be important in the CVD development

(114, 115). It is very likely that these systemic inflammatory responses of the host promote atherosclerotic plaque vulnerability and atherothrombotic states (116, 117). In addition, literature has shown that infectious respiratory diseases (chronic bronchitis, pneumonia, and upper respiratory infections) predicted IHD stronger than non-infectious respiratory diseases (asthma, emphysema, and pneumoconiosis) (93). Influenza vaccination reduced the hospitalizations for cardiac disease and stroke among the elderly patients (118). Altogether, these observations not only highlight the importance of acute lung inflammation and infection in triggering acute cardiovascular events, especially ACS, MI, and stroke, but also raise the possibility that a proper animal model of plaque rupture could be built upon these clinical observations.

1.10 Current Animal Model of Plaque Vulnerability Related to Lung Inflammation

It was demonstrated nicely in rabbits that chronic exposure to urban air pollution particulate matters increases ~70% of the atherosclerotic burden in rabbit coronary arteries (89). The plaque volume in coronary arteries was also positively correlated to its inflammatory response in the lungs. Furthermore, the synthesized plaques in these rabbits exposed to small particulate matters displayed features of vulnerability, including a larger lipid core, increased number of inflammatory cells, and a thinner fibrous cap compared to control animal exposed to saline (89). Similarly, Sun et al. (120) used an ApoE KO mouse model to study the effect of long-term exposure to low concentration of air pollution particles (with a mean aerodynamic diameter of less than 2.5 μm, or PM2.5). They found PM2.5 exposure altered vasomotor tone, induced vascular inflammation, and potentiated atherosclerosis. The chronic exposure to PM2.5 for 6 months increased the atherosclerotic burden in abdominal aorta, worsened endothelial function, and increased expression of reactive oxygen species (120). These models might be a useful

chronic model for studying plaque progression, development, and compositional changes, but it did not show consistent signs of acute plaque rupture and erosion. Importantly, Kido et al. (121) exposed mice to PM10, and Suda et al. (87, 88) exposed mice to bacterial lipopolysaccharide (LPS). They found that these particles induced an acute inflammatory response in the lungs and consequent systemic inflammation, and cause an IL-6 dependent endothelial dysfunction in the systemic blood vessels. Mutlu et al. (122) exposed mice to small air pollution particles acutely and found that there is increased plasma expression of fibrinogen and platelets, enhanced factor VIII activity, and accelerated blood coagulation to ferric chloride application on common carotid arteries, suggesting a prothrombotic state in these mice. Alveolar macrophages in the lungs and IL-6 were found important in modulating this prothrombotic state in the common carotid arteries (122). The results of these valuable models indicate that acute lung inflammation can trigger an acute systemic inflammatory response and promote athrothrombotic state. However, no murine plaque vulnerability and rupture model induced by acute lung inflammation was established (81).

1.11 LPS Induced Lung Inflammation in Animal Models

LPS is a complex glycolipid embedded in Gram-negative bacteria outer membrane, such as *Escherichia coli*. It consists of a hydrophobic lipid A domain, an oligosaccharide core, and a polysaccharide chain (also known as the O antigen). The lipid A domain alone is a powerful stimulator of the innate immune response that can stimulate the production of proinflammatory cytokines and acute-phase proteins through activation of TLR4 pathway (123). Literature shows that LPS lipid A acyl chains can bind to the extracellular domain of TLR4, the lipid binding protein MD2, and the co-receptor CD14 complex on the surface of the extracellular membrane, and cause conformational changes and dimerization of the TLR4. TLR4 is a class 1

transmembrane receptor with a globular cytoplasmic TIR (Toll interleukin-1 receptor) domain. The TIR domain, when dimmerized, can activate the downstream intracellular signaling pathway through the two pairs of adaptor protein, TRAM-TRIF and MAL-MyD88. The recruitment and activation of these cytoplasmic adaptors MyD88 and TRIF eventually lead to activation of the transcription factor NF-ƙB, mitogen-activated protein (MAP) kinases and production of inflammatory cytokines (124). TLR4 receptors are expressed in many different cell types, including monocyte-macrophage lineage cells, lymphoid cells, endothelial cells, epithelial cells, and vascular smooth muscle cells. Mice exposed to inhaled LPS developed acute lung injury, acute bronchconstriction, tumour necrosis factor (TNF), interkeukins and keratinocyte-derived chemokine (KC) production, increased lung permeability, neutrophil infiltration, and endothelial dysfunction (87, 88, 125-127). Intratracheal instillations of LPS in experimental murine model are now widely used to induce acute lung injury for mimicking the inflammatory aspect of reparatory infections, pneumonia, and COPD exacerbation (87, 88, 125, 128-132); however, its effect on plaque destabilization and rupture is unknown.

1.12 Widespread Inflammation and Neutrophil Myeloperoxidase (MPO)

For establishing a relevant model of plaque rupture to validate the possible triggers and molecular contributors, it is important that we should not be just limited to plaque alone, but we should consider the concept of plaque rupture in the bigger picture. Clinical studies have shown that patients with unstable angina in their coronary arteries have widespread inflammations in all their coronary branches, which indicates that inflammation is not limited to the location of the vulnerable plaque (133). However, in patients with stable angina, no widespread inflammation was found. This phenomenon suggests that the factors causing coronary inflammation and

unstable angina are not local, but probably is upstream to where unstable angina is located (133). As 100% of cardiac output flow is through the lungs, the inflammatory state of the lung would be an important factor for coronary inflammation. In addition, in these inflamed coronary arteries, neutrophils were activated and the myeloperoxidase (MPO) stored in their primary granules were released in these coronary arteries. In contrast, in the stable patients, no widespread inflammation was found in the coronary arteries along with no release of myeloperoxidase from neutrophils in the coronary arteries (133). Neutrophils are densely granulated bone marrow-derived white blood cells that can migrate from bloodstream to site of inflammation following chemotactic signals and degranulate during respiratory burst. Neutrophils contain at least four different types of granules, including primary granules, secondary granules, tertiary granules, and secretory vesicles. The degranulation processes are highly controlled by activation of specific intracellular signaling pathways. For instance, formyl peptide receptor, CXCR1, β-arrestins, Rho GTPase Rac2, various soluble NSF attached protein (SNAP) receptors, the src family tyrosine kinases Hck and the protein tyrosine phosphatase MEG2 are found critical in the pathway of neutrophil primary granule release in response to bacterial tripeptide fMLP (Met-Leu-Phe) and IL-8 (134).

MPO is a 150-kDa heme peroxidase-cyclooxygenase stored in the primary (azurophilic) granules of neutrophils. Its major function is to suborn bacterial killing by generating various reactive oxidants and diffusible radical species during infections. Upon its release, it can utilize hydrogen peroxide (H_2O_2) to produce hypochlorous acid (HOCl), also known as bleach, that could damage tissues and chlorinate proteins (135). Studies have shown that MPO is the most abundant protein in neutrophils, accounting for up to 5% of their dry mass (136). In humans, it is also present in monocytes at lower levels. The ability of monocytes to produce this protein decreases during

maturation into tissue macrophages. In humans, MPO is localized in atherosclerotic plaques especially at the site of plaque rupture (135, 137-140). In contrary, there is controversial evidence of MPO localization in the plaque in the mouse atherosclerosis model (141, 142). Clinically, it is now well established that circulating MPO levels are associated with acute CV events among patients who present to emergency departments with chest pain (143-147). In these and other studies, plasma MPO levels predicted the presence of plaque erosions, and importantly, the prognosis of patients who presented to hospitals with unstable angina (144, 146). Patients with elevated plasma levels of MPO at hospital presentation have two to three times higher risk of death or nonfatal MI within the next 6 months compared to patients who have low MPO levels (independent of other well established risk factors for CVD, such as age, sex, and diabetes) (143, 144, 146). A genetic study also showed that individuals with partial or total deficiency of MPO were protected against CVD (148). Consistent with this observation, irradiated atherogenic mice that repopulated with macrophages containing human MPO gene developed atherosclerosis at a rate that was two times faster than control mice repopulated with wild-type mouse bone marrow (142). However, the pathological role of MPO in plaque vulnerability had not yet been validated experimentally. In an appropriate animal model of plaque vulnerability, this important phenomenon of widespread inflammation should be considered and possible cellular and molecular contributors, such as neutrophils and MPO should be validated (149). Possible mechanisms of neutrophil and MPO mediated plaque destabilization proposed by Soehnlein (149) are illustrated in Figure 5, which is obtained from an article by Soehnlein (149), reused with permission from Wolters Kluwer Health, Inc.

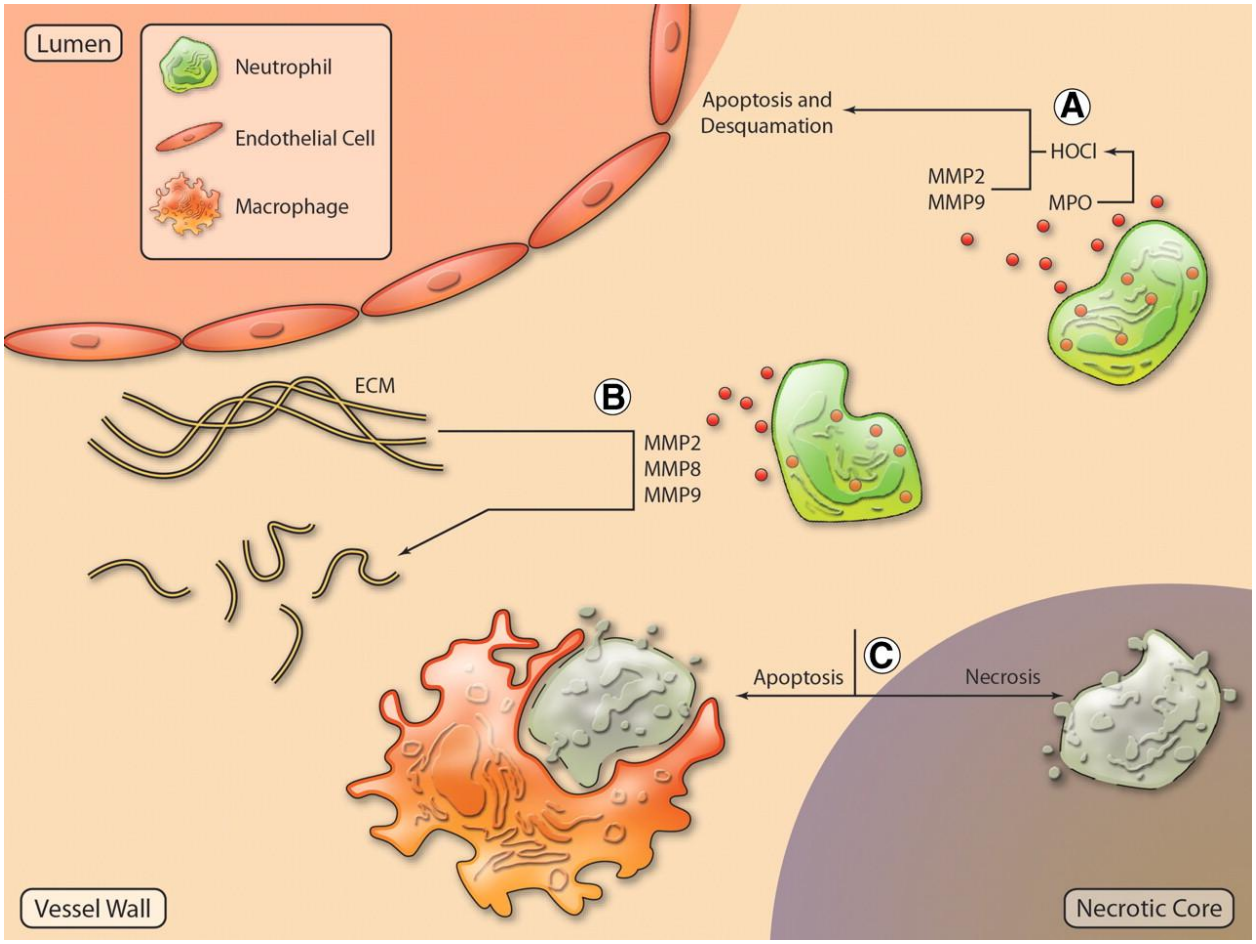

Figure 5: Possible Mechanisms of Neutrophil-driven Plaque Destabilization.

Figure obtained from Soehnlein (149), reused with permission from Wolters Kluwer Health, Inc. A, Myeloperoxidase-dependent oxidative stress and neutrophil-derived matrix metalloproteinases may induce apoptosis in endothelial cells, degradation of the basement membrane, and subsequent endothelial cell desquamation. B, Neutrophil-derived matrix metalloproteinases cleave components of the extracellular matrix. C, Neutrophils undergo apoptosis and secondary necrosis, which possibly contributes to necrotic core formation. ECM, extracellular matrix; MMP, matrix metalloproteinase; MPO, myeloperoxidase. Illustration credit: Cosmocyte/Ben Smith. Promotional and commercial use of the material in print, digital or mobile device format is prohibited without the permission from the publisher Wolters Kluwer Health. Please contact healthpermissions@wolterskluwer.com for further information.

Chapter 2: Experimental Approaches

2.1 Rationale

A physiological murine model of plaque vulnerability is lacking. Literature has implicated lung inflammation as a risk factor for acute coronary syndrome and stroke, but the underlying mechanisms linking lung injury to plaque destabilization are largely unknown. Neutrophil's role in plaque destabilization has not been validated experimentally in animal models. Plasma myeloperoxidase (MPO) is an inflammatory biomarker for acute CVD, but the effect of MPO enzymatic inhibition on plaque stability is unclear.

2.2 Hypothesis

Intratracheal exposure to Lipopolysaccharide will lead to acute plaque destabilization in ApoE KO mice fed on a short-term Western-type diet (WD). Circulating neutrophils and MPO are important contributors to plaque vulnerability.

2.3 Aims

1) Determine if intratracheal LPS exposure induces atherosclerotic plaque destabilization and plaque vulnerability in the right brachiocephalic artery of ApoE KO mice fed a short-term WD [Chapter 3:].
2) Determine if LPS exposure intrapertioneally induces acute plaque vulnerability in the right brachiocephalic artery of ApoE KO mice fed a short-term WD [Chapter 3:].
3) Determine the role of circulating neutrophils in LPS induced acute lung injury and plaque vulnerability in the developed plaque vulnerability model by depletion of circulating neutrophils [Chapter 4:].

4) Determine the role of myeloperoxidase in plaque vulnerability during LPS induced acute lung inflammatory episode using an enzymatic inhibitor 4-Aminobenzoic Acid Hydrazide (4-ABAH) [Chapter 5:].

Chapter 3: Lung Exposure to Lipopolysaccharide Causes Atherosclerotic Plaque Destabilization

3.1 Introduction

Lung injury and inflammation are considered to be major triggers of acute cardiovascular events (81). For instance, acute respiratory tract infections and heavy exposure to air pollution increase the risk of IHD, MI or stroke by two- to four-fold (90, 96, 97, 101, 102, 150). Most acute cardiovascular events arise from rupture and thrombosis of vulnerable (or unstable) atheromas (37, 38, 43, 151, 152). Vulnerable atheromas, independent of their size, are characterized by a thin cap, an enlarged "necrotic" core (acellular spaces normally occupied by lipids), increased inflammatory cell infiltration at shoulder regions, and areas of hemorrhage resulting from a loss of plaque integrity or leakage of microvessels (81). Stable atheromas, on the other hand, have a thicker cap, a smaller necrotic core, and fewer inflammatory cells. As a result, they are morphologically robust and unlikely to rupture. Although it is generally believed that vulnerable atheromas arise from stable ones, it is not clear how (or even if) acute lung inflammation induces this transition. One major barrier to investigate this crucial transition has been the lack of robust animal models that demonstrate atheromatous (plaque) rupture. In small rodents, atheromatous plaques tend to be very stable and rarely demonstrate vulnerability without external manipulation. In this study, we established a novel murine model that uses one-time exposure of lipopolysaccharide (LPS) instilled directly into the lungs via the trachea to promote the transition of stable atheromas to vulnerable ones (inducing plaque rupture).

3.2 Materials and Methods

3.2.1 Animal and Study Design

Male apolipoprotein E-null mice (ApoE-/-) on a C57BL/6J background (Jackson Laboratory, Bar Harbor, ME; Stock number: 002052) were fed a Western-type diet (WD) containing 21% fat from lard and 0.15% cholesterol (TD88137, Harlan Laboratories Inc., Madison, USA) for 8 weeks to induce atheromatous plaque formation in the brachiocephalic trunk (BCT) (153). These mice were then randomly divided into 3 groups: 1) LPS (N=28), 2) saline (N=20) or 3) WD (N=6). The experimental scheme is illustrated in Figure 6.

In the LPS group, a single dose of 100 µg LPS (Escherichia coli O111:B4; 3mg/kg) (L2630, Sigma-Aldrich, St. Louis, MO), dissolved in 50 µl of sterile saline, was sprayed as aerosol particles (16-22 µm in mass median diameter) directly into the lungs through the vocal cords using a microsprayer (MSA-250-M, Penn-Century Inc., Wyndmoor, PA). In the saline group, a single dose of 50 µl sterile saline aerosol was sprayed into the lungs in the same manner (87, 88).

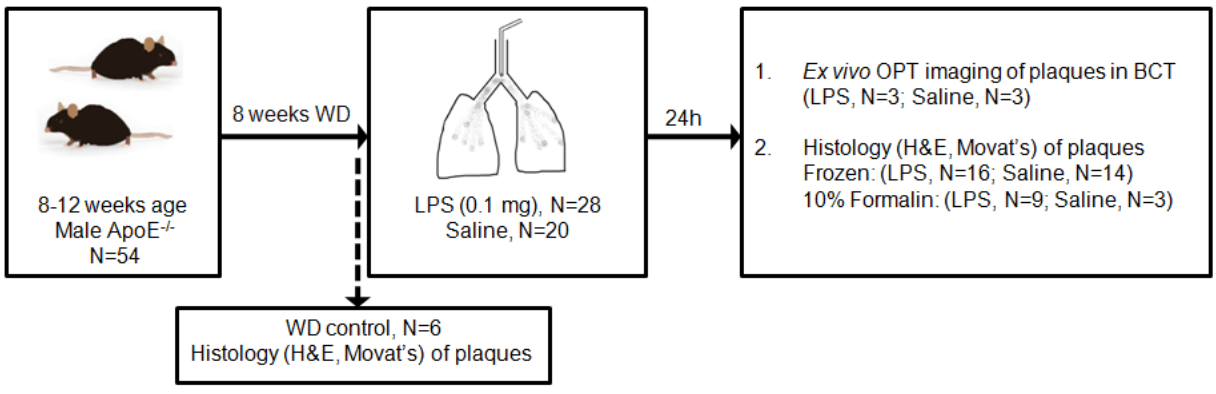

Figure 6: Scheme Diagram of the Mouse Model of Atherosclerotic Plaque Destabilization by Intratracheal LPS Exposure.

54 male apolipoprotein E-null mice (ApoE-/-) were fed a Western-type diet (WD) containing 21% fat from lard and 0.15% for 8 weeks to induce atheromatous plaque formation in the brachiocephalic trunk (BCT) and then randomly divided into 3 groups: 1) LPS (N=28), 2) saline (N=20) or 3) WD control (N=6). In the LPS group, a single dose of 100 µg LPS, dissolved in 50 µl of sterile saline, was sprayed as aerosol particles directly into the lungs through the vocal cords using a microsprayer In the saline group, a single dose of 50 µl sterile saline aerosol was sprayed into the lungs in the same manner. No LPS or saline exposure for the WD group.

3.2.2 LPS Dosage and Timeline Determination

The LPS dosage and timeline were determined based on a pilot study [Figure 7]. In order to optimize the atheroma destabilization model, three different LPS doses and three different time-points were investigated. Mice instilled with intratracheal LPS (25µg, 50 µg, 100 µg) were sacrificed after 4 hours, 24 hours and 48 hours (N=4 each). Saline-instilled mice that were sacrificed at the same time-points were used as controls. Experiment with LPS (100 µg) at 48 hours time-point resulted in sudden deaths and occurrence of paralysis in some mice. Atheromas were evaluated based on histological evidence described in this study. Fisher exact test were used to compare plaque destabilization rate in the right brachiocephalic trunk (BCT) between LPS and saline group at each time-point. Fourteen mice in total were in the saline 24 hours control group.

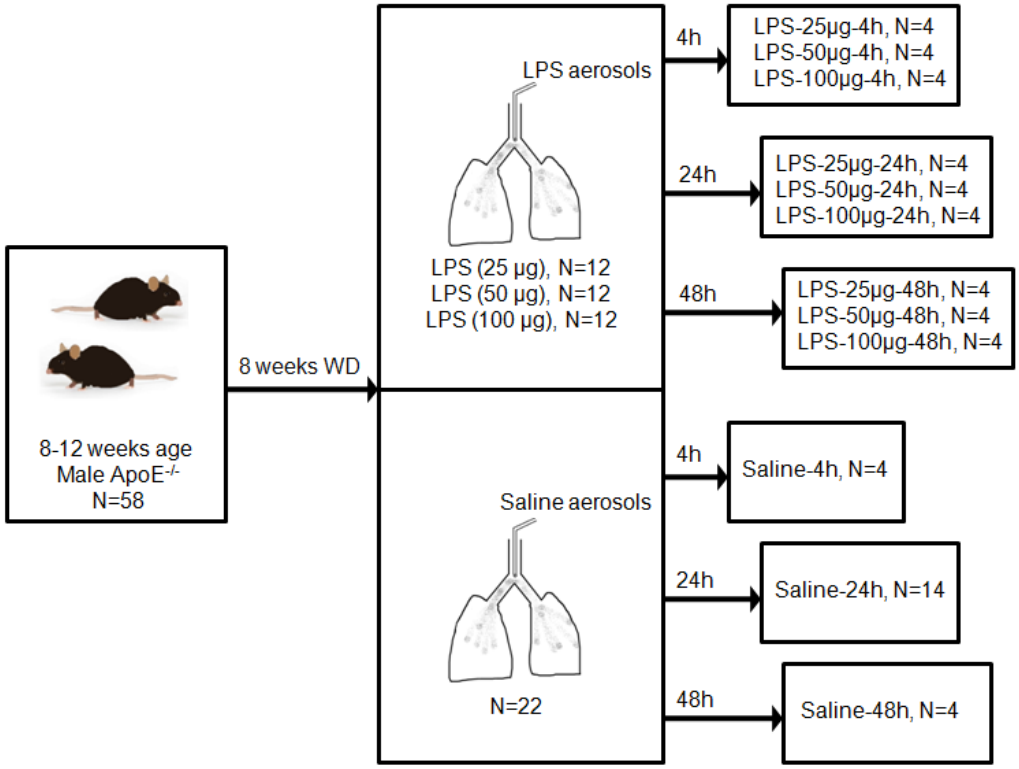

Figure 7: Scheme Diagram of LPS Dosage and Timeline Experiment.

Mice instilled with intratracheal LPS (25µg, 50 µg, 100 µg) were sacrificed after 4 hours, 24 hours and 48 hours (N=4 each). Saline-instilled mice that were sacrificed at the same time-points were used as controls. Experiment with LPS (100 µg) at 48 hours time-point failed due to sudden deaths and occurrence of paralysis in mice. Atheromas were evaluated based on histological evidence described in this study. Fisher exact test were used to compare plaque destabilization rate in the right brachiocephalic trunk (BCT) between LPS and saline group at each time-point. Fourteen mice in total for the saline 24 hours control group.

3.2.3 Investigation of Early Atheromatous Destabilization via Intratracheal Route versus Intraperitoneal Route of LPS Exposure

To determine the early changes in the plaque, we evaluated plaque morphology at 8 hours post-1) intratracheal LPS-exposure (LPS-IT; N=16) or 2) intratracheal saline-exposure (Saline-IT; N=14). To determine whether the route of LPS instillation modified the response in the plaques,

two additional groups were used: 1) intraperitoneal LPS-exposure (LPS-IP; N=5) and 2) intraperitoneal saline-exposure (Saline-IP; N=5). In the LPS-IP group, 100 µg of LPS dissolved in 50 µl of sterile saline was injected directly into the intraperitoneal space. In the saline-IP group, 50 µl of sterile saline was used. See [Figure 8] for experimental design. The same anesthetic procedures were used in both IT and IP groups.

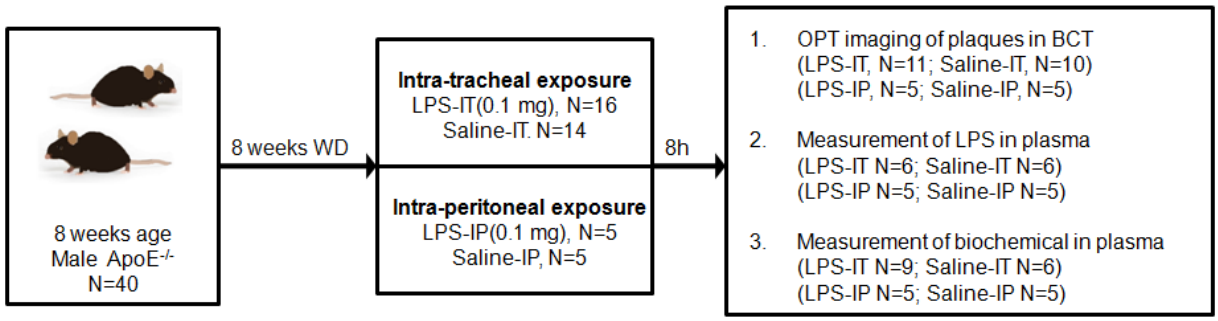

Figure 8: Early Stage of Atheroma Destabilization via Different Routes of LPS Exposure.

To determine the early changes of the plaques at 8 hours time point, plaque morphology at 8 hours post- 1) intratracheal LPS-exposure (LPS-IT; N=16) or 2) intratracheal saline-exposure (Saline-IT; N=14) were evaluated. To determine whether the same dosage intraperitoneal LPS would modify the response in the plaques, two additional groups were used: 1) intraperitoneal LPS-exposure (LPS-IP; N=5) and 2) intraperitoneal saline-exposure (Saline-IP; N=5). The same anesthetic procedures were used in both IT and IP groups during LPS instillation.

3.2.4 Organ and Tissue Procurement and Bronchoalveolar Lavage (BAL)

Under anesthesia (isoflurane 5% inhalation), blood was collected from the inferior vena cava (IVC) using a 25 gauge catheter needle (ProtectIV® Plus Safety I.V. Catheter, Smiths Medical International Ltd. Rossendale, Lancashire, UK) 24 hours after LPS challenge for cytokine and chemical measurements. Immediate procurement of the heart and blood vessels was performed

after blood collection. The heart, aortic arch and branching arteries containing the BCT were carefully harvested and perfused with 3ml of phosphate buffered saline (PBS) injected directly into the left ventricle at an infusion rate of 1 ml/minute (Harvard Apparatus, Massachusetts, USA). Bronchoalveolar lavage (BAL) fluid was collected by washing the right lung once with 600 µl of PBS. The left lung was harvested and perfused with 400 µl of 10% formalin. Extrapulmonary organs including liver and kidneys were also harvested and their hematoxylin and eosin stained (H&E) sections were used for morphological examination.

3.2.5 Optical Projection Tomography (OPT)

To visualize the plaques ex vivo without disturbing the plaques, optical projection tomography, OPT, (Bioptonics 3001M, MRC Technology, London, UK) was used, which enabled three-dimensional imaging of the entire aortic arch and BCT of mice (154, 155). The plaques were assessed in a blinded manner and plaques were considered vulnerable if there was a visible thrombus or evidence for hemorrhage in these plaques (with a size greater than 0.0005 mm^3). Thrombus and erythrocytes produced a distinct autofluorescence signal that was 10-fold higher in intensity than the arterial wall, which enabled volume quantification by threshold segmentation.

To enable imaging, the aortic arch containing branching arteries was carefully removed from the surrounding fat tissues. The samples were then immediately fixed in 10% formalin for 48 hours, after which, the samples were rinsed in PBS 3 times (30 minutes for each wash) and then embedded in 1% low melting point agarose. Next, the solidified agarose blocks were immersed in 100% methanol for 48 hours, which was changed five times during the procedure to ensure

complete removal of water from the blocks. After dehydration, the samples were stored in Benzyl Alcohol Benzyl Benzoate (BABB) solution for 72 hours. The samples were then imaged using an OPT scanner. UV light in the OPT scanner (metal-halide 120W UV source) was filtered to enable an excitation wavelength of 425 nm/40 nm with an emission wavelength of LP475 nm. The projection images were acquired by a charge-coupled device (CCD) camera every 0.9 degrees while the samples were rotated. In total, 400 projection images with a pixel size of 6.4 µm were captured per sample. The projection images were then reconstructed using the SkyScan NRecon software (Bruker microCT, Kontich, Belgium), resulting in a three-dimensional (3D) picture with an isotropic voxel size of 6.4 µm in all directions. All volume rendering and quantification was performed using the Amira visualization software (Amira V6.0, FEI Visualization Sciences Group, Burlington, MA, USA). Blood clots and hemorrhage in samples were detected via autofluorescence of red blood cells that occur at wavelength of 425 nm and were segmented and quantified three dimensionally (in volume) using Amira V6.0 visualization software.

3.2.6 Serial Cross-Sectioning of BCT: Frozen Sections

BCT was carefully removed from the surrounding fat tissues then embedded with optimum cutting temperature compound (OCT) (Sakura Finetek, Torrance, CA) on dry ice, followed by cryopreservation in liquid nitrogen and storage at -80°C. Using a cryostat (Leica, UK), serial 5 µm sections of vessels perpendicular to the long axis were obtained at approximately 50 µm intervals starting from the arch (proximal end) to the site of the BCT bifurcation. For each specimen, light microscopy was performed to confirm the quality of the cross-sections. Serial

cross-sections (approximately 18 cross-sections per mouse) were stained with hematoxylin and eosin (H&E) and Movat's pentachrome for morphological analysis.

3.2.7 Serial Cross-Sectioning of BCT: Formalin Perfusion and Paraffin Embedment

In order to further preserve the histological features of plaque rupture and validate the thrombus and intraplaque hemorrhage observed in this model, we also performed immediate formalin perfusion [Figure 4]. LPS was microsprayed as described previously into the lungs of 9 mice, and saline was microsprayed into 3 mice as saline controls After 24 hours, the aortic tree was harvested and immediately perfused with 3.0 ml of 10% formalin at constant perfusion rate (1ml per minute) following complete blood withdrawal. After 48 hour of formalin fixation, the aortic tree was paraffin embedded and continuous sections were obtained for H&E and Movat's pentachrome staining.

3.2.8 Quantitative Histology and Definition of Vulnerable Plaque

To correlate the findings of OPT images with histology, the serial cross sections of the entire BCT, which had been embedded in paraffin (or in optimal cutting temperature compound and frozen in liquid nitrogen) were stained with H&E and Movat's pentachrome and examined under the microscope.(156) Vulnerable plaque was defined by the presence of a thrombus or intraplaque hemorrhage. Intraplaque hemorrhage was noted when there were erythrocytes inside the atheroma on at least two contiguous sections spaced 50 μm apart. The presence of the vulnerability signals in a given plaque was determined by 2 independent investigators in a blinded manner. The decision was made by the third independent investigators when inconsistency occurred between them. For illustration of morphometric analyses, see Figure 9

and Figure 10. To phenotype the plaques in detail, we chose the cross-section of the frozen BCT that contained the largest plaque area and performed morphometric analysis. BCTs with formalin fixation may not be adequate for this purpose due to possible vessel shrinkage. All measurements were performed on H&E stained images using Image Pro software (Media Cybernetics Inc. Rockville, Maryland, USA) at 200X magnification. From these images, plaque size was determined by ascertaining the area enclosed by the internal elastic lamina (IEL) minus the area enclosed by the endothelial layer (lumen area). The necrotic core was defined as the component of the plaque that did not contain any matrix material (either collagen or elastin) or cells. This area was quantified by using color segmentation (illustrated in Figure 9). The percent (%) necrotic core was calculated by dividing the necrotic core area by the total plaque size. The cap-to-plaque thickness ratio was determined by first generating linear rays from the midpoint of IEL of the plaque and then measuring the distance from the endothelium to necrotic core and dividing this value by the distance from endothelium to the origin of the rays [Figure 10]. This method is suggested by Dr. Joanne Wright, who is an experienced pathologist. This approach allowed unbiased measurement of average cap thickness of plaque, as the cap thickness throughout a given plaque structure varies (heterogenic)

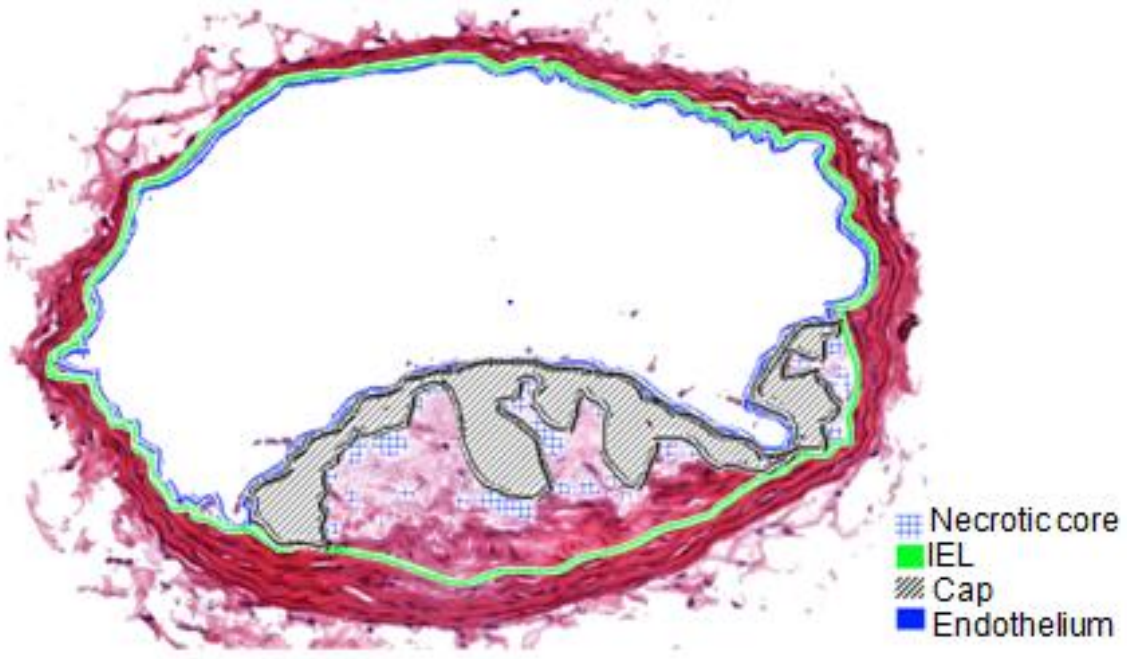

Figure 9: A Representative Figure of Different Morphological Components of a Plaque.

Vessel lumen, plaque area, necrotic core and cap region in a cross section of BCT. Plaque area was determined by ascertaining the area enclosed by the internal elastic lamina (IEL) minus the area enclosed by the endothelial layer (lumen area). The necrotic core was defined as the component of the plaque that did not contain any matrix material (either collagen or elastin) or cells. This area was quantified by using color segmentation. The percent (%) necrotic core was calculated by dividing the necrotic core area by the total plaque area.

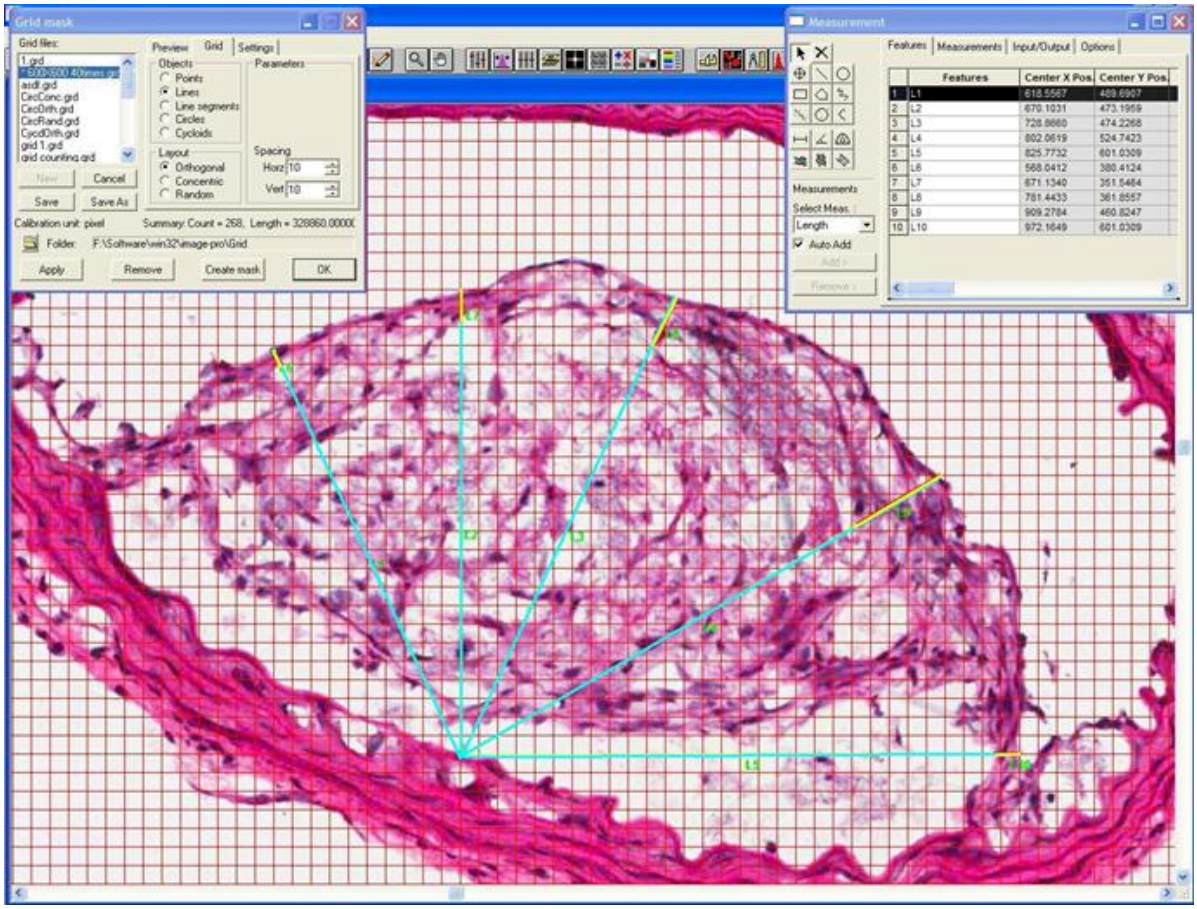

Figure 10: Determination of Cap-Plaque Thickness.

A plaque image was overlaid with a known pattern ray originating from the mid portion of internal elastic lamina (IEL) of the plaque. The cap-plaque thickness ratio was calculated by determining the distance from the endothelium to the necrotic core (yellow line) and then dividing this number by the distance from the endothelium to the spectrum origin (yellow line + blue line). An arithmetic mean value of five measurements was calculated and used for statistical analysis.

3.2.9 Immunofluorescent Staining and Signal Quantitation

Thrombin and Endothelial Co-staining: The frozen mouse BCT cross-sections were fixed in methanol for 10 minutes and then rinsed in running water for two minutes. The sections were incubated with 10% chicken serum (Gene Tex Inc., USA) and donkey serum (Sigma-Aldrich,

USA) for 30 minutes and then incubated with the anti-mouse CD31 monoclonal antibody rat IgG (5ug/ml; Cedarlane, ON, Canada) and the anti-mouse thrombin polyclonal antibody rabbit IgG (2.5mg/ml; Abcam, Toronto, ON, Canada) for 2 hours at 4°C. After PBS washes (4X of PBS incubation for 5 minutes each), the BCT sections were incubated with the secondary antibodies: Donkey anti-rat 488 (400X dilution; Invitrogen, USA) and Chicken anti-rabbit 594 (400X dilution; Invitrogen, USA) were used as the secondary antibodies for another 2 hours at room temperature. After washes (4X of PBS incubation for 5 minutes each), the sections were air dried for 30 minutes and mounted using the Vectashield mounting medium with DAPI (Vector Lab Inc, USA). Immunofluorescence images of the 3 serial sections containing the largest plaque areas were captured under a fixed computerized setting with Nikon immunofluorescence light microscope Eclipse TE300 (Nikon, Japan) at 100X, 200X and 600X magnification. Normal rabbit and rat IgG were used as the primary antibodies for negative controls.

MMP9 Staining: The standard staining procedure was followed according to manufactures' recommendation with primary antibody: goat anti-MMP9 polyclonal IgG (sc6840; Santa Cruz Biotechnology, Dallas, Texas USA); and secondary antibody: donkey anti-goat 488 (400X dilution, Invitrogen, USA)

3.2.10 Evaluation of Lung Inflammation: Differential Cell Counts in BAL

After centrifugation, cell pellet in the BAL fluid was re-suspended with PBS, gently mixed and cytospun down to a glass slide and fixed with methanol before staining with H&E and Giemsa-Wright stain. PMN (neutrophil) counts were obtained by dividing the cell pellet into 4 equal quadrants and then taking 4 random fields from each quadrant using Image Pro software at 400X

magnification (157). PMNs were morphologically identified by evaluating their size, shape, multinucleation, and presence of granules. Monocytes and alveolar macrophages were also determined by morphology. The arithmetic mean of measurements was used for statistical analysis. An automated hemocytometer for total blood cell count was also used to confirm the cell counts in BAL and blood.

3.2.11 Histology of the Left Lung

To evaluate the histological changes of the lungs, mouse left lungs were harvested and inflated at a pressure of 25 cmH2O using 400 μl 10% phosphate-buffered formalin. Left lungs were fixed in 10% phosphate-buffered formalin over 24 hours and embedded in paraffin. Paraffin-embedded left lungs were coronally sectioned in 4 μm slice thickness and were stained with H&E. The H&E slides were scanned with Aperio ScanScope XT (Aperio Technology Inc, USA) at 400X.

3.2.12 Evaluation of Systemic Inflammation: Serum Cytokines

Serum samples were used to measure the proinflammatory cytokines, including monocyte chemotactic protein-1 (MCP-1), keratinocyte chemoattractant (KC), interleukin-6 (IL-6), and tumor necrosis factor alpha (TNF-α) using Luminex MagPix (EMD Millipore, MA) and mouse multiplex assay kit according to the manufacturer's protocols.

3.2.13 Plasma LPS Measurements and Blood Chemical Test

Plasma concentrations of LPS were measured in duplicate using a commercially-available kinetic turbidimetric Limulus amebocyte lysate (LAL) assay kit (Lonza, Walkersville, MD) according to the manufacturer's protocol. Plasma samples were heat-inactivated and then diluted

1:500 in 10mM MgCl2 solutions to enable positive product control recoveries within 50-200%. Plasma urea and creatinine, lactate dehydrogenase (LD), albumin, alkaline phosphatase (ALKP), total bilirubin, (TBIL), aspartate aminotransferase (AST), alanine aminotransferase (ALT), and gamma-glutamyl transpeptidase (GGT)) were measured using the ADVIA 1800® Clinical Chemistry System (Siemens, Munich, Germany).

3.2.14 Statistical Analysis

All results were expressed as mean value ± standard deviation unless otherwise indicated. Data were analyzed using a Fisher's exact test (for comparison of rupture incidence between two independent groups), t-tests (for comparison of two independent groups that were normally distributed), and Mann Whitney U tests (for comparison of two independent groups that were not normally distributed). Kruskal Wallis test was used to compare more than two independent groups when distributions of the variables were not normal. All analyses were conducted using Prism 5 (GraphPad Software Inc., La Jolla CA, USA) and p-values less than 0.05 (two-tailed) were considered statistically significant.

3.3 Results

3.3.1 Male ApoE KO Mice Fed with an 8 Week Western-Type Diet (WD) Exhibit Stable Plaque Formation in the Brachiocephalic Trunk (BCT)

Morphological measurements of atheroma in brachiocephalic trunk (BCT) following 8 weeks of a Western-type Diet are shown in Table 3. These mice consistently developed atheromatous plaques in BCT, which were characterized by intimal thickening, foam cell accumulation, a

necrotic core, and a cap [Figure 11]. None of the plaques demonstrated histological features of vulnerability (hemorrhage or thrombus) before LPS or saline exposure.

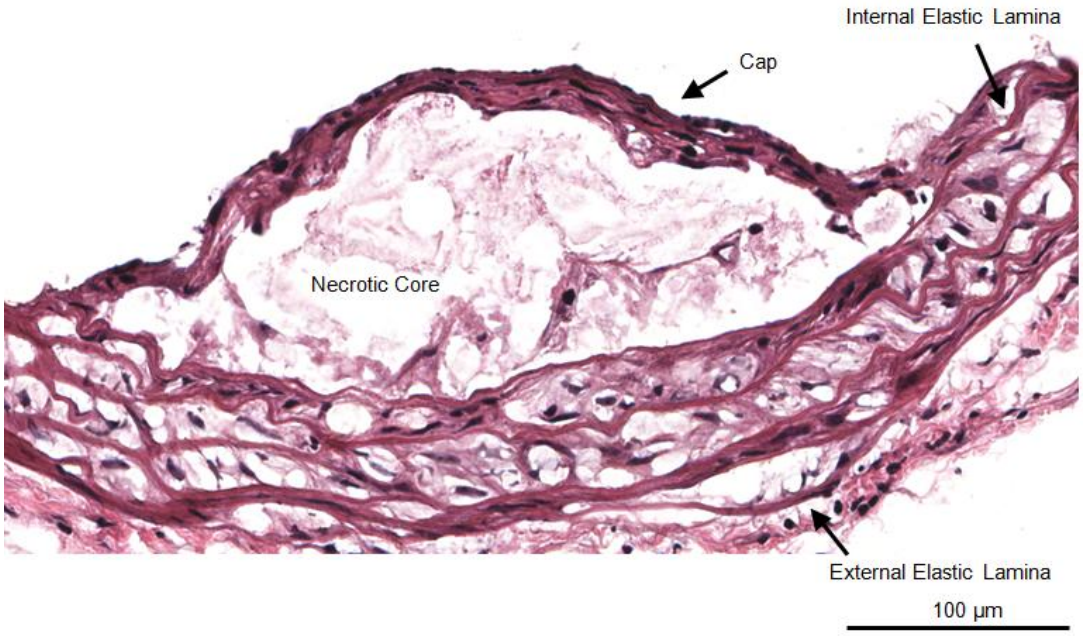

Figure 11: A Hematoxylin and Eosin (H&E) Stained Cross-section of an Frozen Atherosclerotic Plaque in the Brachiocephalic Trunk (BCT) of an ApoE KO Mice Fed an 8 Weeks Western-type Diet (WD).

Table 3: Morphometry of Atheromatous Plaques Developed in the BCT of ApoE KO Mice Fed an 8 Weeks Western-type Diet.

2D Cross-sectional Parameters	WD (N=6)
Cap-plaque thickness ratio (%)	37 ± 21
Necrotic core / Plaque size (%)	22.7 ± 10.2
Plaque size × 10^3 (μm^2)	42.3 ± 24.9

The cross-section of BCT containing maximal plaque size was stained by H&E and quantified by Image-Pro Plus. The data are shown as mean ± standard deviation.

3.3.2 LPS-induced Lung Inflammation and Systemic Inflammation

Direct instillation of LPS into the lungs of atherogenic mice resulted in neutrophilic lung inflammation [Figure 12], and systemic inflammation characterized by elevated proinflammatory cytokines [Figure 13].

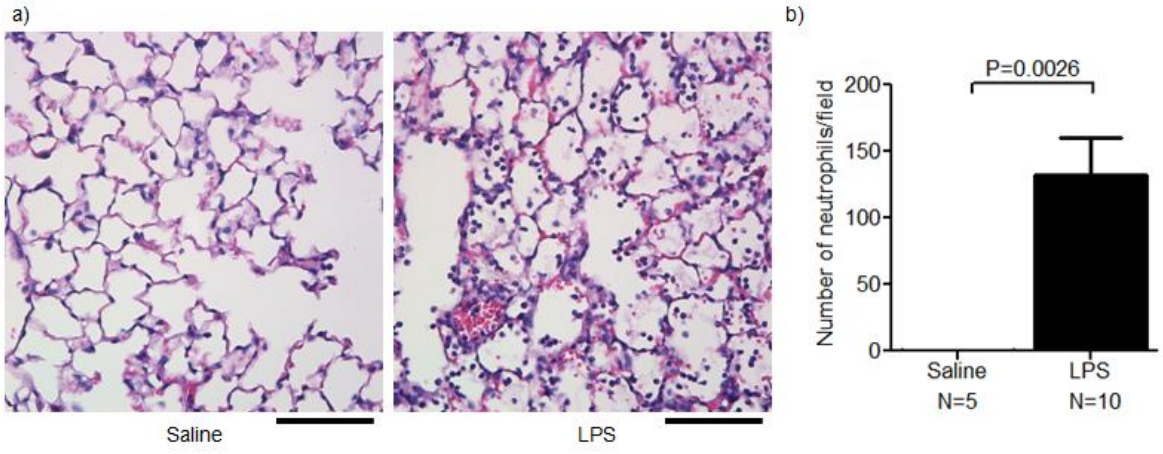

Figure 12: Intratracheal LPS Exposure Induced Neutrophilic Lung Inflammation.

a) H&E stained mouse left lung images 24 hours after intratracheal exposure to 50 µl sterile saline (left) and 100µg LPS dissolved in 50 µl sterile saline (right). There were increased numbers of neutrophils, disrupted epithelial cells, blood congestion, and edema in the parenchyma of mouse lungs exposed to LPS; b) Quantitation of neutrophils in bronchoalveolar lavage (BAL) fluid from saline and LPS exposed mice at 24 hours were shown. Error bars represent standard error of the mean. Cells in the BAL were gently mixed and cytospun down to a glass slide and fixed with methanol before staining with H&E stain. neutrophils were morphologically identified by evaluating size, shape, and

presence of granules and multinucleation. Monocytes and alveolar macrophages were also determined by morphology.

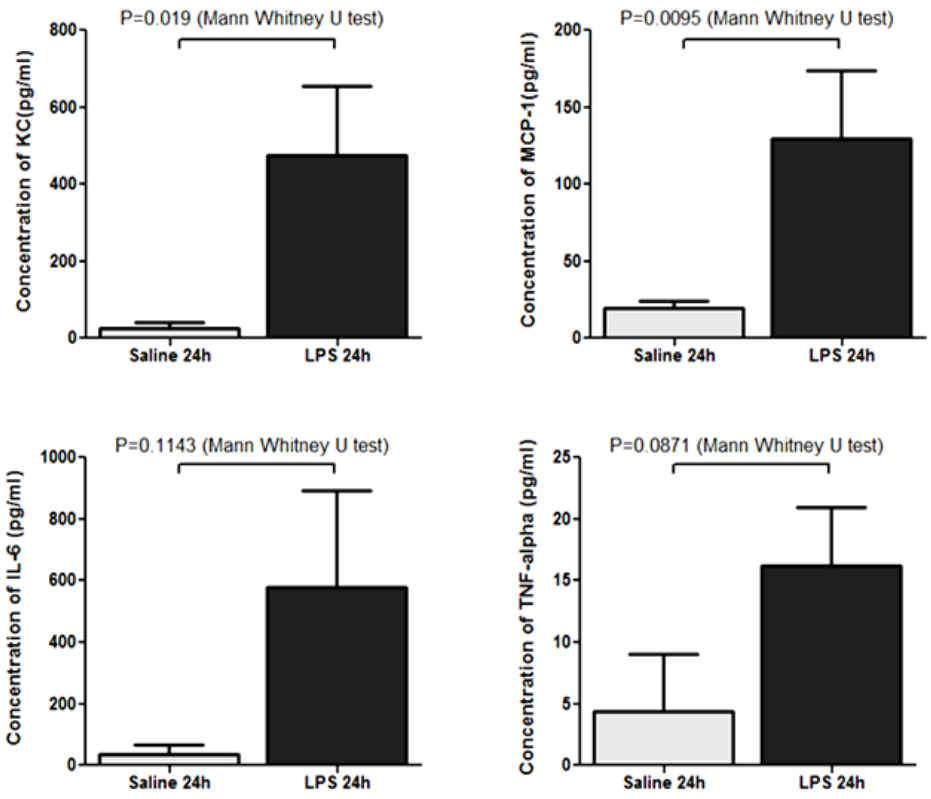

Figure 13: The Level of Inflammatory Cytokines in Serum.

Evaluation of systemic inflammation characterized by proinflammatory cytokines: a) Keratinocyte chemoattractant (KC), b) monocyte chemotactic protein-1 (MCP-1), c) interleukin-6 (IL-6), and d) tumor necrosis factor alpha (TNF-α) in the mouse plasma 24 hours after intratracheal exposure to saline (N=4) or LPS (N=4); error bars represent the standard errors.

3.3.3 LPS Dosage and Timeline Study

Mice exposed to intratracheal LPS at dosage of 50 µg and 100 µg had superimposed high rates of atheroma destabilization at 4 hours and 24 hours, by 24 hours they were significantly different

from that of saline exposed mice. The 24 hour time point was therefore chosen as the primary time point for investigation of plaque vulnerability. Some histology is shown in following figures.

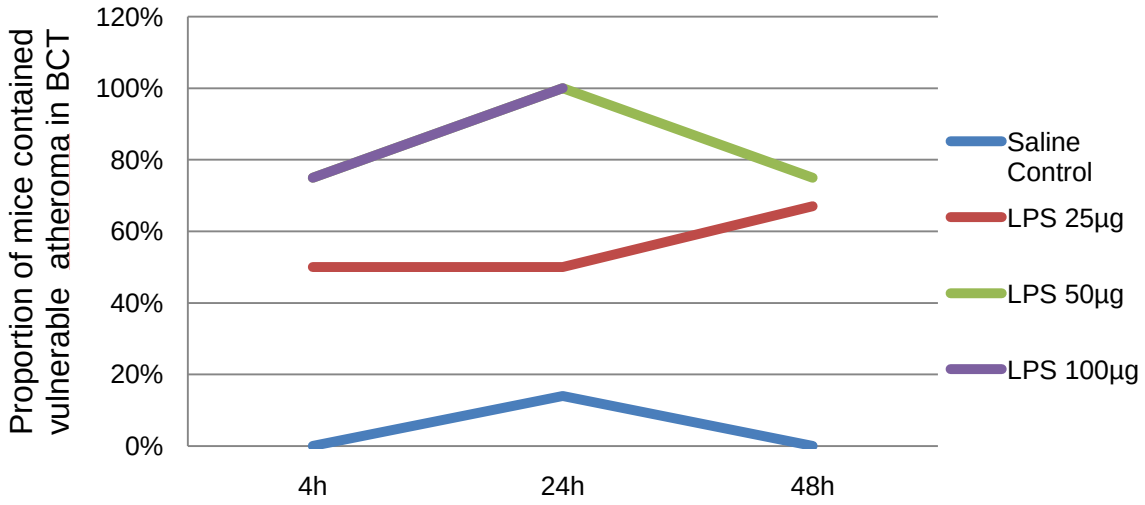

Figure 14: LPS Dosage and Timeline Pilot Study.

ApoE$^{-/-}$Mice were sacrificed at 4, 24, 48 hours post intratracheal LPS (25µg, 50µg, 100µg) administration (N=4 each). Saline-instilled mice that were sacrificed at these same time points were pooled as controls. The 48 hour post-LPS (100 ug) time point experiment was terminated prematurely because mice experienced sudden deaths and paralysis. Plaque instability was defined based on histological evidences of intraplaque hemorrhage and thrombus formation. Mice exposed to intratracheal LPS at dosage of 50 µg and 100 µg demonstrated similar rates of atheroma destabilization at 4 hours and 24 hours (overlap). 24 hours post-LPS administration was chosen as the primary time point for investigation because LPS 24 hours versus Saline 24 hours demonstrated significant change in plaque vulnerability (Fisher exact test $P<0.005$).

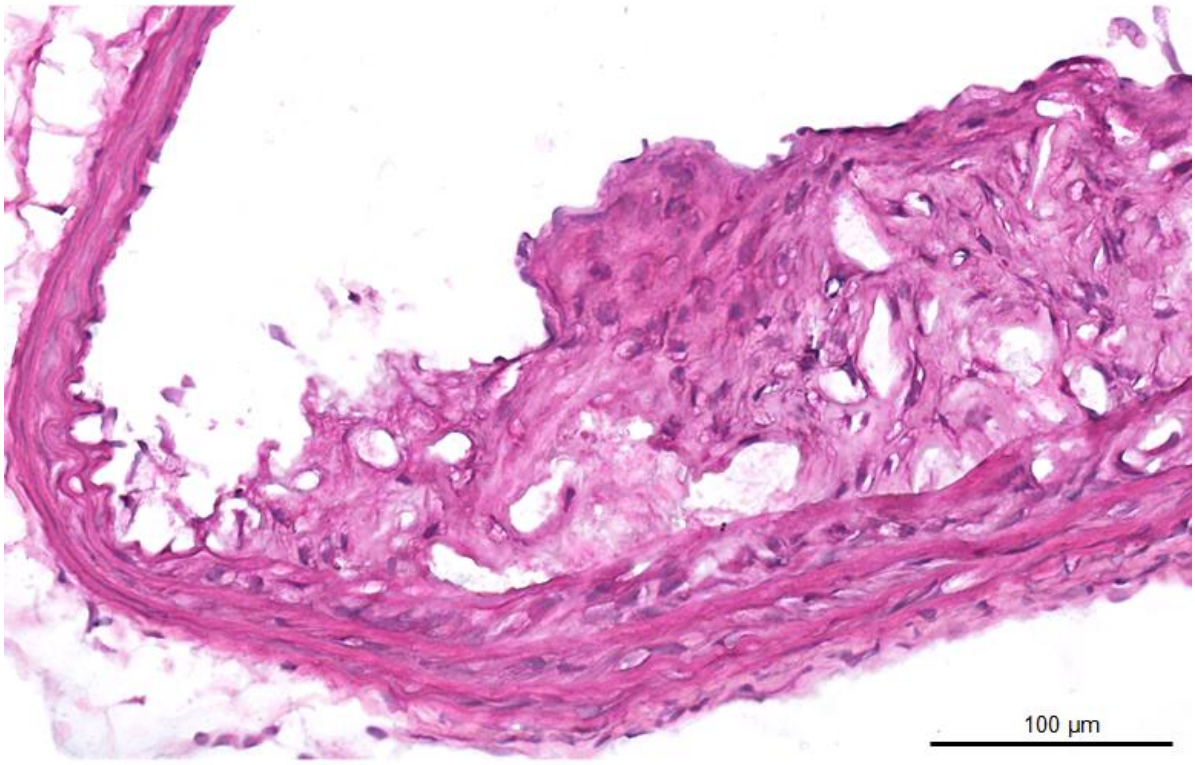

Figure 15: H&E Stained Frozen Cross-section of Saline-Exposed Mouse at 4 Hours Time-point.

No Sign of hemorrhage or thrombosis observed. Little tissue disruption at the plaque shoulders, but no inflammatory cell infiltration observed. The disruption may be caused by cross-sectioning.

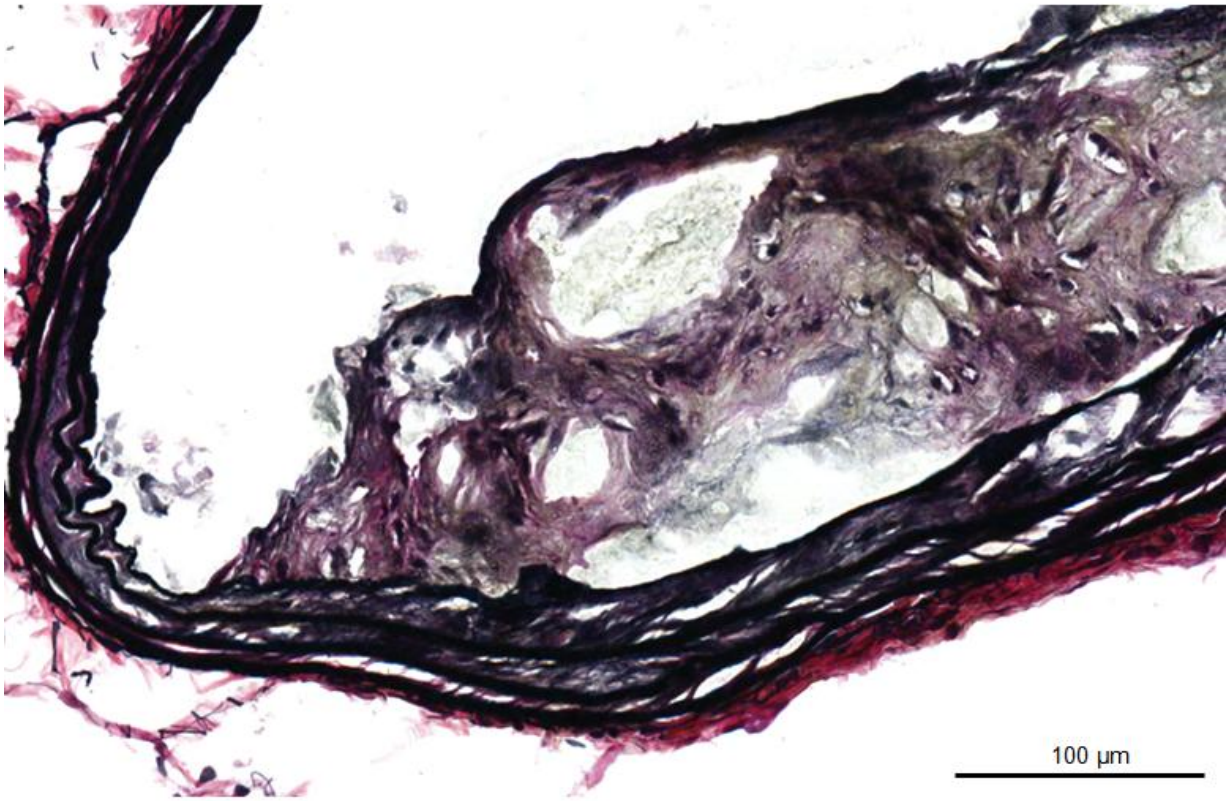

Figure 16: Movat's Stained Frozen Cross-section of Saline-Exposed Mouse at 24 Hours Time-point.

The Cap structure overlaying necrotic core is intact. No Sign of hemorrhage or thrombosis observed. Little tissue disruption at the plaque shoulders, but no inflammatory cell infiltration observed. The disruption may be caused by cross-sectioning.

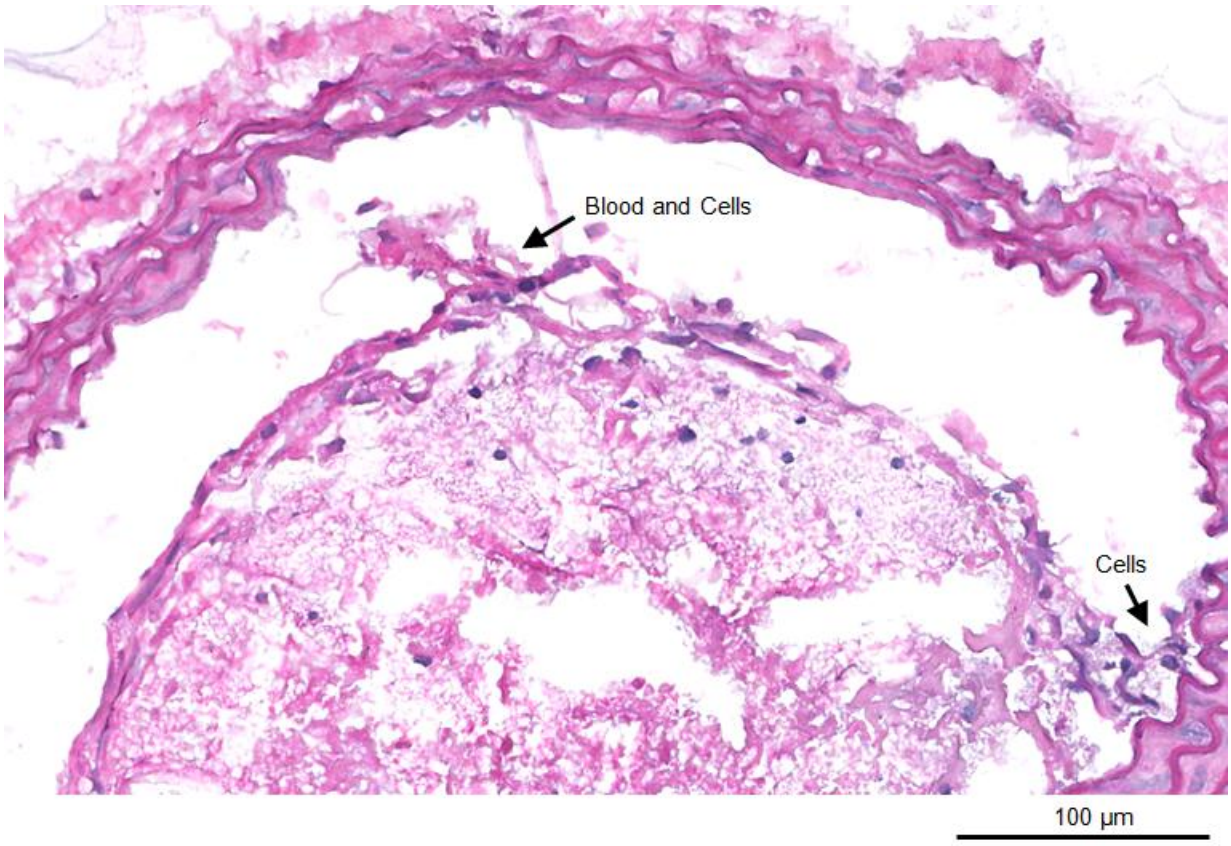

Figure 17: H&E Stained Frozen Cross-section of LPS-Exposed Mouse at 4 Hours Time-point.

The surface of plaque is mixed with cells and platelets. Little tissue disruption at the plaque shoulders with many inflammatory cells observed.

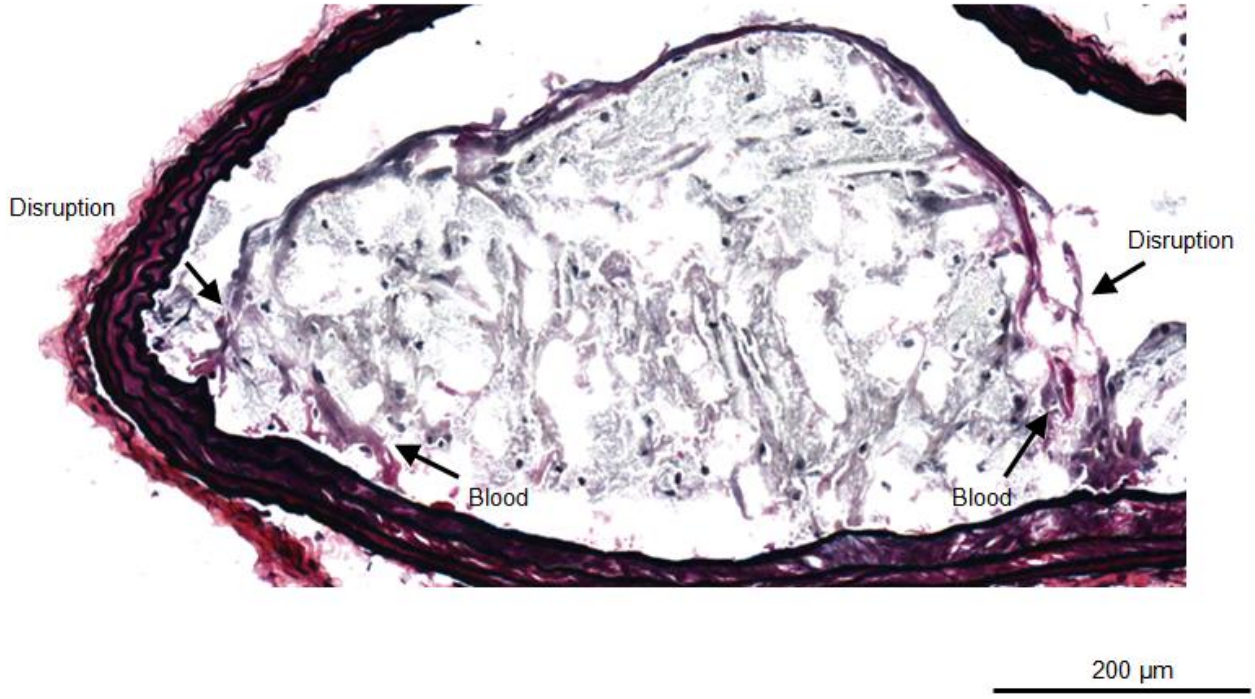

Figure 18: A Movat's Stained Frozen Cross-section of LPS-Exposed Mouse at 4 Hours Time-point.

Blood and platelets were localized at the shoulder regions of the plaque where the elastin layer of the cap is disrupted.

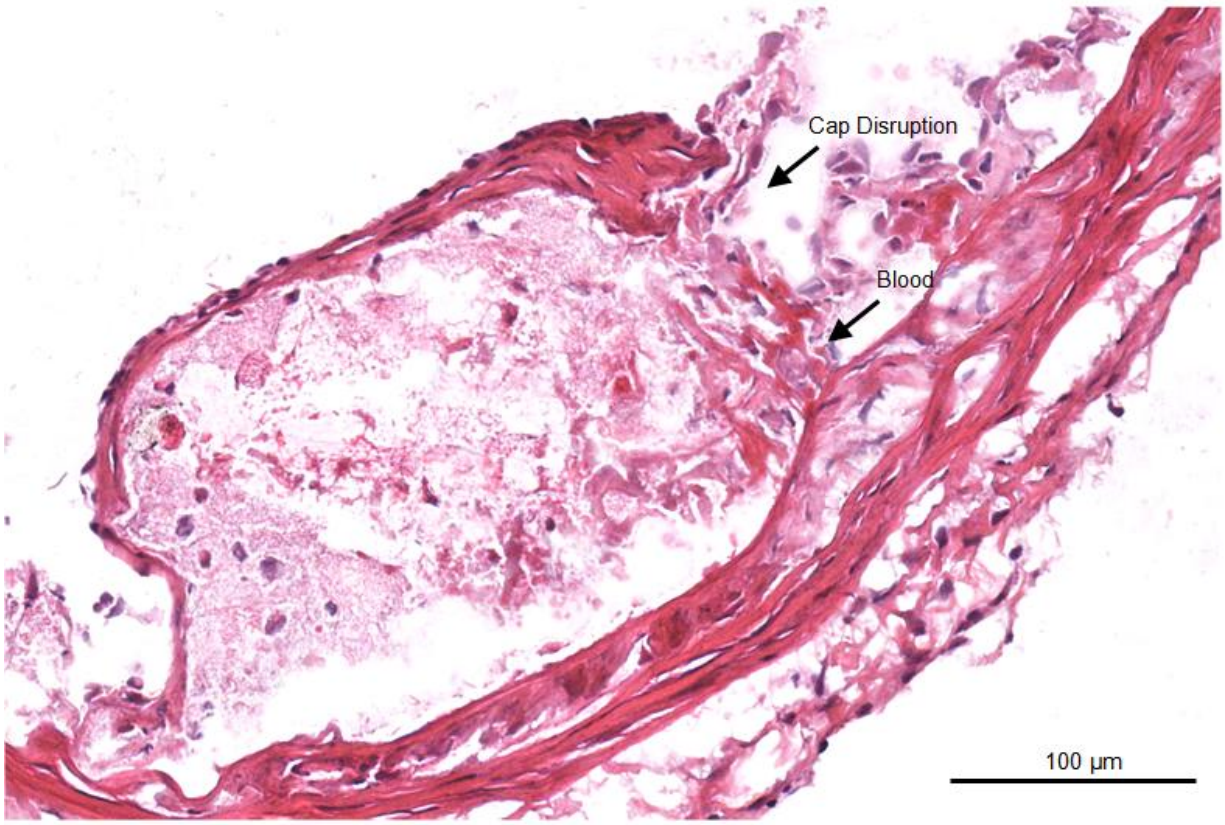

Figure 19: A H&E Stained Frozen Cross-section of LPS-Exposed Mouse at 24 Hours Time-point.

Blood and platelets were observed at the shoulder regions of the plaque where cap structure is disrupted. Inflammatory cells infiltrated at the site of breakage.

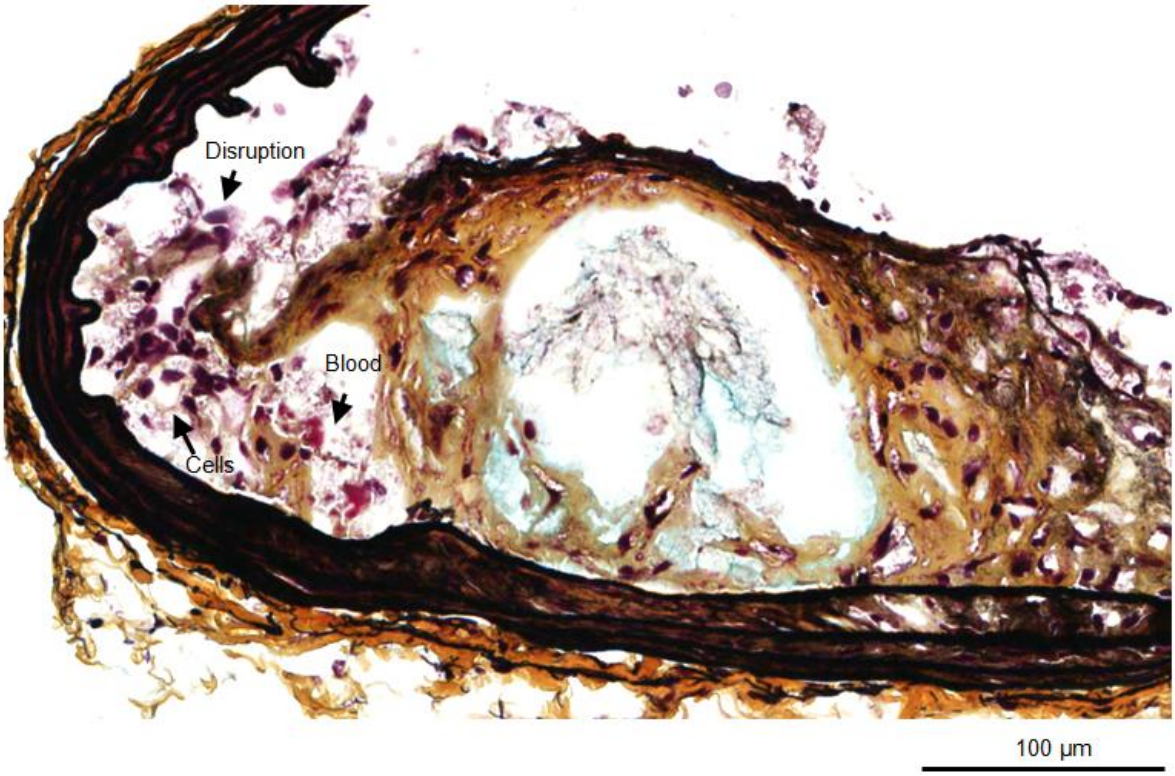

Figure 20: A Movat's Stained Frozen Cross-section of LPS-Exposed Mouse at 24 Hours Time-point.

Blood and platelets were observed at the shoulder regions of the plaque where the elastin and collagen structure of the cap is disrupted. Inflammatory cells and platelet were presented at the breakage of the plaque.

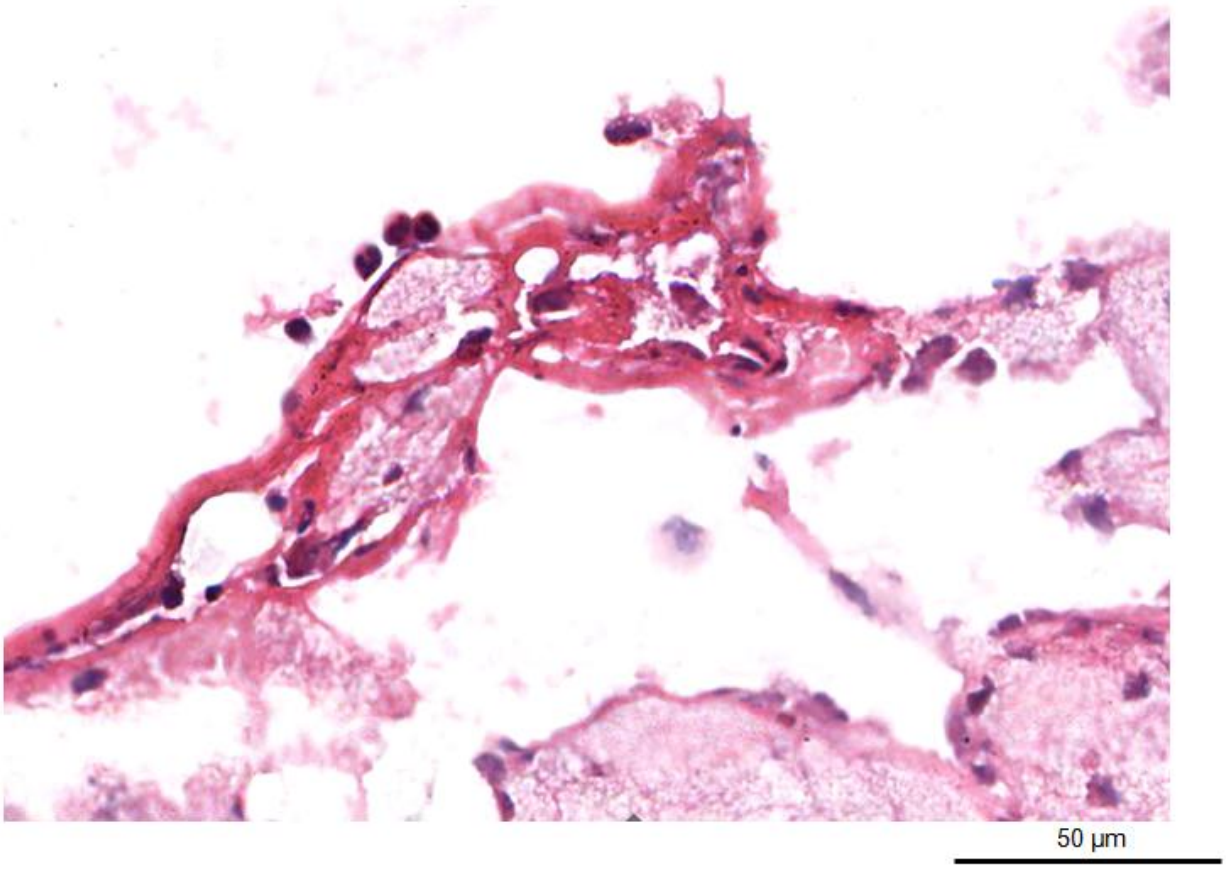

Figure 21: A H&E Stained Frozen Cross-section of LPS-Exposed Mouse at 24 Hours Time-point.

Blood and platelets were observed at the shoulder regions of the plaque where the plaque is disrupted. Inflammatory cells and platelet were mixed with the plaque tissue.

3.3.4 Thrombus and Intraplaque Hemorrhage Detected by OPT in LPS-exposed Mice

As shown in Figure 22, the high-resolution OPT revealed the presence of thrombus in 2 of 3 LPS-exposed mice (Video 1 in Appendix), but none in the 3 saline-exposed mice (Video 2 in Appendix). Thrombi were located mostly on the edges of the plaque and extended into the aortic arch (Video 3 in Appendix). We also detected hemorrhage inside the plaques and the absence of

luminal thrombi in 1/3 of LPS-exposed mice (Video 4 in Appendix), but none of these phenotypes were observed in saline-treated mice (0/3 mice).

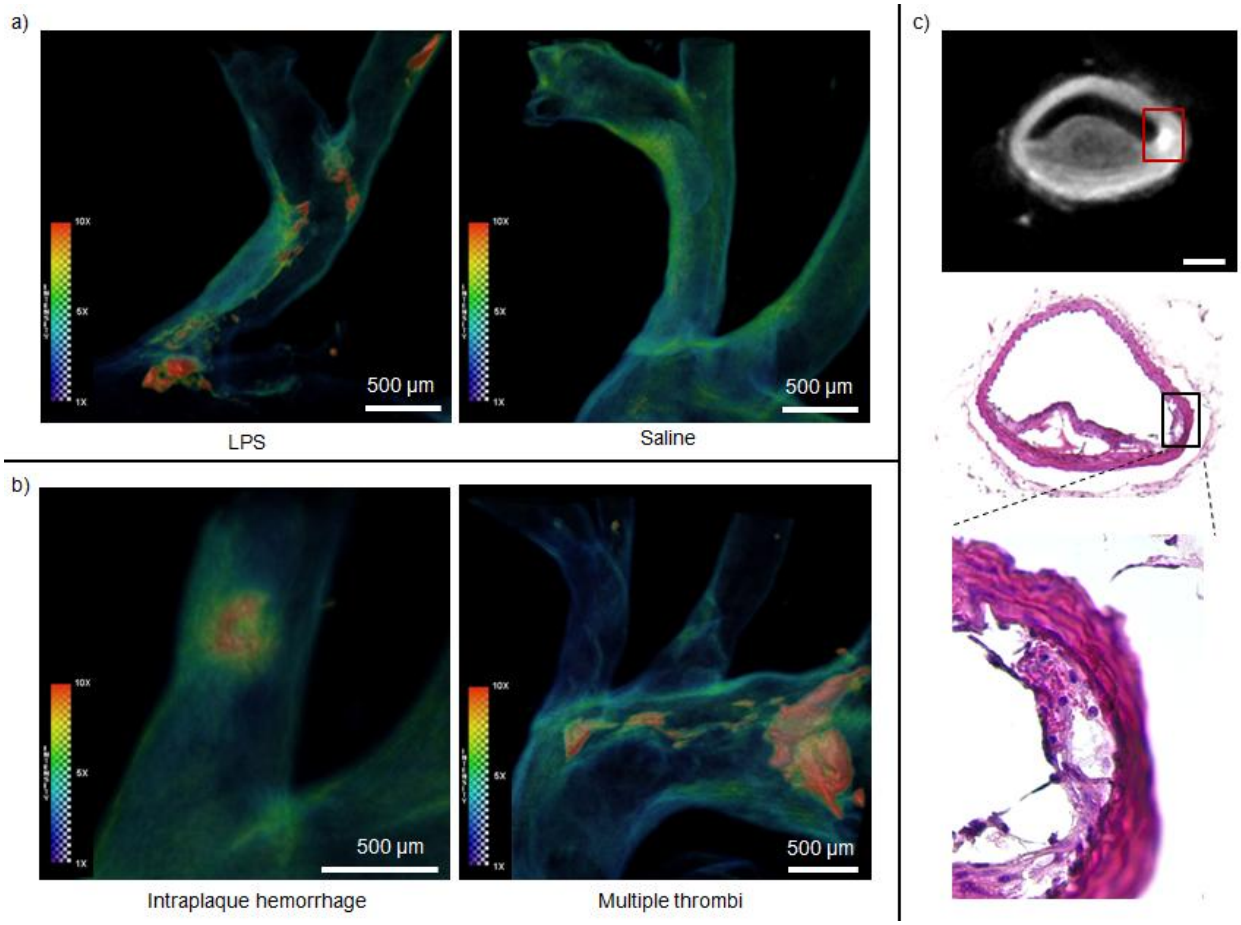

Figure 22: Optical Projection Tomography (OPT) Fluorescence Intensity Maps and Histology of Brachiocephalic Trunk (BCT).

a) Left: An intensity map of BCT from a LPS-exposed mouse. Blood and thrombus (red) were determined by their auto-fluorescence intensity (10 times higher than the vessel wall base intensity). Thrombi were frequently localized at the edges of the vulnerable plaque in LPS-exposed mice; Right: An Intensity map from a saline-exposed mouse. No/rare thrombus or intraplaque hemorrhage was observed in the plaques of saline-exposed mice; b) Intensity maps from other LPS-exposed mice, showing intraplaque hemorrhage (auto-fluorescent 10 times higher than the vessel wall) (left) and multiple thrombi were observed along the aortic arch (right). The three-dimensional demonstration

and navigation of these BCTs are shown in Video 1, 2, 3, 4 in Appendix respectively; c) A two-dimensional (cross-sectional) reconstruction of OPT (upper) from a LPS-exposed mouse; blood and hemorrhage was observed at the atheroma edge by their high auto-fluorescent signal and confirmed with histology (middle and lower).

3.3.5 Quantitation and Characterization of Plaque Vulnerability

We quantitated vulnerable plaques using serial histological cross sections of BCT. This revealed that 17 out of the 25 (68%) LPS-exposed mice harbored vulnerable plaques, which contained histological features of intraplaque hemorrhage or thrombus [Figure 23]. Eight (32%) LPS-exposed mice demonstrated luminal blood clot or thrombus, which were mostly located at the edges of the plaque. Nine (36%) LPS-exposed mice displayed hemorrhage inside the atheroma. Plaque complications are summarized in [Figure 24]. In contrast, only 2 out of the 17 (12%) saline-exposed control mice demonstrated intraplaque hemorrhage and none of these animals harbored plaques that contained thrombus (p=0.0004 comparing LPS vs. saline group) [Figure 23].

The morphometrical data of atheroma are shown in Table 4. The mean cap thickness (relative to plaque thickness) in the LPS-exposed mice was approximately 1/3 of that in the saline-exposed mice (13±10% vs 39±26%, p=0.0004). The size of the necrotic core in LPS-exposed mice was two times of that in the saline-exposed mice (36.9±12.9% vs. 18.6±11.8%, p=0.0004). However, the overall plaque size of the LPS-exposed mice (101±41 ×103 μm^2) was not significantly different than that of the saline-exposed mice (78±34 ×103 μm^2, p=0.102).

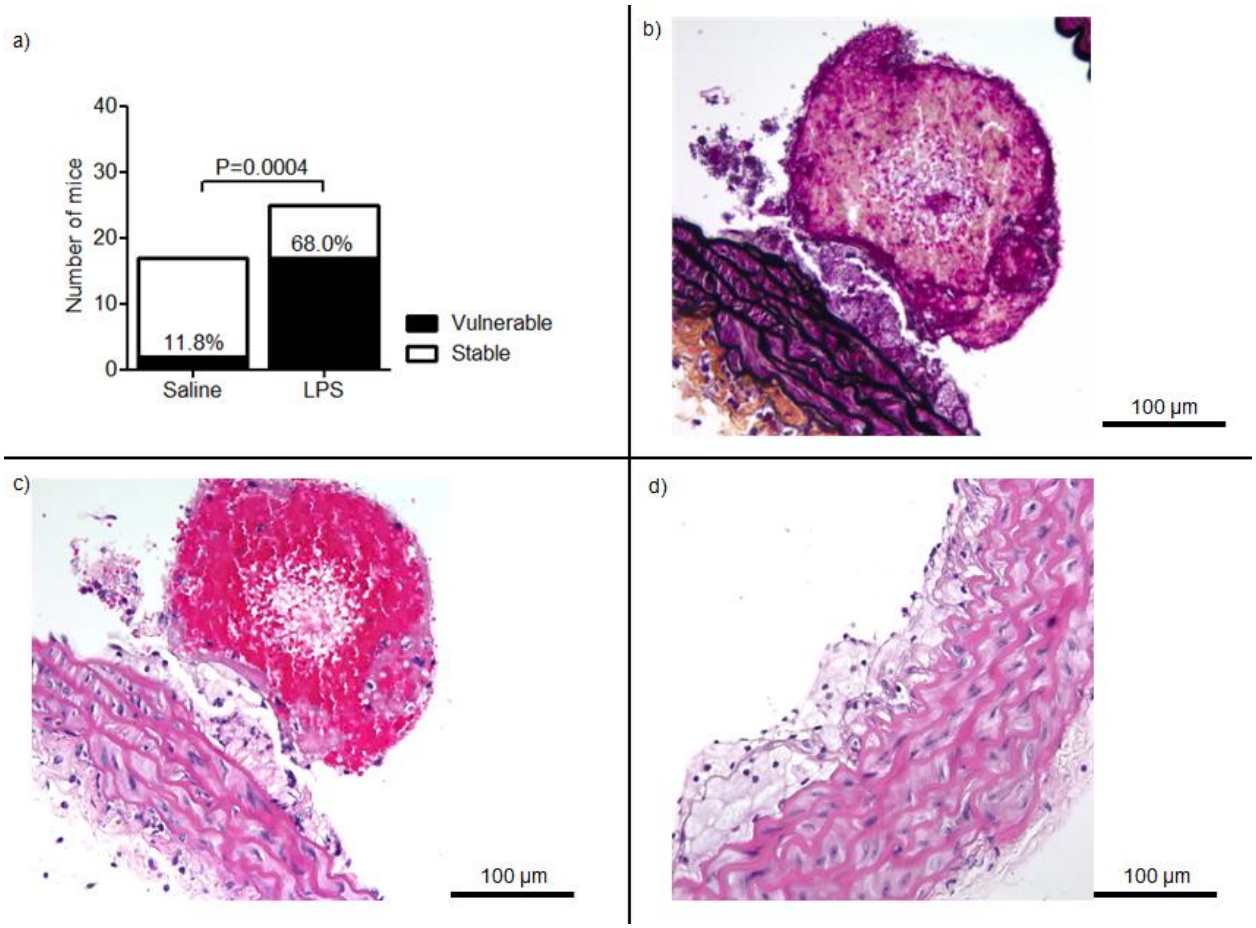

Figure 23: Plaque Vulnerability in LPS-exposed Mice versus Saline-exposed Mice.

a) Quantitation of vulnerable plaques in mice: A vulnerable plaque was defined by intraplaque hemorrhage or luminal thrombus in at least two continuous cross-sections (50 µm intervals) stained with H&E and Movat's pentachrome. b) A representative BCT cross-sectional image stained by Movat's pentachrome from a LPS-exposed mouse. A thrombus was present in the lumen of BCT at edge region of plaque, and loss of endothelium was observed at adjacent edge of atheroma. c) The representative H&E stained cross-sectional image of BCT from the same LPS-exposed mouse. Fibrin deposition around thrombus was observed. Loss of endothelium at the edges of plaque was observed. d) A representative H&E cross-section of an atheroma edge from a saline-exposed animal. Endothelium integrity was preserved; No thrombus detected in all saline-exposed animals. The presence of the vulnerability signals in a given plaque was determined by 2 independent investigators in a blinded manner. The final decision was made by the third independent investigators when a conflict occurred between them.

Table 4: Morphometry of Atheroma Using the Frozen Cross-Sections of BCT that Contained the Maximal Plaque Size.

Cross-sectional Parameter	Saline (N=14)	LPS (N=16)	P value
Cap-Plaque Thickness ratio (%)	39 ± 26	13 ± 10*	<0.001
Cap thickness (μm)	70 ± 67	29 ± 15*	0.003
Necrotic core / Plaque (%)	18.6 ± 11.8	36.9 ± 12.9†	<0.001
Plaque size $\times 10^3$ (μm^2)	78 ± 34	101 ± 41†‡	0.102

The data are shown as mean ± standard deviation.

* Distribution was not normal and Mann-Whitney U test was performed

† Distribution was normal and unpaired student T test was performed

‡ The comparisons across the groups were done with the parameter normalized by perimeter of EEL.

Lipopolysaccharide: LPS; brachiocephalic trunk: BCT; external elastic lamina: EEL.

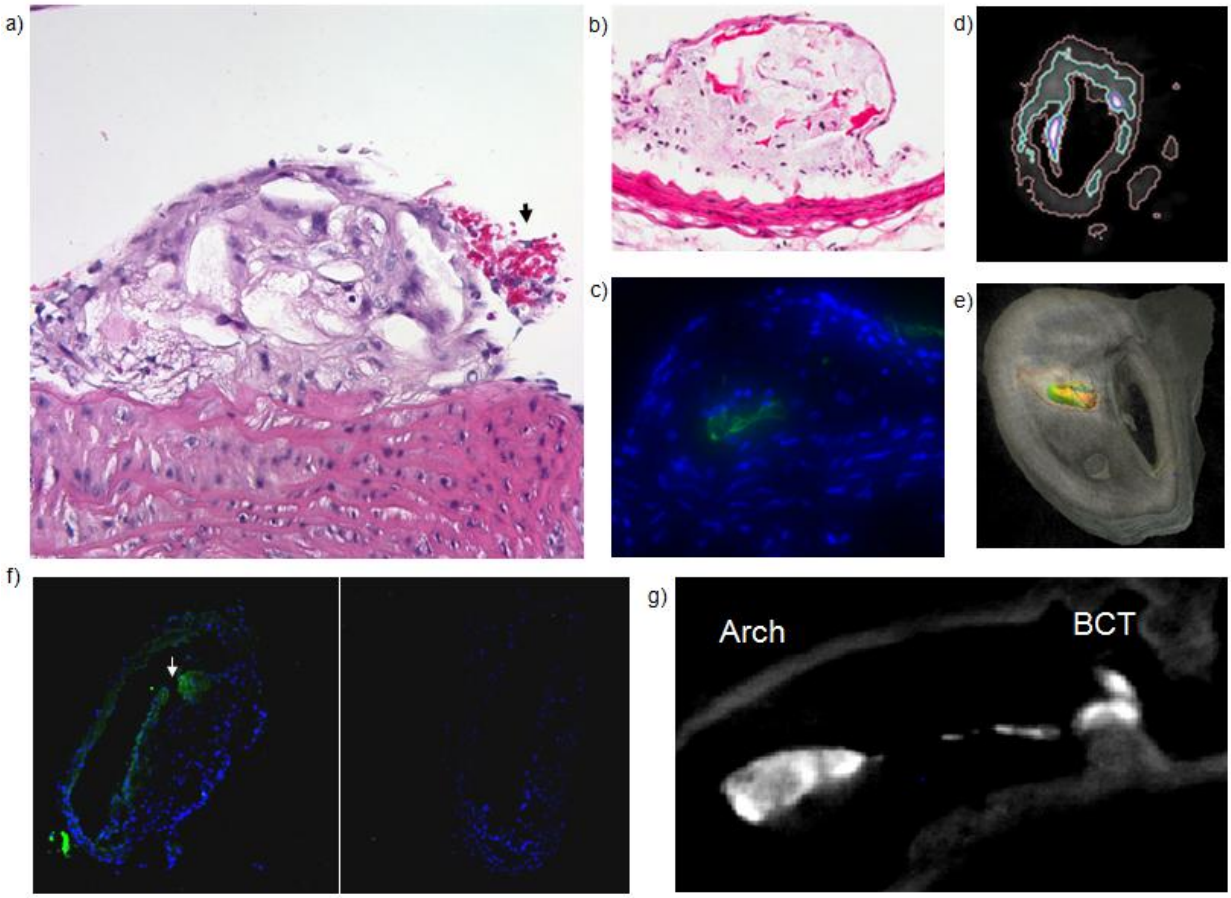

Figure 24: Acute Plaque Complications Following LPS Lung Exposure.

a) The edge region of plaque in LPS-exposed mice displayed blood attached on the surface of plaque and mixed with plaque tissue (H&E). Loss of endothelium integrity was observed at the edge of plaque. b) The necrotic core region in the plaque of LPS treated mice showed intraplaque hemorrhage. c) Immunofluorescent staining of thrombin (green) in the plaque is shown. d) Both intraplaque hemorrhage and luminal thrombus were detected in the BCT of LPS-exposed mice by OPT (high relative intensity signals are demarcated by a blue line, vessel wall is demarked by a pink line, and the perimeter of the plaque is demarcated by a green line). e) 3-D OPT cross-sectional image of a plaque containing hemorrhage (Green: lower intensity blood signal, Yellow: medium intensity blood signal; Red: highest intensity blood signal). f) Immunfluorescent staining of MMP-9 (green) of plaque in LPS-exposed mice (left) and saline-exposed mice (right). There was MMP-9 in the sub-endothelial region and in areas where plaque had been perturbed; in contrast, there was no MMP-9 signal detected in saline treated plaque. g)

Luminal blood clots (high intensity signal) were detected on plaque shoulders of BCT and extended into aortic arch in the LPS lung exposed animal.

3.3.6 Early Stage of Plaque Destabilization at 8 Hours via Intratracheal Route of LPS but not via Intraperitoneal Route of LPS

To investigate the earlier stages of atheromatous destabilization, we examined plaques in BCT at 8 hours post-intratracheal LPS instillation using a dissection microscope and OPT. At 8 hours, there was evidence for plaque vulnerability in BCT (LPS-IT: 8/16 vs Saline-IT: 1/14, P=0.017). As shown in Figure 25, thrombus and hemorrhage were detectable in BCT. The vulnerability signals of randomly selected BCT (11 LPS-IT mice vs 10 Saline-IT mice) were quantitated. LPS-IT group demonstrated a significantly greater signal than that in the saline-IT group (P=0.04). We then investigated whether or not similar changes could be found by injecting the same LPS dose intraperitoneally. There was no significant difference in the occurrence of vulnerable plaques between intraperitoneal LPS instillation and saline controls (LPS-IP: 1/5 vs Saline-IP 0/5; p=1.0). Both LPS groups (IT and IP) demonstrated higher plasma LPS levels compared with the saline control groups. Interestingly, plasma LPS levels increased by 17,000-fold when LPS was injected intraperitoneally but the same dose given IT increased the plasma LPS levels by only 40-fold [Figure 25c]. Mice injected with intraperitoneal LPS also demonstrated higher plasma lactate dehydrogenase and urea levels compared with mice exposed to intratracheal LPS [Figure 25d]. The BAL cell count data showed that neutrophil and macrophage counts were not significantly different between the LPS-IP and Saline-IP groups; however, LPS-IT group demonstrated higher neutrophil counts [Figure 26c and d]. Circulating white blood cell counts revealed very similar patterns between IT route and IP route of LPS

exposure [Figure 27]. Together, these data suggested that IT administration of LPS induced neutrophilic lung inflammation but resulted in less systemic absorption and reduced injury to the liver and kidneys compared with intraperitoneal administration of LPS. Importantly, intratracheal LPS instillation (but not IP injection) promoted transition of stable plaques to vulnerable ones in this model.

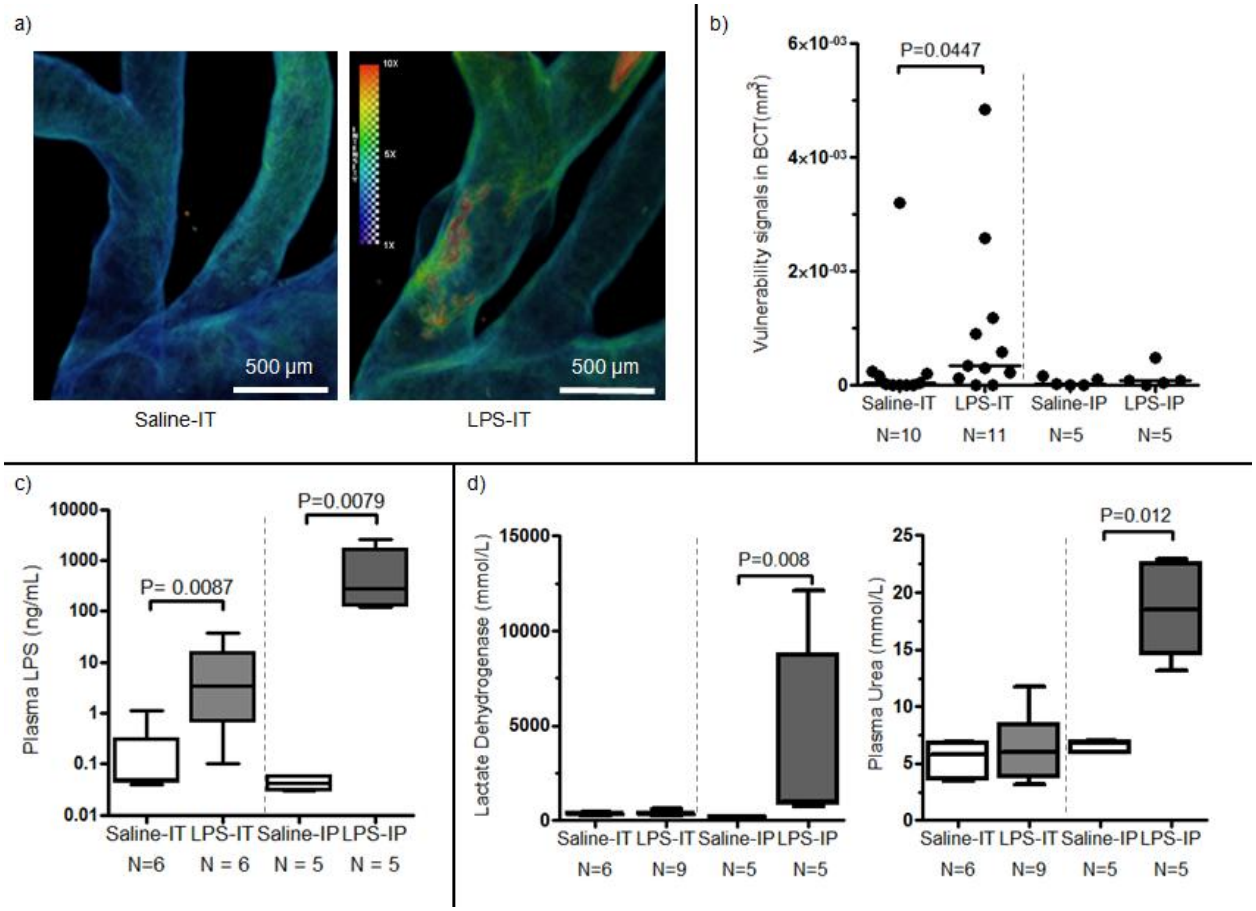

Figure 25: Early Stages of Plaque Destabilization, LPS Translocation and Tissue Damage via Different Routes of LPS Exposure.

a) The representative OPT intensity map of BCT from an intratracheal saline control mouse (Saline-IT, left) and a LPS-exposed mouse (LPS-IT, right). Vulnerability signals are shown in red. b) Quantitation of vulnerability signals in the BCT. The median signal intensity (in volume) of LPS-IT group was higher than that of Saline-IT group

(P=0.04). Over 45% of intratracheal LPS-exposed mice demonstrated signs of destabilization, but these signs only occurred in 10% of intratracheal saline controls; the median signal intensity of the intraperitoneal LPS-exposed mice (LPS-IP) was no different from that of the intraperitoneal saline control (Saline-IP) group. There was no increase in plaque vulnerability between the LPS-IP and Saline-IP groups. Bars represent the medians. c) Plasma LPS level in LPS-IT group was slightly (less than 40-fold) higher than that in Saline-IT group. Plasma LPS level in the LPS-IP group were markedly higher (17000-fold) than that in Saline-IP group. d) Lactate dehydrogenase (LD) in the plasma after different routes of saline or LPS exposure (left). Elevation of Plasma LD was observed in LPS-IP group when compared to Saline-IP group. Plasma LD is commonly used as an indicator for systemic tissue damage (muscles, liver, heart, etc); Urea level in the plasma after different route of LPS and saline exposures (right). Plasma urea is a common marker of kidney damage. It was elevated in LPS-IP group, but not LPS-IT group.

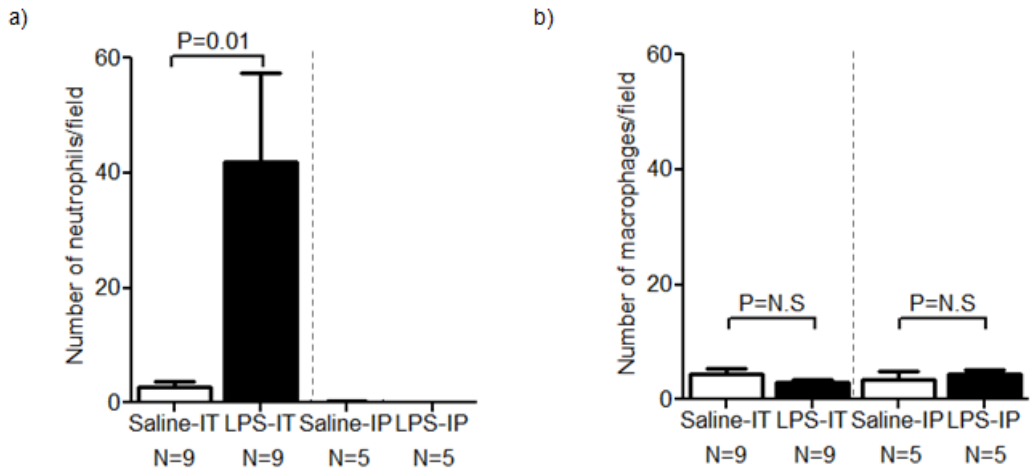

Figure 26: Comparisons of White Blood Cell Counts in BAL between IT (Intratracheal) Route and IP (Intraperitoneal) Route at the 8 Hour Time Point.

a) LPS exposure via IT route induced neutrophil lung inflammation, but not LPS exposure via IP route. b) There were no significant changes in the macrophage counts between these groups. Eosinophil and basophil counts were consistently rare (less than 1% of the total cell counts); thus, they were not included in these data. Error bars represent standard error.

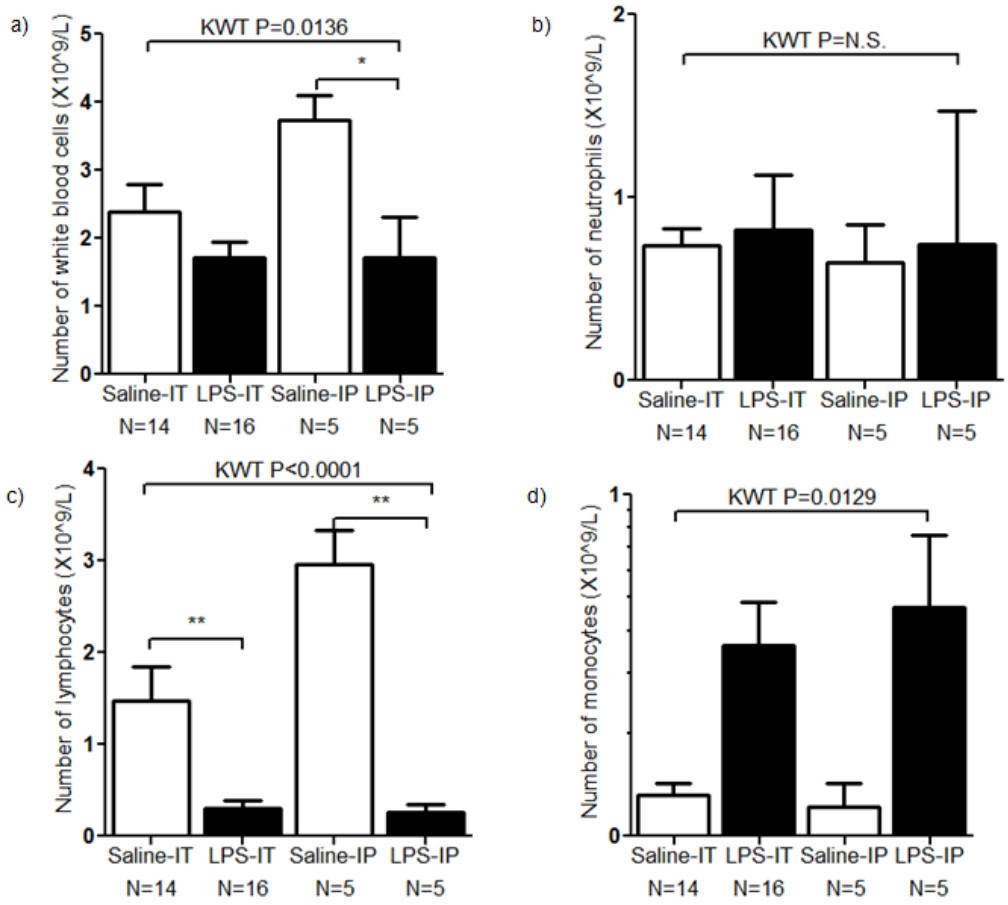

Figure 27: Circulating White Blood Cell Counts from IT (Intratracheal) and IP (Intraperitoneal) Groups.

a) Total white blood cells, b) neutrophils, c) lymphocytes, and d) monocytes in mouse blood 8 hours after saline and LPS administration demonstrated a similar pattern change. Eosinophil and basophil counts were consistently rare (less than 1% of the total cell counts); thus, they were not included in these data. Error bars represent the mean ± SE.

3.4 Discussion

The most important finding of this study is that we found that a single intratracheal administration of LPS caused the stable atheromatous plaques in mice to become vulnerable within 24 hours of exposure. By 8 hours post-instillation, plaques demonstrated features of vulnerability including hemorrhage and thrombus formation, which could be detected and

quantified by optical projection tomography. However, administration of the same dose of LPS intraperitoneally failed to induce these acute changes, despite causing greater rises in serum LPS levels and more end-organ damage in liver and kidneys. These findings highlight the importance of lung inflammation and injury in the pathogenesis of acute plaque rupture. As 100% of total cardiac output flow through the lungs, the inflammatory condition of the lung could intensify and modulate the downstream blood vessels.

The comparison of lung and systemic inflammation after IT and IP LPS administration in C57Bl6 wild-type mice has been documented in the literature (158). It has been shown that 6 hours after LPS IT and IP administration is an optimal time point for comparison. In that case, LPS IT induced neutrophilic lung inflammation while LPS IP did not. We collected BCTs at 8 hours for examining changes in the following the optimal time point. The signal of plaque destabilization, if happened, would not diminish in this short period of time. Therefore, if the plaque indeed ruptured earlier, the signal should be still detectable using OPT. At 8 hours, we found that IP injection of saline or LPS did not induce neutrophilic lung inflammation, nor macrophage counts. However, instillation of LPS IT caused significant neutrophilic lung inflammation, while macrophage counts did not change. The pattern of WBC counts and differentials were not different between IT, and IP administration of LPS when compared to their saline controls. Under this differential lung inflammatory condition dominated by neutrophils, the signal of plaque complication in the IP group is very low (even if 4x the sample size N=20 was used, we would not be able to find significance), but the signal of plaque complication in LPS-IT groups is significantly higher compared to the saline-IT group.

Our study has several strengths. It is widely believed that one of the very early plaque changes leading to acute CV events is the transition of stable plaques to vulnerable ones, characterized by hemorrhage followed by rupture and then thrombosis. However, the mechanism(s) by which this sequence of events occurs are largely unknown. A major barrier to mechanistic studies and therapeutic discoveries in this field has been the lack of a simple animal model of plaque rupture. To address this critical gap, previous studies have used a variety of interventional approaches using surgery (for example by creating tandem stenosis to arteries (159)) or drugs (e.g. angiotensin II infusions directly into plaque containing arteries (75) or prolonged feeding with a high-fat diet (57, 160). In this experiment, dissimilar to previous studies, which focused on chronic factors, we exploited the strong epidemiological association between lung injury and acute cardiovascular events and demonstrated that a single dose of intratracheal (but not intraperitoneal) LPS can consistently cause stable plaques to become vulnerable and induce acute plaque rupture in the BCT of ApoE KO mice fed a short-term WD. Furthermore, dissimilar to previous studies, which solely relied on histology to demonstrate plaque rupture, we used OPT, a novel ex vivo micro-imaging tool that does not require tissue sectioning and thus preserves the architecture of the vessel. This technique enables high-resolution, three-dimensional imaging of organs/tissues (154, 155). It can also be combined with whole-mount immuno-fluorescent staining technology for studying distribution of specific molecules in organs and tissues. By combining this new technique with our histological findings, we provide convincing evidence that acute lung injury induces plaque destablization. This novel model can now be used to determine mechanistic pathways and most importantly test novel compounds to prevent acute plaque rupture related to acute lung inflammation.

Epidemiological studies have shown that lung infections and inflammation could transiently increase the risk of MI, ACS, and strokes [Table 2]. We have used LPS as a convenient trigger to induce lung injury and inflammation, simulating an acute lung infection with gram negative bacteria. Future studies should explore more common human pathogens, such as respiratory viruses or bacteria that would enhance the application and generalizability of this model to clinical conditions. However, the trade-off could be a more complicated model of lung inflammation and host responses that may be difficult to fully characterize. Interestingly, LPS administered intraperitoneally did not induce plaque rupture, suggesting that the systemic inflammatory response induced by lung injury may be unique with regard to its downstream effect on blood vessels. This concept needs further evaluation.

In this model we showed that neutrophils migration into the lungs from circulation pool. The inflammatory cytokine and chemokines, such as KC (equivalent to IL-8) and MCP-1 are elevated in circulation. Whether and how these circulating neutrophils contribute to the LPS-induced acute destabilization and rupture of plaques is not known. The cellular mediators and downstream molecules that were directly responsible for plaque rupture need to be determined in the future study. Based on some preliminary experiments, we speculate that neutrophils upon LPS instillation into the lung could be an important contributor in this process. Neutrophil related myeloperoxidase and metalloproteinases could also be important downstream molecular factors in this process. Additional studies are needed to determine the exact molecular pathways that lead to acute plaque destabilization and rupture. It should also be noted that we did not identify the exact mediators responsible for the activation and recruitment of neutrophils into the lungs following LPS lung exposure. Whether or not neutrophils and MPO are acutely localized

on the plaques and contribute to plaque vulnerability is not addressed here. Further work will be needed to unravel the molecular underpinnings of this process.

3.5 Conclusion

Notwithstanding these limitations, this study has established a new mouse model in which lung exposure to LPS leads to lung inflammation and causes acute plaque destabilization; furthermore, we showed that OPT can be used to determine plaque vulnerability. This animal model, and the OPT imaging technique, could be a useful tool to interrogate possible therapeutic targets aimed to prevent acute plaque destabilization and thereby reduce cardiovascular morbidity and mortality related to lung inflammation.

Chapter 4: Neutrophils Contribute to Plaque Vulnerability Induced by LPS Lung Exposure

4.1 Introduction

The role of neutrophils in atherosclerotic plaque vulnerability and rupture is largely under-recognized. Historically, investigations of the inflammatory processes during plaque destabilization and thrombotic occlusion were mostly centered on intraplaque macrophages and T lymphocytes. Although neutrophils are widely recognized as important mediators of inflammation and vascular injury, little is known regarding their role in acute plaque destabilization. Since the last decade, there has been accumulating evidence suggesting a link between neutrophilic inflammation and acute cardiovascular diseases. Previous studies have shown that neutrophils are activated systemically during an acute coronary event and causing widespread neutrophilic inflammation across all coronary vasculatures independent of the location of the vulnerable plaques (133). Pathological studies have shown that there are increased neutrophils in the disease-causing plaques from patients who have died following AMI, specifically at the site of plaque rupture and erosion (139, 140). The neutrophil numbers in the plaques were also found to be strongly associated with the histopathologic features of plaque vulnerability (161). Upon neutrophil activation and degranulation, myeloperoxidase (MPO), a heme enzyme within the azurophilic granules of neutrophils, is released into the plasma and vasculature. Thus, Plasma MPO is now considered a biomarker of coronary heart disease (CHD) and acute coronary syndromes (ACS) (145-147, 162, 163). In animal models, neutrophils are also known as important contributors to atherogenesis (164, 165). However, the role of

neutrophils in acute plaque rupture has not yet been determined due to the lack of well-established animal model of plaque rupture.

In a previous study, we established an acute plaque rupture model related to lung inflammation by instilling lipopolysaccharide, LPS, into the lungs of ApoE KO mice fed a short-term Western-type diet (WD). In this study, we investigated the role of circulating neutrophils in the process of plaque rupture using this model.

4.2 Methods

4.2.1 Animals

Male apolipoprotein E-null mice ($ApoE^{-/-}$) on a C57BL/6J background (Jackson Laboratory, Bar Harbor, ME; Stock number: 002052) were fed a Western-type diet (WD) containing 21% fat from lard and 0.15% cholesterol (TD88137, Harlan Laboratories Inc., Madison, USA) for 8 weeks to induce atheromatous plaque formation in their brachiocephalic trunk (BCT).

4.2.2 LPS-induced Plaque Vulnerability

For intratracheal LPS instillation, a single dose of 100 µg LPS (Escherichia coli O111:B4; 3mg/kg) (L2630, Sigma-Aldrich, St. Louis, MO), dissolved in 50 µl of sterile saline, was sprayed as aerosol particles (16-22 µm in mass median diameter) directly into the lungs through the vocal cords using a microsprayer (MSA-250-M, Penn-Century Inc., Wyndmoor, PA).

4.2.3 Neutrophil Depletion (ND) *in vivo* with Antibody Injections

To determine the role of neutrophils in plaque rupture in this model, the LPS-exposed mice were injected twice intraperitoneally with either 1) rat anti-mouse Ly6G clone 1A8 antibodies (BE0075-1, Bio X cell, New Hampshire, USA) (LPS-ND group, N=15) to deplete circulating neutrophils, or 2) rat IgG2A isotype clone 2A3 antibodies (BE0089, Bio X cell, New Hampshire, USA) as controls (LPS-Ctrl, N=14). The first dose was given 24 hours prior to the LPS challenge and the other dose was given immediately after the LPS challenge [Figure 28]. Each dose (400µg) was diluted in 400µl sterile phosphate buffered saline (PBS) (166). In order to investigate if injections of antibodies on their own induce plaque vulnerability, we included additional comparator groups (without LPS exposure) including: 1) mice injected intraperitoneally with non-specific control IgG antibodies as controls (Ctrl; N=4) and 2) mice injected intraperitoneally with specific anti-Ly6G antibodies, as the neutrophil-specific antibody control group (ND; N=5).

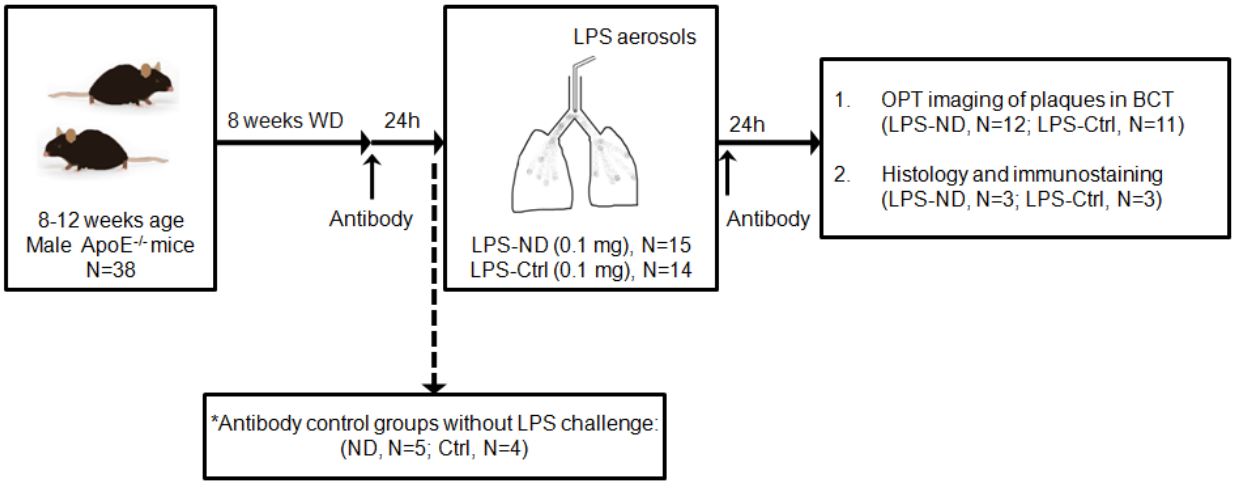

Figure 28: Scheme Diagram of Neutrophil Depletion in LPS-exposed Mice by Antibody Injections.

29 LPS-exposed mice were injected twice intraperitoneally with either 1) rat anti-mouse Ly6G clone 1A8 antibodies (LPS-ND group, N=15) to deplete circulating neutrophils, or 2) rat IgG2A isotype clone 2A3 antibodies as controls (LPS-Ctrl, N=14). The first dose was given 24 hours prior to the LPS challenge and the other dose was given immediately after the LPS challenge. Each dose (400µg) was diluted in 400µl sterile phosphate buffered saline (PBS). Additional comtrol groups (without LPS exposure) including: 1) mice injected intraperitoneally with non-specific control IgG antibodies as controls (Ctrl; N=4) and 2) mice injected intraperitoneally with specific anti-Ly6G antibodies, as the neutrophil-specific antibody control group (ND; N=5).

4.2.4 Organ and Tissue Procurement and Bronchoalveolar Lavage (BAL)

Under anesthesia (isoflurane 5% inhalation), blood was collected from the inferior vena cava using a 25 gauge catheter needle (ProtectIV® Plus Safety I.V. Catheter, Smiths Medical International Ltd. Rossendale, Lancashire, UK)) 24 hours after LPS challenge for white blood cell count measurements. Immediate procurement of the heart and blood vessels was performed after blood collection. The heart, aortic arch and branching arteries containing the BCT were carefully harvested and perfused with 3ml of phosphate buffered saline (PBS) injected directly into the left ventricle at an infusion rate of 1 ml/minute (Harvard Apparatus, Massachusetts, USA). Bronchoalveolar lavage (BAL) fluid was collected as previously described [Section 3.2.4]

4.2.5 Optical Projection Tomography (OPT)

To visualize the plaques ex vivo without disturbing the plaques, optical projection tomography, OPT, (Bioptonics 3001M, MRC Technology, London, UK) was used, which enabled three-dimensional imaging of the entire aortic arch and the BCT of mice (154, 155). The plaques were assessed in a blinded manner and plaques were considered vulnerable if there was a visible

thrombus or evidence for intraplaque hemorrhage (with a size greater than 0.0005 mm^3). Thrombus and erythrocytes produce a distinct autofluorescence signal that was 10-fold higher in intensity than the arterial wall, which enabled volume quantification by threshold segmentation. Plaque vulnerability signals were detected at wavelength of 425 nm and were segmented and quantified three dimensionally (in volume) using Amira V6.0 visualization software.

4.2.6 Definition of Vulnerable Plaque

To correlate the findings of OPT images with histology, the serial cross sections of the entire BCT, which had been embedded in optimal cutting temperature compound and frozen in liquid nitrogen, were stained with H&E and Movat's pentachrome and examined under the microscope (156).Vulnerable plaque was defined by the presence of a thrombus or intraplaque hemorrhage. Intraplaque hemorrhage was noted when there were erythrocytes inside the atheroma on at least two contiguous sections spaced 50 µm apart.

4.2.7 Myeloperoxidase (Peripheral Neutrophil Marker) and CD68 Co-staining:

The frozen BCT cross-sections were fixed in 10% formalin for 10 min and then rinsed in running water for 2 min. The sections were incubated with 10% chicken serum (Gene Tex Inc., USA) and donkey serum (Sigma-Aldrich, USA) for 30 min and then incubated with the mouse MPO affinity purified polyclonal goat IgG antibody (5µg/ml; R&D, USA) and the mouse macrophage/smooth muscle CD68 monoclonal rabbit IgG antibody (2.5µg/ml; Abcam, Toronto, ON, Canada) for 2 hours at 4°C. After 4 incubations in PBS for 5 min, the BCT sections were incubated with secondary antibodies: donkey anti-goat 488 (400X dilution; Invitrogen, USA) and chicken anti-rabbit 594 (400X dilution; Invitrogen, USA) for another 2 hours at room

temperature. After 4 washes in PBS for 5 min, the cross-sections were air dried for 30 min and mounted using the Vectashield mounting medium with DAPI (Vector Lab Inc, USA). Immunofluorescent images of the 3 serial sections containing the largest plaque areas were captured under a fixed computerized setting using a Nikon immunofluorescence light microscope Eclipse TE300 (Nikon, Japan) at 100X, 200X and 600X magnification. The MPO signals in the given plaques were quantified by color segmentation in the original unit of pixels. The value of %MPO was calculated by dividing the MPO signal by the plaque size using Image-Pro Plus software. The values for the 3 serial cross sections with the largest plaque size were averaged to represent the center plaque region, and values for the 3 serial sections with the smallest plaque size were averaged to represent the shoulder region. The arithmetic mean was used for statistical analysis. Normal rabbit and goat IgG were used for negative controls. The frozen lungs of LPS-treated mice were used for positive controls.

4.3 Results

4.3.1 Neutrophil Depletion and Characterization of Plaque Vulnerability

We characterized the vulnerable plaques in the BCT of LPS-ND and LPS-Ctrl groups using both histology and OPT [Figure 29]. Altogether, 10 out of the 14 (71.4%) LPS-Ctrl mice harbored vulnerable plaques, which contained vulnerability signal of intraplaque hemorrhage or thrombus. In contrast, only 4 out of the 15 (26.7%) LPS-ND mice harbored vulnerable plaques ($p=0.0268$) [Figure 31a]. Further plaque characterizations are shown in Figure 30a and b. 5 out of the 14 (35.7%) LPS-Ctrl mice demonstrated luminal blood clot or thrombus [Figure 29a]. Similar to previous findings, these complications were mostly located at the edges of the plaque [Figure 30c]. There were 8 out of the 14 (57.1%) LPS-Ctrl mice displayed hemorrhage inside the

atheroma [Figure 30b]. In contrast, only 2 out of the 15 (13.3%) LPS-ND mice demonstrated intraplaque hemorrhage (P=0.0209) and only 2 (13.3%) of these animals harbored plaques that contained blood clots. The representative BCT images from LPS-Ctrl and LPS-ND mice are demonstrated in Video 5 in Appendix A; the representative plaque histology is demonstrated in Figure 31b. LPS-exposed mice treated with neutrophil-specific antibodies had reduced plaque vulnerability detected by OPT (LPS-ND vs. LPS-Ctrl; P=0.0042, Figure 31c). Without LPS challenge, the injections of non-specific control IgG antibodies and neutrophil-specific antibodies did not induce plaque vulnerability or change the plaque phenotype (0/4 and 0/5 plaque ruptured respectively; [Figure 30d]). Immunofluorescent staining of MPO showed that MPO+ polymorphonuclear cells were localized at the edges and in the core area of plaques in the LPS-Ctrl mice, but were markedly reduced in the plaques of LPS-ND mice [Figure 30e-g, and Figure 31d].

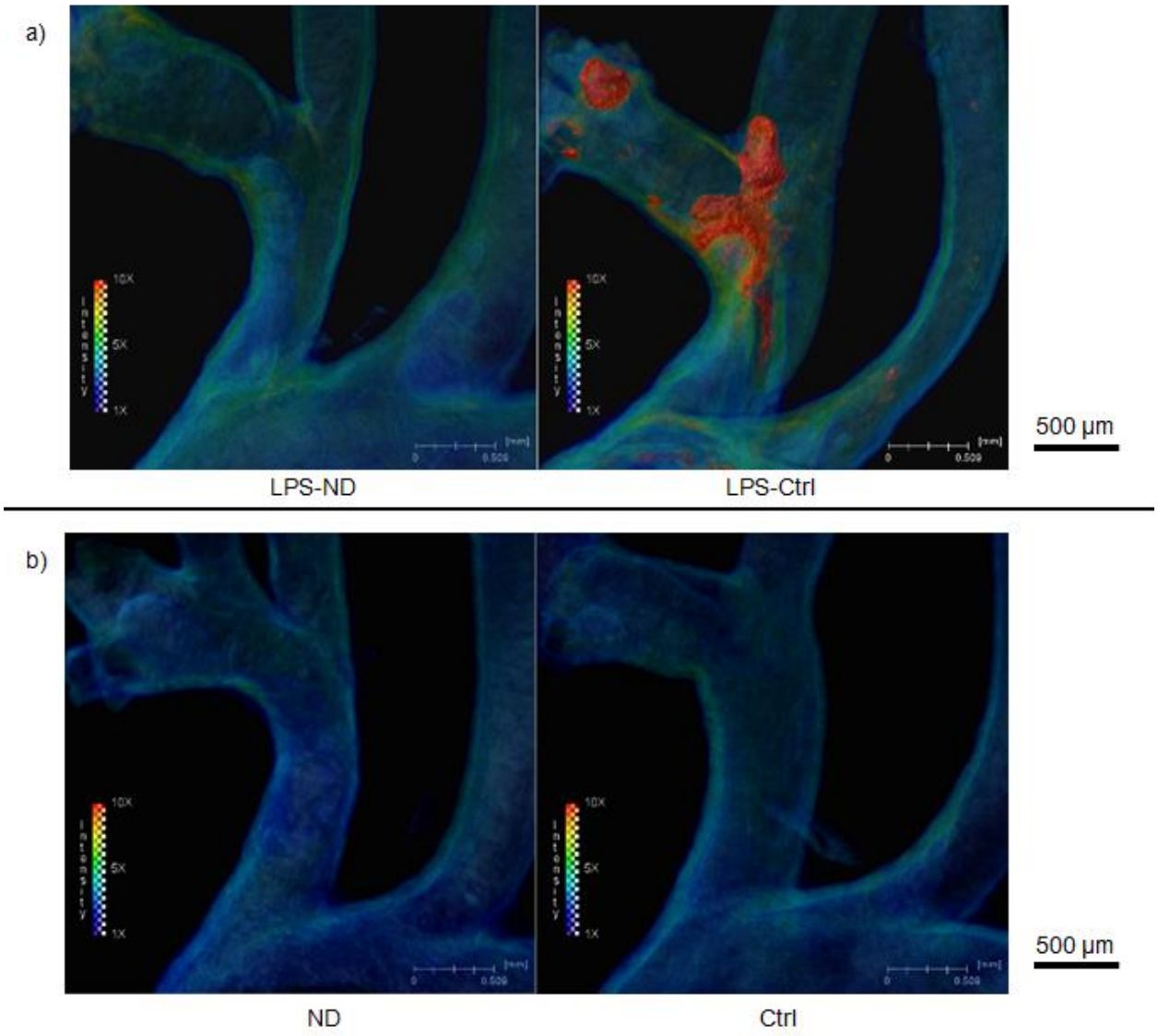

Figure 29: Optical Projection Tomography (OPT) Fluorescence Intensity Maps of Brachiocephalic Trunk (BCT).

a) Left: An intensity map of BCT from a LPS-exposed mouse treated with neutrophil-specific antibodies (LPS-ND). Right: An intensity map of BCT from a LPS-exposed mouse treated with control antibodies (LPS-Ctrl). Blood and thrombus (red) were determined by their auto-fluorescence intensity (10 times higher than the vessel wall base intensity). Thrombi were frequently localized at the edges of the vulnerable plaque in LPS-Ctrl mice; No or rare thrombus or intraplaque hemorrhage was observed in the plaques of LPS-ND mice; the three-dimensional demonstration and navigation of these BCTs are shown together in Video 5. b) Intensity maps from antibody control

mice: a BCT from a mouse injected with neutrophil-specific antibodies without LPS exposure (left) and a BCT from a mouse injected with control antibodies without LPS exposure (right). No plaque vulnerability was observed in these groups.

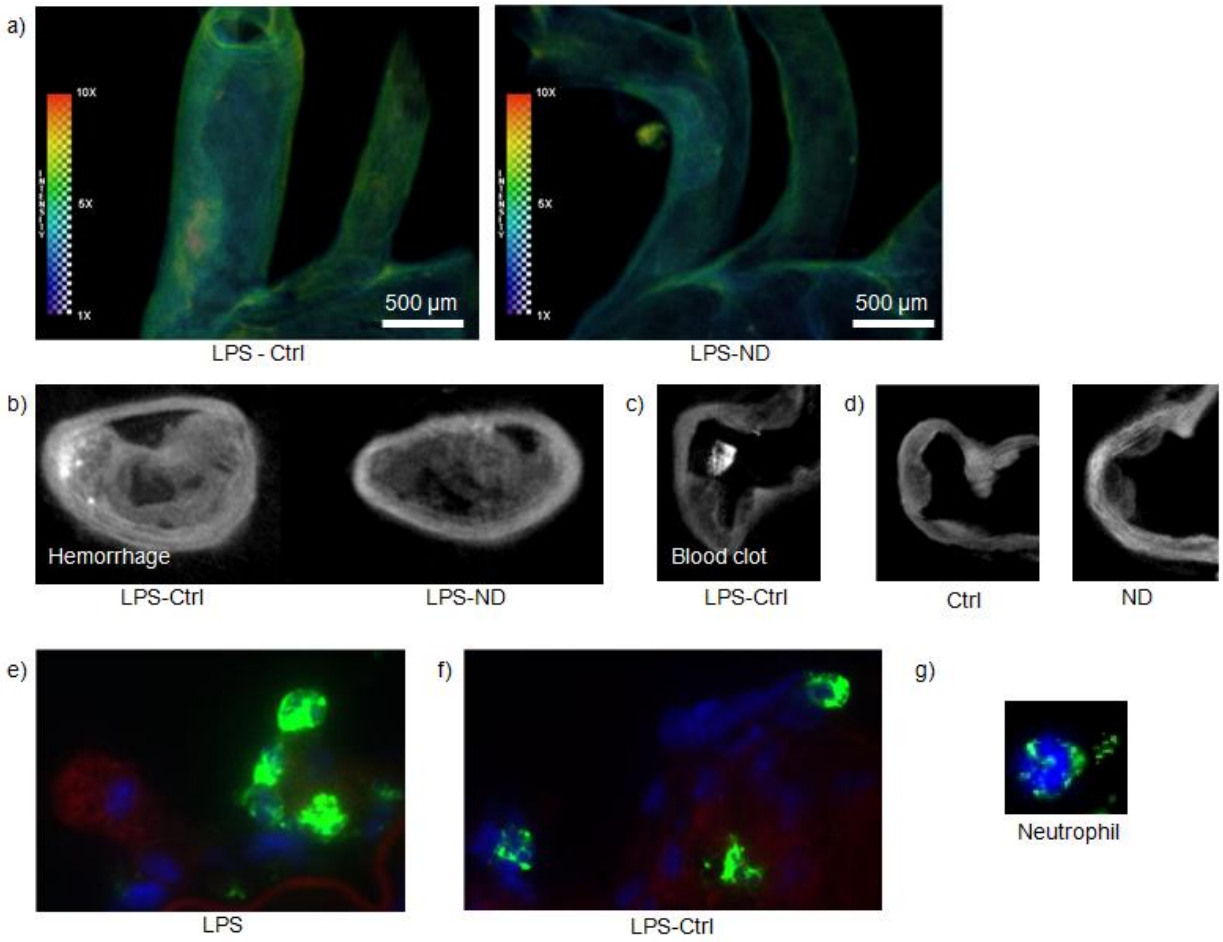

Figure 30: Depletion of Neutrophils Attenuated Plaque Vulnerability in LPS-exposed Mice.

a) A representative auto-fluorescence intensity map of mouse BCT from LPS-Ctrl group demonstrating intraplaque high intensity signal consistent with intraplaque hemorrhage (left) and that from LPS-ND group demonstrating lower signal intensity consistent with a stable plaque (right). b) A representative OPT cross-sectional image of mouse BCT from LPS-Ctrl group that shows high intensity signal at the shoulder region consistent with intraplaque hemorrhage (left) and that from LPS-ND group that shows a stable phenotype (right). c) An OPT cross-sectional image from the proximal end of BCT from a LPS-Ctrl mouse that shows a luminal blood clot at the edge of a plaque. d) OPT cross-sectional images from the proximal end of BCT of a mouse injected with control antibodies

(Ctrl, left) and of a mouse injected with neutrophil-specific antibody (ND, right). Both images show a stable plaque phenotype with no features of vulnerability. e) Immunofluorescent staining of MPO (green) and CD68 (red) in cross-sections of BCT from LPS-exposed mice that shows MPO+ polymorphonuclear cells and CD68+ macrophages localized at the edges of a plaque, and f) these MPO+ polymorphonuclear cells (green) also observed in the plaques of LPS-Ctrl mice (mouse treated with control antibodies) g) An confocal image of representative neutrophil stained with MPO (green) found in an area of plaque rupture.

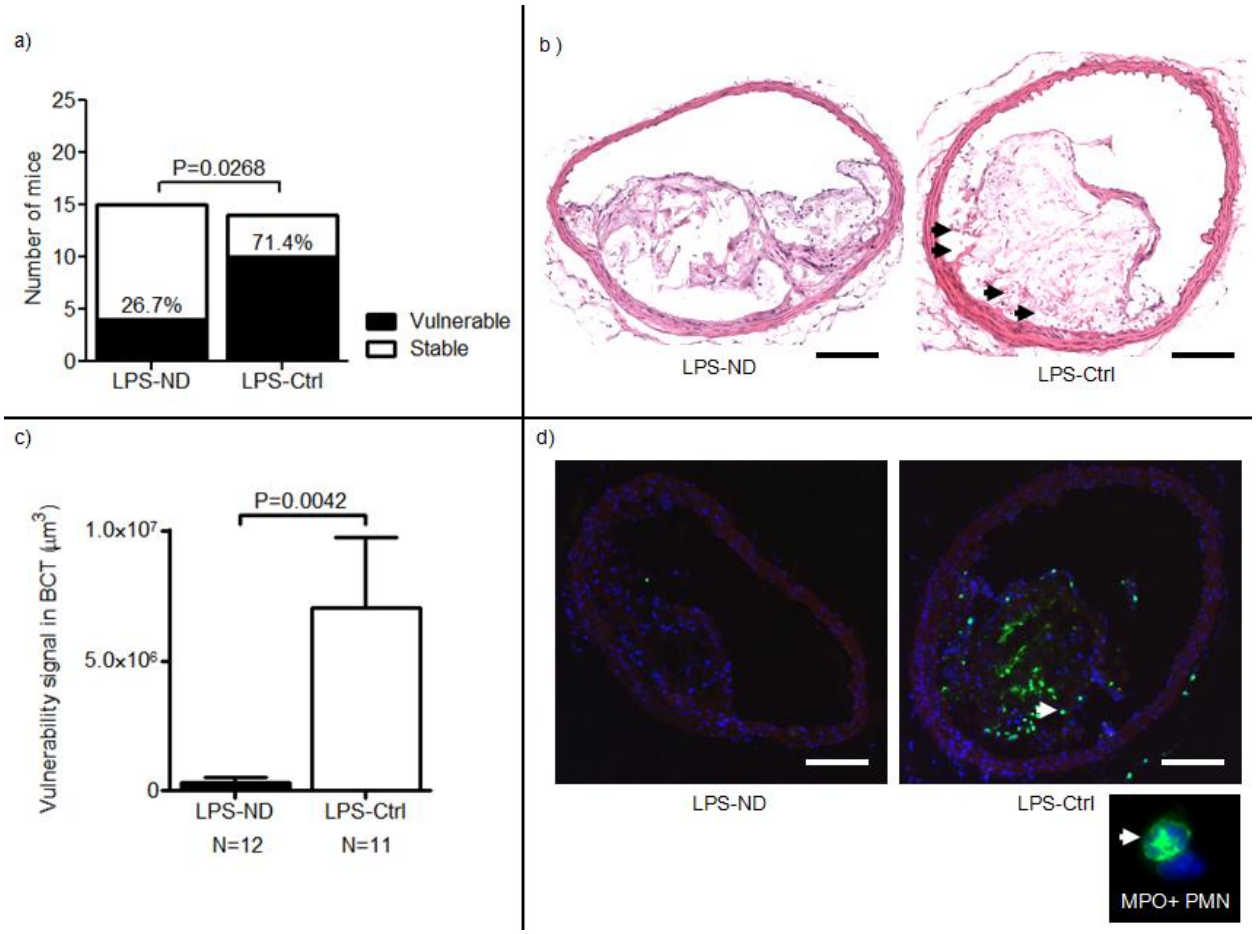

Figure 31: Quantitation of Plaque Vulnerability in LPS-ND and LPS-Ctrl Mice.

a) Quantitation of vulnerable plaque in mice: A vulnerable plaque was defined by the presence of intraplaque hemorrhage or luminal thrombus in the BCT based on histology and OPT. b) H&E stained cross-sections of BCT from LPS-ND group (left) and LPS-Ctrl (Right). Intraplaque hemorrhages (indicated by the black arrows) were

observed in the BCT of LPS-Ctrl mice. c) Quantitation of vulnerability signals in BCT detected by OPT; Error bars represent standard error of the mean. d) Immunofluorescent stained cross-sections of myeloperoxidase (MPO; green), a general marker for peripheral neutrophils (blue: nuclear). Neutrophil/MPO signal (indicated by white arrow in the bottom image) was located at plaque edges and in the core area of LPS-exposed mice injected with control IgG antibodies (LPS-Ctrl; right). MPO+ neutrophils in the atheroma of LPS-ND mice were markedly reduced by injections of neutrophi-specific antibodies (LPS-ND; left); Scale bar represents 100 μm.

4.3.2 Neutrophil Recruitment in the Lungs and Circulating White Blood Cell Counts

In the absence of LPS exposure, injections of non-specific control IgG antibodies or neutrophil-specific antibodies into mice did not induce neutrophil infiltrations in their lungs [Figure 32a]. In the presence of LPS, neutrophil lung infiltrations were observed; Neutrophil counts in the BAL were consistently elevated in the LPS and LPS-Ctrl group [Figure 33]. However, it was significantly attenuated by the injections of neutrophil-specific antibodies (LPS-ND group vs. LPS-Ctrl group, P=0.0002). Macrophage number in the BAL remained consistent among the antibody control groups in both the absence and presence of LPS [Figure 32b]. Administration of neutrophil-specific antibodies significantly reduced the circulating neutrophil counts in the presence of LPS (LPS-ND group: 0.10±0.06 vs. LPS-Ctrl group: 0.8±0.5 $X10^9$/L; Mann-Whitney test P=0.0021). All lymphocyte and monocyte counts in the blood were not significantly different between LPS-ND and LPS-Ctrl groups, or between ND and Ctrl groups. The white blood cell counts of the various groups are shown in Table 5.

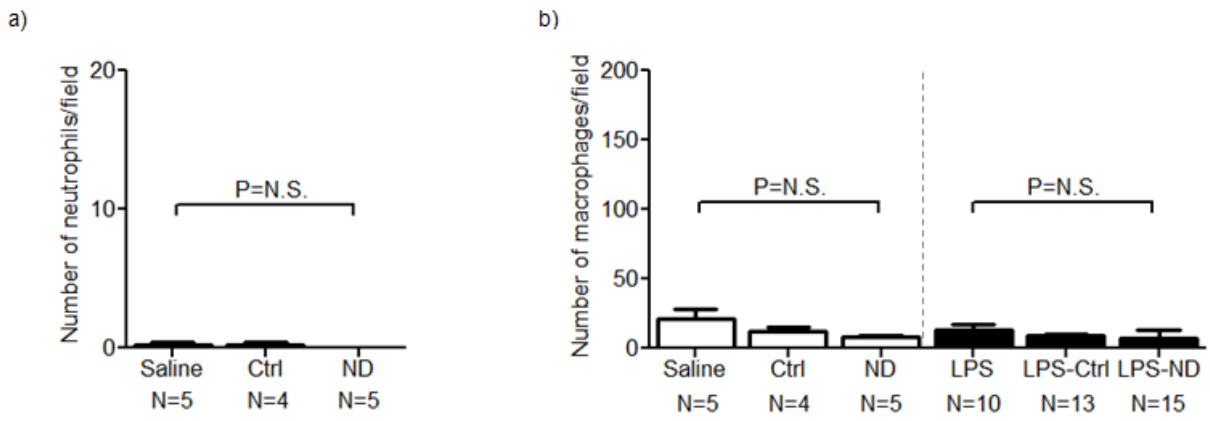

Figure 32: Inflammatory Cell Counts from the BAL.

a) BAL neutrophil counts from saline group, Ctrl group (with injections of control IgG antibodies), and ND group (injections of neutrophil-specific antibodies) are shown. Injections of antibodies into mice *in vivo* did not induce neutrophil lung infiltration. b) Quantitation of macrophage in the BAL of mice in the saline group, Ctrl group, ND group, LPS group, LPS-Ctrl group (LPS group with injections of control IgG antibodies), and LPS-ND group (LPS group with injections of neutrophil specific antibodies). Error bars represent standard error of the mean.

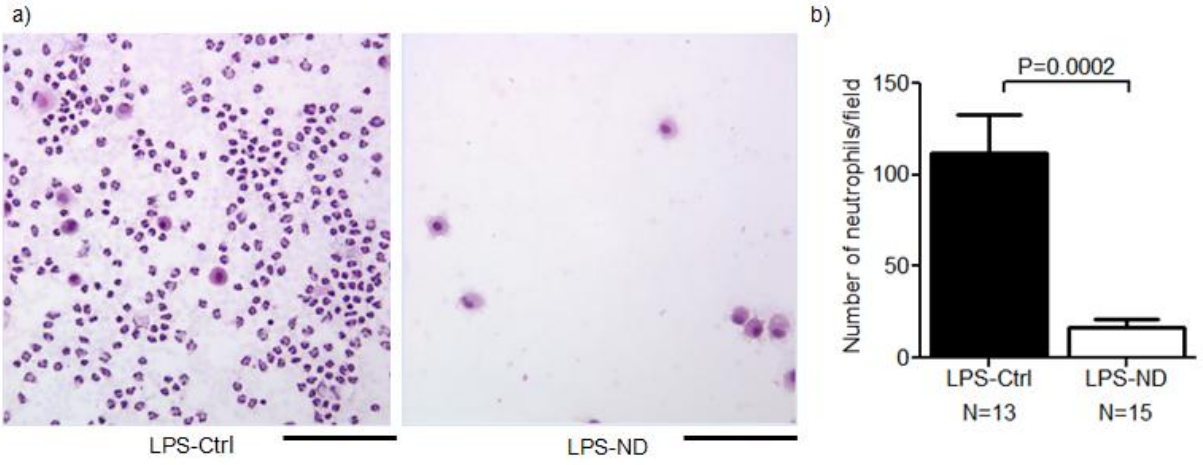

Figure 33: Neutrophil Depletion Reduced Neutrophil Infiltration into the Lungs of LPS-exposed Mice.

a) Cytospin images of bronchoalveolar lavage (BAL) from LPS-Ctrl group (LPS-exposed mice injected with control antibodies (left) and LPS-ND group (LPS-exposed mice injected with neutrophil specific anti-Ly6G antibodies,

right); b) Quantitation of neutrophil count in the BAL. Error bars represent standard error of the mean. Neutrophil depletion in the LPS-exposed mice significantly attenuated the number of neutrophils in BAL.

Table 5: White Blood Cell Counts

(X10^9/L)	WBC	Neutrophils	Lymphocytes	Monocytes
WD (N=3)	7.1 ± 1.4	3.2 ± 1.5	2.9 ± 0.3	0.9 ± 0.2
Saline (N=7)	3.9 ± 2.1	1.0 ± 0.5	2.6 ± 2.4	0.2 ± 0.1
LPS (N=7)	1.8 ± 0.5	1.6 ± 0.9	0.8 ± 1.6	0.8 ± 2.0
LPS-PBS (N=7)	1.9 ± 1.0	1.5 ± 0.9	0.3 ± 0.2	0.03 ± 0.02
Ctrl (N=4)	4.9 ± 4.2	2.4 ± 2.5	2.0 ± 1.6	0.3 ± 0.3
ND (N=4)	3.1 ± 1.4	0.6 ± 0.2	2.2 ± 1.2	0.06 ± 0.03
LPS-Ctrl (N=7)	0.9 ± 0.5[a]	0.8 ± 0.5	0.10 ± 0.03 [abf]	0.01 ± 0.01[abe]
LPS-ND (N=7)	0.27 ± 0.04[abef]	0.10 ± 0.06[acde]	0.06 ± 0.03[abef]	0.06 ± 0.07
P value	<0.0001	=0.0002	<0.0001	<0.0001

The data are shown as mean ± standard deviation. Kruskal-wallis test was used to compare all groups; Dunn's multiple comparison tests were performed to compare between all individual groups. Dunn's test shown a: Significant differences compared to WD group; b: Significantly different from Saline group; c: Significantly different from LPS group; d: Significantly different from LPS-PBS group; e: Significantly different from Ctrl group; f: Significantly different from ND group. WD: 8 weeks western-style diet control group; Saline: intratracheal saline exposure group; LPS: intratracheal lipopolysaccharide exposure group; PBS: intraperitoneal injections of

phosphate buffered saline; Ctrl: intraperitoneal injection with control IgG antibody; ND: intraperitoneal injection with anti-Ly6G antibody for neutrophil depletion

4.4 Discussion

The most important finding of this study is that the depletion of circulating neutrophils *in vivo* using neutrophil-specific antibodies attenuated atherosclerotic plaque vulnerability induced by LPS lung exposure. This result indicates that neutrophils play an important role in acute plaque destabilization in the context of the LPS induced lung inflammatory episode. In the previous study, we established the mouse model of acute plaque destabilization by exposing mice lungs to bacterial LPS, based on the observations that acute respiratory infection and pneumonia transiently increased the risk of acute CV events in human. We found that the atherosclerotic plaques in the BCT were destabilized following the LPS-induced lung inflammation. However, we did not identify the cellular or molecular mediators in this process. In this study we found that during the LPS induced lung inflammation episode, neutrophils not only recruited into the lungs (where LPS was instilled) but also infiltrated into the atherosclerotic plaques downstream in the brachiocephalic arteries, notably recruited into the plaque shoulders and sub-endothelial regions. These regions are also the frequent site of plaque breakage and complications characterized by intraplaque hemorrhage and thrombus formation. Depletion of the circulating neutrophils prior to intratracheal LPS exposure attenuated the neutrophil infiltration into both the lungs and the atherosclerotic plaques and results in less plaque vulnerability, suggesting neutrophils play a cause-effect role in acute plaque destabilization.

Our findings are consistent with the concept that there is widespread neutrophilic inflammation in the coronary arteries during acute CV events. It is postulated that during acute CV events, neutrophils are activated and recruited to the arteries where they release azurophilic (primary) granules, amplifying the original inflammatory signal (133). Studies have shown that neutrophil infiltrations were observed in the ruptured and eroded plaques in the patients suffering ACS. Nearly 44% of unstable angina pectoris (UAP) patients demonstrated neutrophil infiltrations in their atherectomy specimens, while only 6% of stable angina pectoris (SAP) patients had neutrophil infiltrations in their atherectomy specimens (139). Similarly, in another study, it was found that neutrophils and monocytes expressing myeloperoxidase localized in fibrous caps and thrombi in unstable coronary plaques (140). Neutrophils were present in 72% of ruptured atheroma, 8% of TCFA, and none of the fibroatheromas. High neutrophil numbers were not only found in the vulnerable plaques in the coronary arteries, but also in the carotid arteries (167). Furthermore, the high intraplaque neutrophil numbers are associated with the characteristics of plaque vulnerability, including a large lipid core, high macrophage numbers, low collagen amount, low smooth muscle cell numbers, high interleukin 8, high plaque level of matrix metalloproteases 8 and 9, and high intraplaque microvessel density (167). Although associations were found between neutrophils and plaque vulnerability in these studies, the cause-effect role was still not established. In the mouse model of atherosclerosis, the role of neutrophils in atherogenesis was already established by depletion of circulating neutrophils using neutrophil-specific antibodies (165). However, due to the lack of well-established animal model of plaque rupture, the experimental validation of the neutrophil's role in plaque destabilization and rupture was still missing. In this study we experimentally validated the role of neutrophils in plaque destabilization for the first time using the well-established neutrophil depletion technique (166).

Circulating neutrophils contributed to the LPS-induced acute plaque destabilization and rupture. It was beyond the purview of this study to evaluate downstream molecules that were directly responsible for plaque rupture. However, based on some preliminary experiments, we speculate that myeloperoxidase and matrix metalloproteinases could be important downstream molecular factors in this process. But, additional studies are needed to determine the exact molecular pathways that lead to acute plaque destabilization and rupture. It should also be noted that we did not identify the mediators responsible for the activation and recruitment of neutrophils into the plaques following LPS stimulation. Further work will be needed to unravel the molecular underpinnings of this process.

4.5 Conclusion

We found that neutrophils infiltrated into atherosclerotic plaque in the BCT following LPS-induced acute lung inflammation. Neutrophil depletion reduced plaque vulnerability characterized by less intraplaque hemorrhage and thrombus formation. Our results suggest that neutrophils contribute to acute plaque destabilization process. Future investigations are needed for identifying the molecular mediators in this process. Therapeutic strategies targeting neutrophilic inflammation might be important in reducing acute CV events in human.

Chapter 5: Acute Localization of Myeloperoxidase in Vulnerable Atheroma Following LPS Lung Exposure and Myeloperoxidase Inhibition Reduced Plaque Vulnerability

5.1 Introduction

Despite the tremendous commitment to the treatment and prevention of CVD over the past 30 years, ischemic heart disease (IHD), acute coronary syndrome (ACS), and stroke remain the leading causes of mortality, accounting for 25% of deaths in 2010, and 31% of deaths in 2012 worldwide (1, 168). If we cannot reduce the prevalence of CVD, it is projected to account for over 40% of deaths worldwide by 2030 (1). One of the major limitations for CVD prevention is the poor understanding of the molecular mechanisms leading to acute atherosclerotic plaque rupture. Of the many processes involved in acute CVD, acute inflammation is thought to be a major driver of plaque rupture (22, 40, 133, 169). In human coronary arteries, there is evidence of widespread inflammation, characterized predominantly by neutrophil activation, in coronary vessels affecting not just the culprit artery but the entire coronary vasculature (133). Once activated, these neutrophils can unleash a cascade of pro-inflammatory and pro-oxidative molecules. Myeloperoxidase (MPO), a 150-kDa heme peroxidase-cyclooxygenase stored in azurophilic granules of neutrophils, is one of the important enzymes released during this process (170). The primary function of MPO is to promote bacterial killing by generating various reactive oxidants and diffusible radical species during infections. A previous study showed that during acute CV events, MPO levels rapidly increase in the coronary and systemic circulation

(143). Indeed, plasma MPO is now accepted to be a good biomarker of acute CV events (147); however, the effect of MPO on plaque vulnerability remains unclear.

In humans, lung inflammation and injury are considered to be major triggers of acute cardiovascular events (81, 85, 90, 96, 97, 101, 102, 150), but the molecular mechanisms by which this occurs remain poorly understood. In a previous study, our group established an experimental murine model of plaque vulnerability by challenging mice with intratracheal lipopolysaccharide (LPS) administration [Section 3.3.5]. It was found that circulating neutrophils contributed to the plaque rupture caused by LPS-induced lung inflammation [Section 4.3.1]. However, the molecular mechanisms by which plaque rupture occurred were not identified. In the current study, our hypothesis is that MPO might be one of the important contributors to plaque rupture in response to lung inflammation. In this study, we determined: 1) the acute localization of MPO in our mouse model of plaque rupture caused by lung injury using a novel three-dimensional (3D) immunofluorescence staining combined with ex vivo high resolution optical projection tomography (OPT) in the whole mount blood vessels, 2) the effect of MPO inhibition on plaque vulnerability using the MPO inhibitor 4-aminobenzoic hydrazide (4-ABAH), and 3) the role of neutrophils in MPO accumulation by examining the effect of neutrophil depletion on intraplaque MPO accumulation.

5.2 Methods

5.2.1 Animals and Experimental Designs

Male apolipoprotein E-null mice ($ApoE^{-/-}$) on a C57BL/6J background (Jackson Laboratory, Bar Harbor, ME; Stock number: 002052) were fed a Western-type diet (WD) containing 21% fat

from lard and 0.15% cholesterol (TD88137; Harlan Laboratories Inc., Madison, WI, USA) for 8 weeks to induce the growth of atherosclerotic plaques in their right brachiocephalic trunk (BCT) [Section 3.2.1]. The experimental scheme is illustrated in Figure 34. The effect of LPS-induced lung inflammation on plaque rupture using this model was previously characterized and reported [Section 3.3.4]. In addition, C57BL/6J wild-type mice (N=40) were used to study the changes of MPO level in BAL and plasma (draw from IVC) at different time-points following intratracheal LPS instillation.

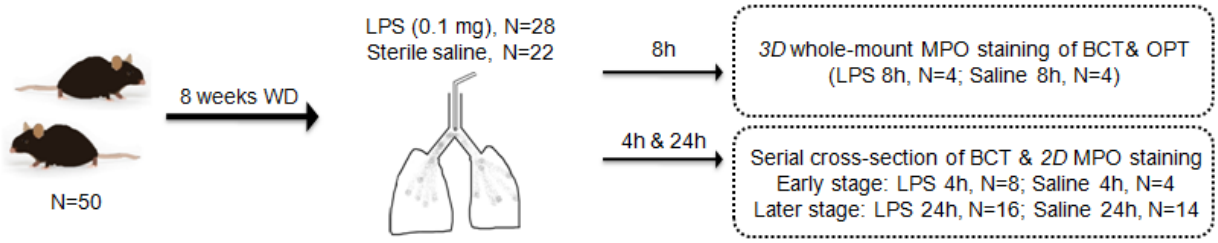

Figure 34: Investigation of Myeloperoxidase (MPO) Localization in Mouse Atherosclerotic Plaques Following LPS Lung Exposure.

50 Male ApopE KO mice on a C57BL/6J background were fed a Western-type diet (WD) containing 21% fat from lard and 0.15% cholesterol for 8 weeks. These mice were randomly divided into 2 groups: 1) LPS-exposed (N=28), or 2) saline-exposed as the control group (N=22). 4, 8, and 24 hours post-instillation, optical projection tomography (OPT) or histology were used to determine plaque vulnerability in the mouse BCT. The presence of myeloperoxidase (MPO) was investigated by 3D and 2D MPO staining.

5.2.2 Investigation of Myeloperoxidase (MPO) Localization in Atherosclerotic Plaques Following LPS Lung Exposure

Male ApoE$^{-/-}$ mice were randomly divided into 2 groups: 1) LPS-exposed (N=28), or 2) saline-exposed as the control group (N=22). In the LPS-exposed group, a single dose of 100 µg LPS (3mg/kg) (L2630, Sigma-Aldrich, St. Louis, MO), dissolved in 50 µl of sterile saline, was sprayed as aerosols (16-22 µm in mass median diameter) directly into the lungs of the mice, bypassing the vocal cords, using a microsprayer (MSA-250-M, Penn-Century Inc., Wyndmoor, PA). In the saline-exposed group (N=22), a single administration of 50 µl sterile saline aerosol was sprayed into the lungs in the same manner. [Section 3.2.1] At 4, 8 and 24 hours post-instillation, the aortic arch with the BCT was collected and stained for MPO using whole-mount immunofluorescence, and imaged using OPT. This approach enabled 3D visualization of the BCT and MPO localization throughout the plaque and vessel. This was complemented by two-dimensional (2D) assessment of MPO using traditional immunofluorescent staining techniques of serial cross-sections of the BCT.

5.2.3 Myeloperoxidase Enzymatic Inhibition by 4-Aminobenzoic Acid Hydrazide (4-ABAH)

To determine the effect of MPO enzymatic inhibition on plaque vulnerability, we challenged another group of male ApoE$^{-/-}$ mice (N=24) with intratracheal LPS (1.5 mg/kg) following 8 weeks of WD and subjected the mice either to: 1) immediate treatment with intraperitoneal (ip) injections of 1 mg of the MPO enzyme inhibitor 4-ABAH (Sigma-Aldrich, USA) dissolved in 400 µl of sterile phosphate-buffered saline (PBS, ~30 mg/kg) administered every 2 hours for a total of 4 injections (LPS+4-ABAH, N=13) (126, 171, 172), or 2) 400 µl of sterile PBS as

vehicle control (LPS+PBS, N=11), as shown in Figure 35. At 24 hours post-instillation of LPS, the BCT was harvested for plaque vulnerability, and morphometric measurements were performed on serial hematoxylin and eosin (H&E) stained cross-sections of the BCT [Section 3.2.6]. Mice fed a WD without exposure to LPS were used as controls (WD control, N=6) and 4-ABAH-injected mice fed the WD without LPS instillation (WD+4ABAH N=4) served as additional controls for plaque vulnerability.

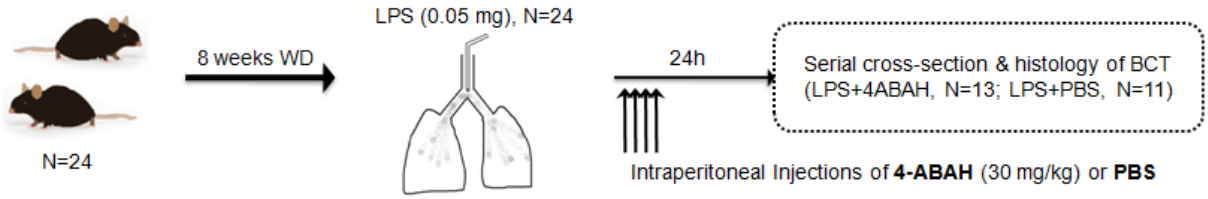

Figure 35: Investigation of MPO Enzymatic Inhibition *in vivo* and Changes of Plaque Phenotypes.

To determine the effect of MPO enzymatic inhibition on plaque vulnerability, we challenged male ApoE KO mice (N=24) with intratracheal LPS (1.5 mg/kg) following 8 weeks of WD and subjected the mice either to: 1) immediate treatment with intraperitoneal (ip) injections of the MPO enzyme inhibitor 4-ABAH (~30 mg/kg) dissolved in 400 µl of sterile phosphate-buffered saline administered every 2 hours for a total of 4 injections (LPS+4-ABAH, N=13), or 2) PBS as vehicle control (LPS+PBS, N=11). At 24 hours post-instillation of LPS, the BCT was harvested for plaque vulnerability, and morphometric measurements were performed on serial hematoxylin and eosin (H&E) stained cross-sections of the BCT.

5.2.4 Neutrophil Depletion (ND) *in vivo* with Anti-Ly6G Antibody Injections

To determine the role of circulating neutrophils in intraplaque MPO accumulation, LPS-exposed mice received 2 ip injections of either: 1) rat anti-mouse Ly6G clone 1A8 antibodies (Bio X cell, New Hampshire, USA) (LPS-ND group, N=6) to deplete circulating neutrophils,16,22 or 2) rat

IgG2A isotype clone 2A3 antibodies (Bio X cell, New Hampshire, USA) (LPS-Ctrl, N=6) as controls. The first dose was given 24 hours prior to LPS challenge and the second dose was given immediately after LPS challenge. Each dose was 400µg diluted in 400µl sterile PBS. At 4 and 24 hours post-LPS instillation, the BCT was collected and serial cross-sections were used for histological assessment and immunostaining of MPO [Figure 36].

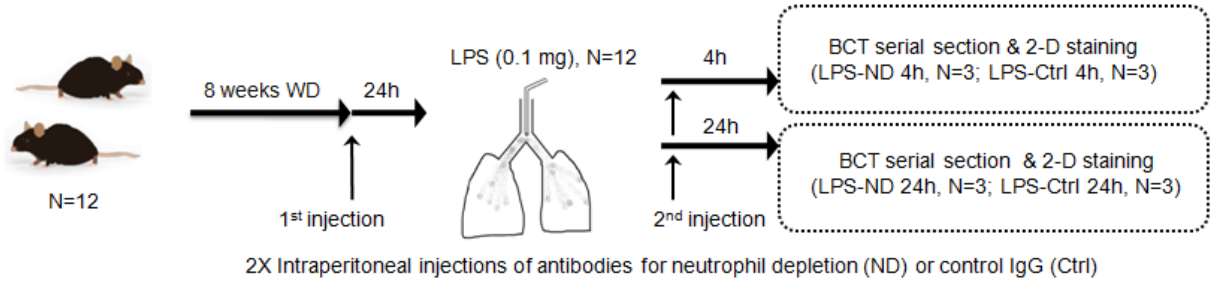

Figure 36: Investigation of the Cellular Origin of Intraplaque MPO.

To determine the role of circulating neutrophils in intraplaque MPO accumulation, LPS-exposed mice received 2 intraperitoneal injections of either: 1) rat anti-mouse Ly6G clone 1A8 antibodies (LPS-ND group, N=6) to deplete circulating neutrophils, or 2) rat IgG2A isotype clone 2A3 antibodies (LPS-Ctrl, N=6) as controls. The first dose was given 24 hours prior to LPS challenge and the second dose was given immediately after LPS challenge. At 4 and 24 hours post-LPS instillation, the BCT was collected and serial cross-sections were used for histological assessment and staining of MPO.

5.2.5 Organ and Tissue Procurement and Bronchoalveolar Lavage (BAL)

Mouse blood was collected from the inferior vena cava (IVC) under anaesthesia (isoflurane 5% inhalation), before sacrifice. The heart, aortic arch, and branching arteries containing the BCT were perfused with 3ml of PBS injected directly into the left ventricle at an infusion rate of 1 ml/min (Harvard Apparatus, Massachusetts, USA). Bronchoalveolar lavage (BAL) fluid was

collected by washing the right lung once with 600 µl of PBS. The left lung was harvested and perfused with 400 µl of 10% formalin.

5.2.6 Whole-Mount Immuno-Fluorescent Staining of MPO

Aortic arches, containing the BCT and carotid arteries, were fixed in 10% formalin for 48 hours. Samples were then placed in descending methanol concentrations of 75%, 50%, and 25% (in PBS) for 10 min each. Following this, samples were washed 3x for 30 mins in wash buffer (1% Triton X100 solution in PBS) and then the autofluorescence signal of samples was quenched using sodium borohydride (3%) for 24 hours. Next, samples were incubated 2x for 1 hour each in blocking buffer (10% donkey serum in wash buffer). The blocking buffer was also injected into the BCT and aortic arch from the distal opening of carotid arteries and thoracic aorta in order to ensure optimal buffer distribution. Following the blocking buffer injection, samples were incubated with additional 2x for 10 min each in the blocking buffer. Next, the samples were transferred to the primary antibody solution containing 20 mg/ml of goat anti-mouse MPO in blocking buffer. The primary antibody solution was also injected into the BCT and aortic arch from the distal opening of carotid arteries and thoracic aorta for optimal antibody distribution. The samples were incubated in the primary antibody solution for the following 4 days at 4°C with intermittent gentle mixing. After that, samples were washed 3x for 1hour in blocking buffer following the same injection protocol, and then washed 3x for 10 min each in the wash buffer. Next, the samples were transferred to the secondary antibody solution (Donkey anti-goat alexa-488 200 X dilutions) following the same injection protocol and incubated for the next 2 days. After incubation, samples were washed 4x for 1hour each in wash buffer.

5.2.7 Optical Projection Tomography (OPT)

We visualize the plaques and the 3D distribution of MPO using the OPT technique. BCT samples were embedded in 1% low melting point agarose solution, dehydrated in 100% methanol, transferred to a benzyl alcohol:benzyl benzoate (BABB) solution, and mounted as described previously [Section 3.2.5].

5.2.8 Vulnerability Signal Detection and Data Acquisition

All prepared BCT samples were scanned with OPT (Bioptonics 3001M, MRC Technology, London, UK) using two different channels. The GFP1 channel (exciter = 425nm/40nm, emitter = LP475nm) was used to visualize and register the sample with its autofluorescence. Thrombus and erythrocytes emit a distinctive autofluorescent signal that is 10-fold higher in intensity than the arterial wall (132). The GFP+ channel (exciter = 480nm/20nm, emitter = LP515nm) was used to visualize and detect the distribution of MPO by the immunofluorescence of alexaflour-488. The data were reconstructed as previously described (132). Semi-automated segmentation of the MPO signal was performed and the 3D MPO-positive signals (signal ranged from 20000-65335) within the whole BCT were quantified. The plaques were assessed in a blinded manner and plaques were considered vulnerable if there was a visible thrombus or evidence of hemorrhage in the plaques with a size greater than 0.0005 mm.

5.2.9 Specimen Recovery for Histological Validation and Confocal Microscopy

To validate plaque stability, post-OPT samples were recovered from the agarose for further analysis. A single edged blade was used to remove excess agarose from the sample, while taking great caution not to damage the tissue. Then, BABB was removed from the specimen by washing

it in 100% methanol with many exchanges. After the complete removal of BABB, specimens were rehydrated in descending concentrations of ethanol (70%, 50%, 30%, 10%). Once rehydrated, specimens were incubated in 0.29 M sucrose for a minimum of 60 min, at which point remaining agarose was trimmed off the tissue. In order to remove the residual pieces of agarose attached to the tissue, samples were placed in 0.29M sucrose that had been preheated to 57°C for 30-60 min. If there was any residual agarose on the tissue, samples were incubated for a longer period of time. Once the agarose was completely eliminated, the samples were washed 2x in fresh 0.29M sucrose at 57°C. The recovered BCT were then embedded in paraffin and sectioned, stained and analyzed using immunofluorescent microscopy and confocal microscopy as previously described [Section 3.2.9].

5.2.10 Serial Cross-Sectioning of BCT: Frozen Sections

Fresh BCTs were embedded with optimum cutting temperature (OCT) (Sakura Finetek, Torrance, CA) on dry ice, followed by cryopreservation in liquid nitrogen and storage at -80°C. Serial 5 µm cross-sections of vessels perpendicular to the long axis were obtained at approximately 50 µm intervals starting from the arch (proximal end) to the site of the BCT bifurcation using a cryostat (Leica, UK). These sections were stained with H&E and Movat's pentachrome for morphological analyses.

5.2.11 Quantitative Histology and Definition of Vulnerable Plaque

A vulnerable plaque was defined by the presence of a thrombus or intraplaque hemorrhage. Intraplaque hemorrhage was noted when there were erythrocytes inside the atheroma on at least two contiguous sections spaced 50 µm apart. The presence of the vulnerability signals in a given

plaque was determined by 2 independent investigators in a blinded manner. The decision was made by a third independent investigator when inconsistency occurred between the first 2 investigators.

5.2.12 Immunofluorescent Staining (IF) of MPO and CD68 and Signal Quantitation

The frozen BCT cross-sections were fixed in 10% formalin for 10 min and then rinsed in running water for 2 min. The sections were incubated with 10% chicken serum (Gene Tex Inc., USA) and donkey serum (Sigma-Aldrich, USA) for 30 min and then incubated with the mouse MPO affinity purified polyclonal antibody to goat IgG (5µg/ml; R&D, USA) and the mouse macrophage/smooth muscle CD68 monoclonal antibody to rabbit IgG (2.5µg/ml; Abcam, Toronto, ON, Canada) for 2 hours at 4°C. After 4 incubations in PBS for 5 min, the BCT sections were incubated with secondary antibodies: donkey anti-goat 488 (400X dilution; Invitrogen, USA) and chicken anti-rabbit 594 (400X dilution; Invitrogen, USA) for another 2 hours at room temperature. After 4 washes in PBS for 5 min, the cross-sections were air dried for 30 min and mounted using the Vectashield mounting medium with DAPI (Vector Lab Inc, USA). Immunofluorescent images of the 3 serial sections containing the largest plaque areas were captured under a fixed computerized setting using a Nikon immunofluorescence light microscope Eclipse TE300 (Nikon, Japan) at 100X, 200X and 600X magnification. The MPO signals in the given plaques were quantified by color segmentation in the original unit of pixels. The value of %MPO was calculated by dividing the MPO signal by the plaque size using Image-Pro Plus software. The values for the 3 serial cross sections with the largest plaque size were averaged to represent the center plaque region, and values for the 3 serial sections with the smallest plaque size were averaged to represent the shoulder region. The arithmetic mean was

used for statistical analysis. Normal rabbit and goat IgG were used for negative controls. The frozen lungs of LPS-treated mice were used for positive controls.

5.2.13 Neutrophil Counts in BAL

As described previously, polymorphonuclear leukocytes (PMNs) were morphologically identified by evaluating size, shape, and presence of granules and multinucleation [Section 3.2.10].

Investigation of MPO Levels Following Intratracheal LPS Instillation in Wild-type Mice

C57BL/6J wild-type male mice (N=40) were used to study the changes in MPO levels in BAL fluid and plasma (drawn from the IVC) at different time-points following intratracheal LPS instillation. The in vitro quantitative determination of mouse MPO in plasma was determined using the HK210 mouse MPO ELISA kit (Hycult biotech, Plymouth Meeting, PA) according to the manufacturer's protocol. The samples were measured in duplicate. The lower detection limit value (1.6 ng/ml) was assigned when there was no detectable MPO.

5.2.14 Myeloperoxidase Enzymatic Activity Assay

MPO activity in BAL fluid (diluted 25X in PBS) was measured using an MPO colorimetric activity kit (Sigma-Aldrich, St. Louis, MO) following the manufacturer's protocol. One unit of MPO activity was defined as the amount of enzyme that hydrolyses taurine and generates taurine chloramines, which in the process consumes 1.0 micromole of 5-thio-2-nitrobenzoic acid (TNB) per min at 25 °C to yield 5-5-dithiobis (2-nitrobenzoic acid) (DTNB). Samples were loaded in

duplicate (one as a blank and one as a test sample) and assayed for 60 min. A zero value was assigned when there was no detectable difference between the sample and blank.

5.3 Results

5.3.1 Acute Localization of MPO Following LPS lung Exposure

As characterized in the previous study, 24 hours following intratracheal LPS instillation, OPT revealed that atherosclerotic plaques in the BCT of these mice became vulnerable, demonstrating the signals of luminal thrombus and intraplaque hemorrhage [Video 6 and Video 7 in Appendix]. In contrast, atherosclerotic plaques in the BCT of saline-exposed mice did not demonstrate these signals [Section 3.3.4]. Importantly, in this study we found that MPO was detected at the edges of the vulnerable plaques, occurring mostly at the site of plaque disruption, and frequently co-localized with luminal thrombi (Figure 37, Video 8 in Appendix). Following intratracheal saline instillation, however, there was no thrombus formation or MPO-positive signal present in the BCT [Video 9 in Appendix].

Confocal microscopy confirmed these findings, demonstrating extracellular MPO deposition and a large number of polymorphonuclear cells containing intracellular MPO in vulnerable plaques, most notably in and around thrombi [Figure 38a and b]. 3D analysis indicated 10X more MPO signal in the BCT of LPS-exposed mice compared to that in the saline-exposed mice ($P=0.0353$, [Figure 38c]).

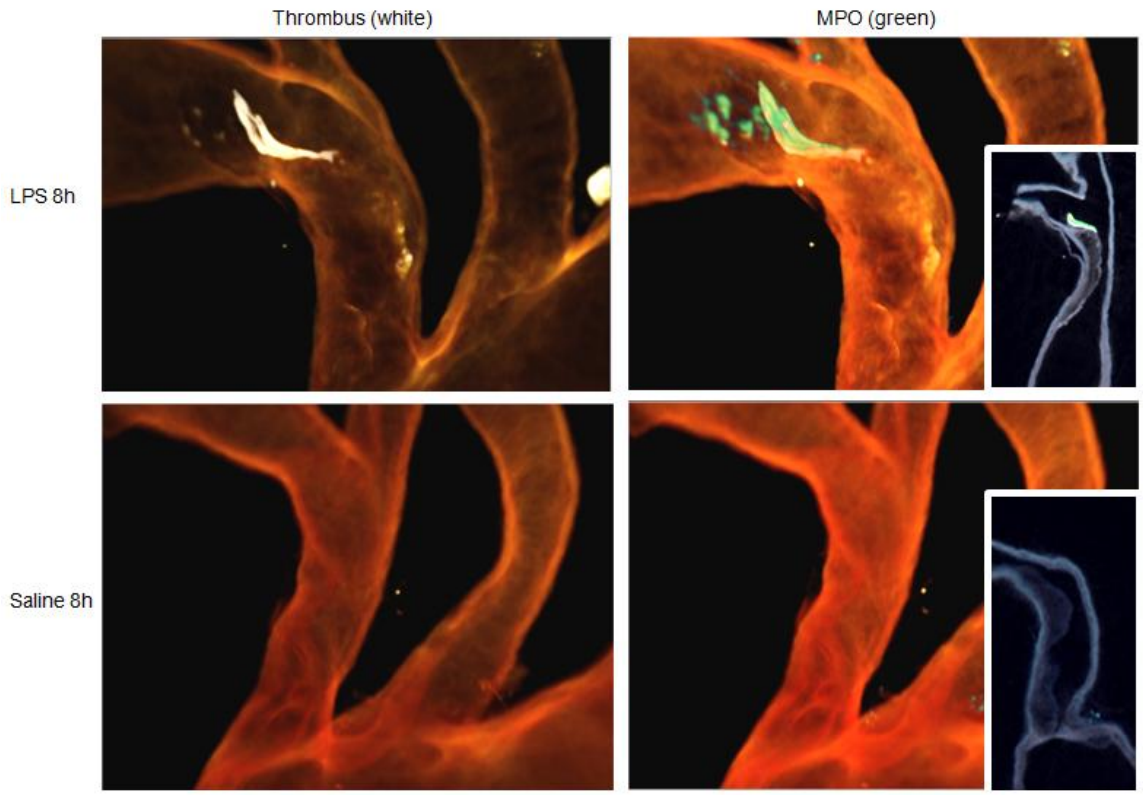

Figure 37: Three-Dimensional (3D) Presentation of Mouse Brachiocephalic Trunk (BCT) and the Distribution of Myeloperoxidase (MPO; green) Detected by Optical Projection Tomography (OPT).

Top left: The BCT (orange) from a LPS-exposed mouse. A thrombus (white) was localized at the distal edge of the atherosclerotic plaque (detected by its auto-fluorescence intensity, 10-fold higher than the vessel wall base intensity). Top right: The MPO (green) signals detected in the same BCT. The MPO signal was co-localized with the thrombus. Sub-panel: a transverse-section of BCT (white) with MPO overlaid (green); Bottom left: The BCT (orange) from a saline-exposed mouse. No thrombus was observed at the atherosclerotic plaque. Bottom right: No MPO (green) signal was detected in the same BCT image Sub-panel: a transverse-section of the same BCT (white) with no MPO detected.

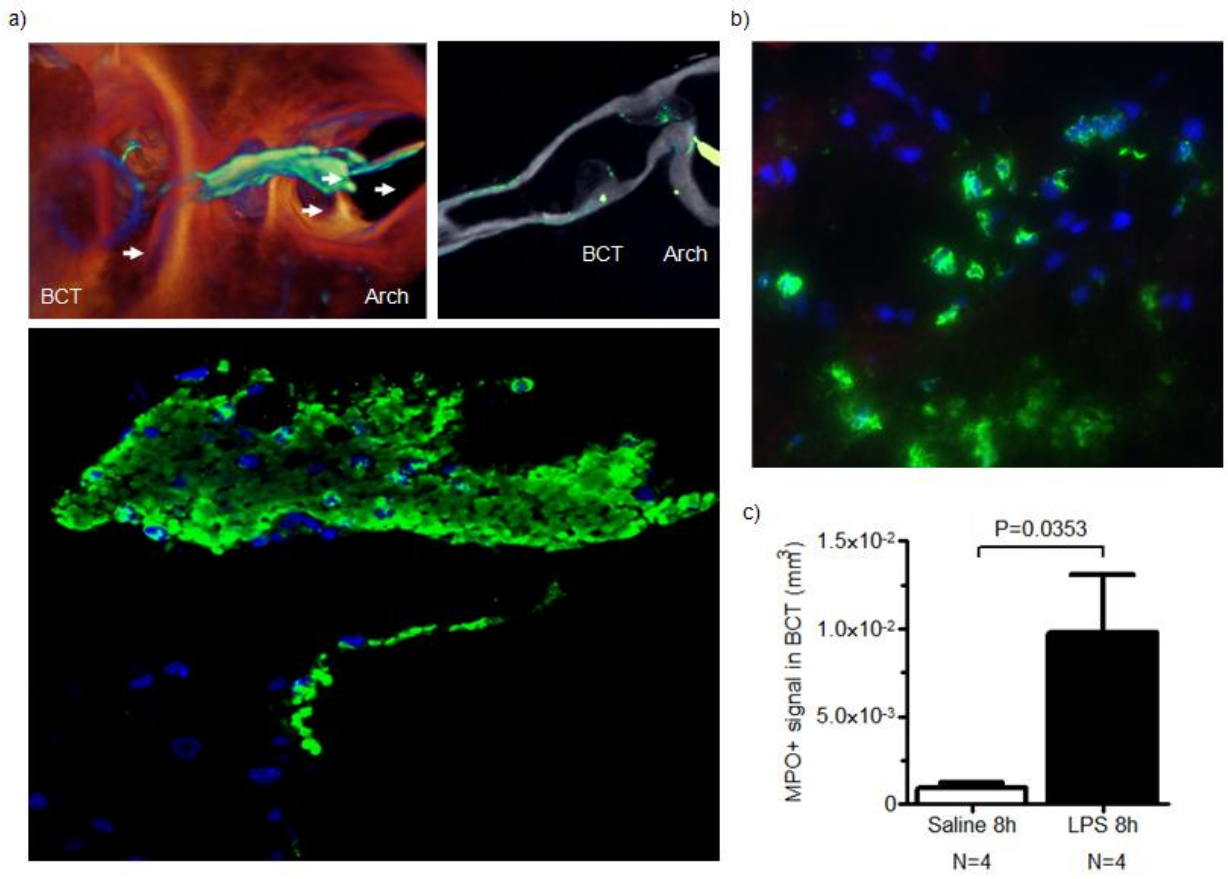

Figure 38: The MPO Signals in the Thrombus and Atherosclerotic Plaque of LPS-exposed Mice.

a) Top-left image: A 3D view from the proximal-end of BCT showing MPO signal (green) in the thrombus attached to the plaque. Top-right image: A 2D transverse-sectional presentation of the same BCT showing MPO signal (green) in the plaque, at the edges of plaque, and in the luminal thrombus and in the thrombus. Bottom: A confocal microscopy image of the luminal thrombus using the whole-mount immunofluorescent staining technique. MPO was detected in green; cell nuclei in blue. Many polymorphonuclear cells with strong intracellular MPO signals were observed in the luminal thrombi. High extra-cellular MPO were also observed in the surrounding thrombus area. b) Many MPO-positive polymorphonuclear cells (green) were detected in the tissue of atherosclerotic plaques and extra-cellular MPO signals were detected in the necrotic core. c) The 3D quantitation of MPO signals in the BCT of LPS-exposed and saline-exposed mice detected by OPT. 10-fold more signals were detected in the LPS-exposed mice compared to that in the saline-exposed mice. Error bars represent SE.

Cross-sections of the BCT showed that, at the earlier phases of acute lung injury (e.g. 4 hours following LPS instillation), MPO-positive polymorphonuclear cells appeared on the surface and edges of atherosclerotic plaques and MPO deposition was noted in the extracellular space surrounding these cells [Figure 39 a-b]. At a later stage (e.g. 24 hours post-instillation of LPS), extracellular MPO was found mainly in the necrotic core [Figure 39c and Figure 40]. There was heavy MPO deposition and a large number of polymorphonuclear cells at the site of plaque rupture in the LPS-exposed mice [Figure 41 a-b]. The 2D MPO quantitation in histologic sections showed a 3.5X higher level of MPO signal at the center of atherosclerotic plaques in LPS-exposed mice (24 hours) compared to that in saline-exposed mice ([Figure 41c], P=0.0047).

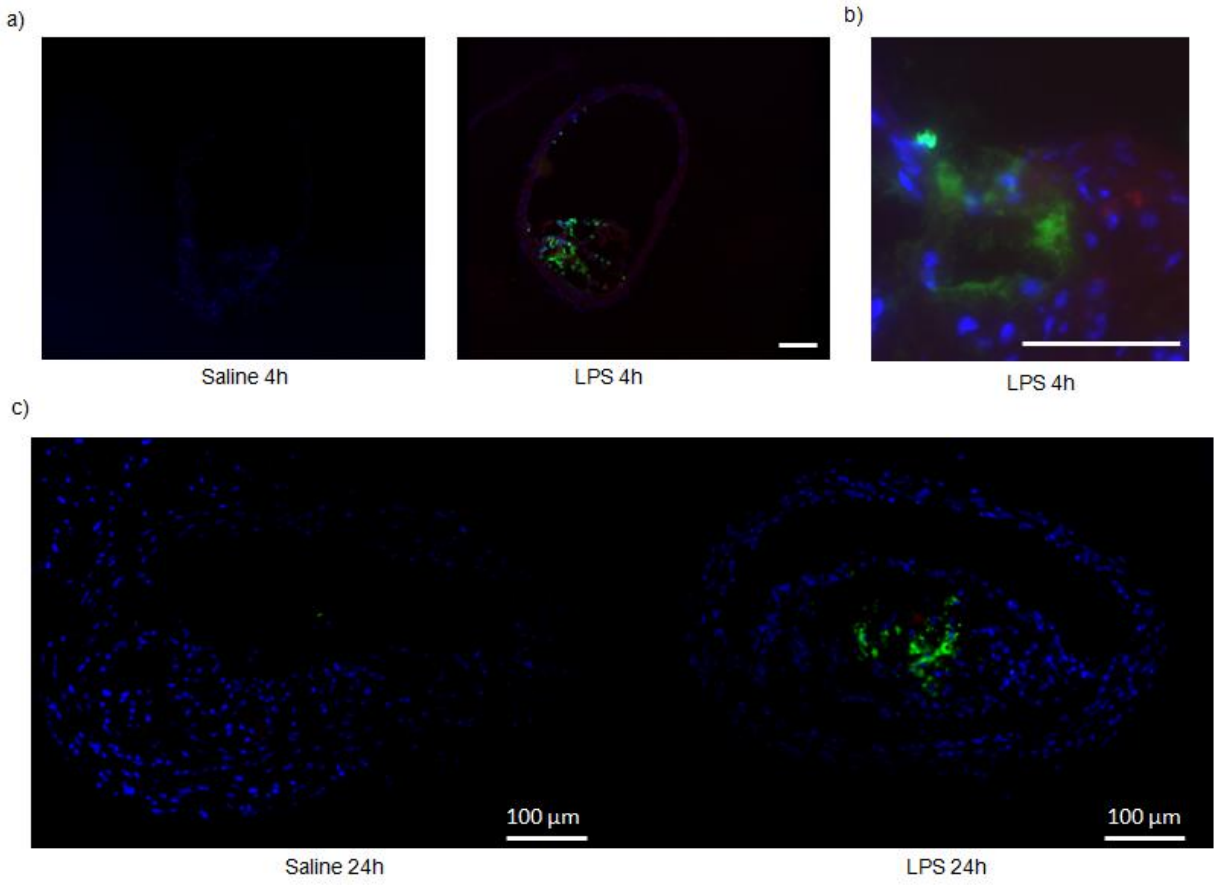

Figure 39: The Two Dimensional (2D) Presentations of the Atherosclerotic Plaques.

a) At the earlier stage, 4 hours post-instillation of saline (left) and LPS (right). MPO-positive cells (green) were detected in the atherosclerotic plaque of the LPS-exposed mice but not in the saline-exposed mice. b) MPO signals were found in a bend cell and surrounding plaque tissue of LPS-exposed mice at 4 hours. c) The presentation of atherosclerotic plaques at the later stage, 24 hours post-instillation of saline (left) and LPS (right). Extra-cellular MPO (green) was mainly presented in the core regions of LPS-exposed mice, but not in the saline-exposed mice.

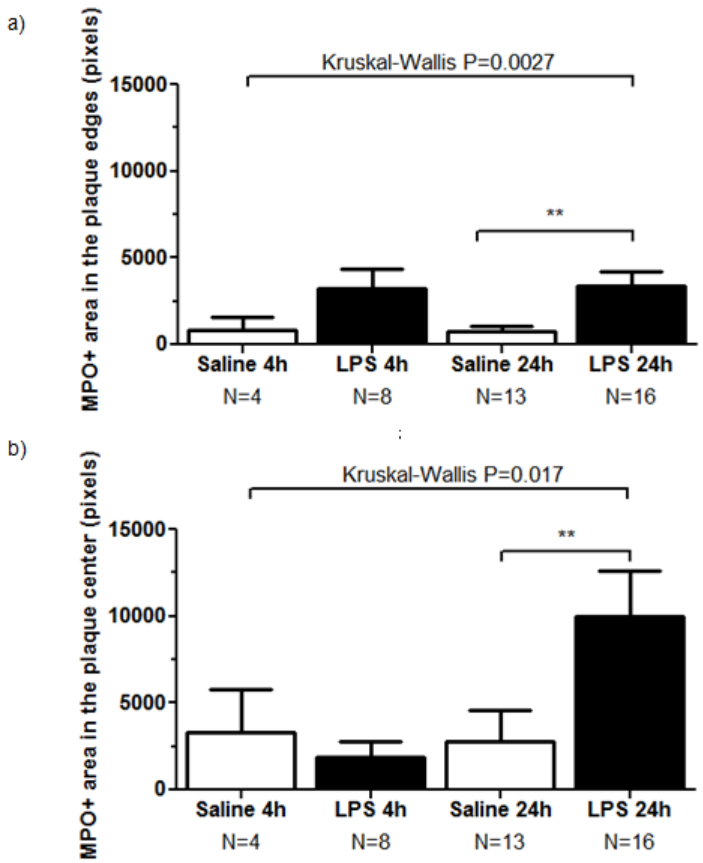

Figure 40: Two Dimensional (2D) Quantitation of MPO in Atherosclerotic Plaques.

a) In the central region of atherosclerotic plaques in the BCT at early stage (4 hours) and later stage (24 hours). b) At the edges of plaques at early stage (4 hours) and later stage (24 hours). The absolute signals in pixels were presented. Error bars represent mean ±-SE.

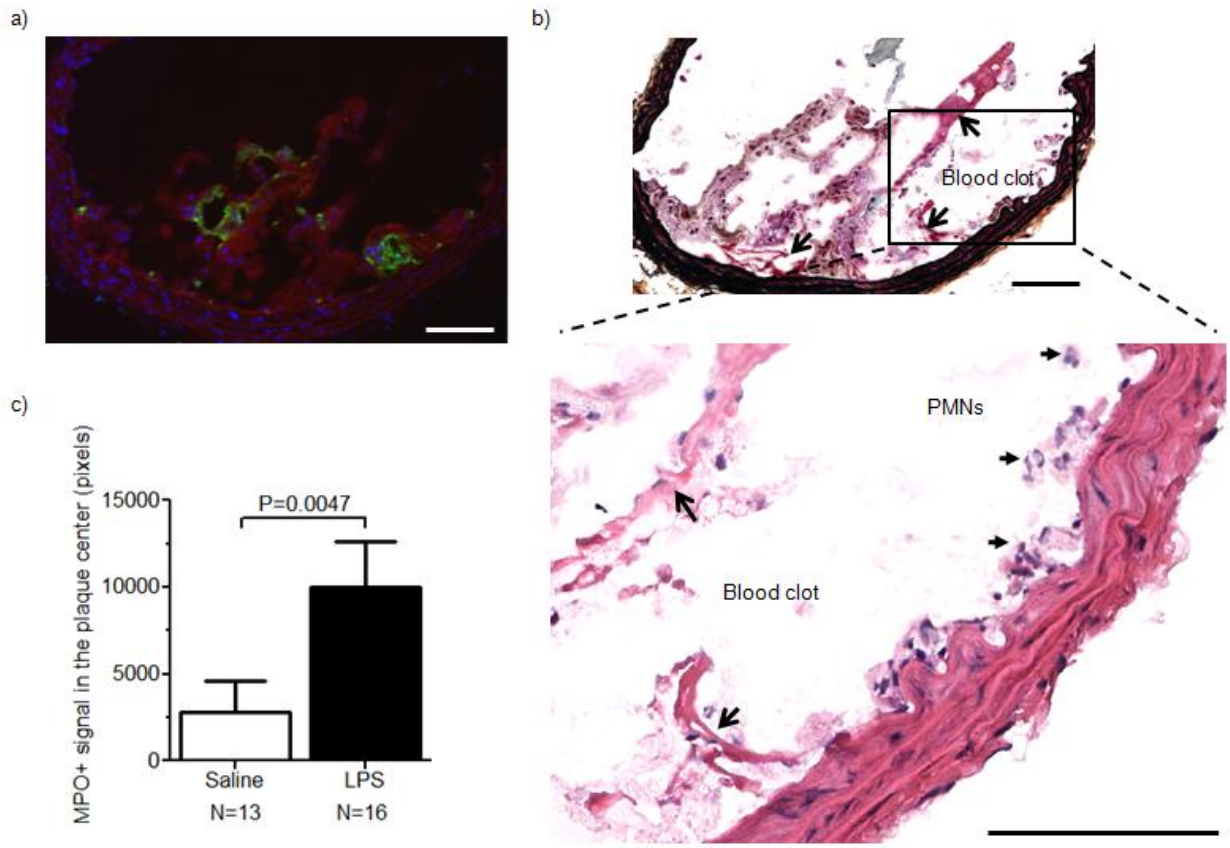

Figure 41: MPO Signals Detected at the site of Plaque Disruption.

a) MPO signals (green) were detected at the ruptured atherosclerotic plaque of LPS-exposed mice at 24 hours. b) Movat's pentachrome stain with Musto's/Harrington modification (upper) and hematoxylin and eosin stain (lower) showed that blood clots and polymorphonuclear cells were observed at the same region of the ruptured plaque. Scale bar represents 100μm. c) The 2D quantitation of MPO in the central region of atherosclerotic plaque: About 3.5-fold increase of MPO signals in the plaques of LPS-exposed mice compared to that in saline-exposed mice at 24 hours post-instillation. Error bars represent 100μm.

5.3.2 MPO Inhibition Attenuated Plaque Vulnerability in LPS-exposed Mice

Histological analysis showed that when LPS-exposed mice were treated with PBS (LPS+PBS), 72.7% of these mice harbored vulnerable plaques (characterized by intraplaque hemorrhage or thrombus formation) in the BCT. In contrast, only 27.3% of LPS-exposed mice that were treated with the MPO enzymatic inhibitor 4-ABAH (LPS+4-ABAH) demonstrated plaques that were vulnerable ([Table 6], P=0.0377). WD control mice and WD+4-ABAH mice did not show plaque vulnerability. Morphologically, the atheroma of LPS-exposed mice treated with 4-ABAH displayed a more stable phenotype, characterized by a thicker cap compared with mice treated with PBS [Figure 42a and Table 7]. Interestingly, treatment with 4-ABAH did not change the level of MPO signal in plaques. However, 4-ABAH treatment attenuated the level of 3-chlorortyrosine, the product of MPO/HOCl mediated protein oxidation, in the plaques [Figure 42b and c]. Furthermore, 4-ABAH treatment significantly reduced the MPO enzymatic activity and neutrophil counts in BAL fluid [Figure 43].

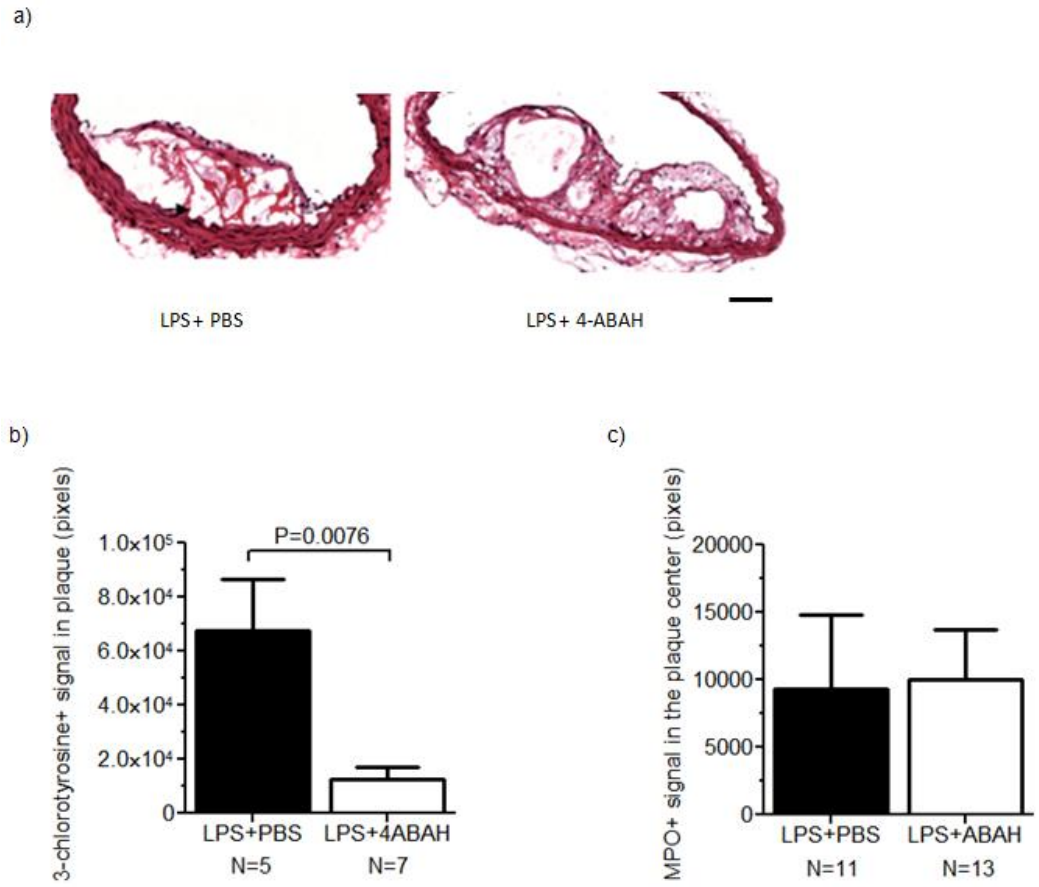

Figure 42: MPO Enzymatic Inhibition Reduced Plaque Vulnerability.

a) Hematoxylin and eosin stained cross-sections of BCT: Left: a vulnerable plaque demonstrated intraplaque hemorrhages (red) in the BCT of LPS-exposed mice treated with phosphate buffered saline (PBS). Right: a plaque in BCT of LPS-exposed mice treated with the MPO inhibitor, 4-aminobenzoic acid hydrazide (4-ABAH), demonstrated enlarged necrotic cores but no signal of plaque rupture. b) The 2D quantification of 3-chlorotyrosine, the specific enzymatic product of MPO/HOCl mediated oxidation, in the atherosclerotic plaques in BCT by immunofluorescent staining. The signal of 3-chlorotyrosine in the plaques of LPS-exposed mice treated with 4-ABAH was significantly lower than that in LPS-exposed mice treated with PBS. c) The 2D quantitation of MPO signal in the plaques of LPS-exposed mice treated with 4-ABAH and PBS. No change in MPO level was found. Error bars represent SE.

Table 6: Comparison of Plaque Vulnerability in the BCT of Mice Based on the Histology of Serial Cross-Sections.

Groups	Vulnerable	Stable	P value
Saline 24h (N=14)	2 (14.3%)	12 (85.7%)	0.011*
LPS 24h (N=16)	10 (62.5%)	6 (37.5%)	
LPS+PBS (N=11)	8 (72.7%)	3 (27.3%)	0.038†
LPS+4ABAH (N=13)	3 (23.1%)	10 (76.9%)	

The presence of the vulnerability signals in a given plaque was determined by 2 independent investigators in a blinded manner (investigators did not know the mice group). The decision was made by the third independent investigator when a conflict occurred between them.

* Fisher's exact test was performed to compare the incidence of plaque vulnerability between LPS 24h group and Saline 24h group.

† Fisher's exact test was performed to compare the incidence of plaque vulnerability between LPS+PBS group and LPS+4ABAH group.

Brachiocephalic trunk: BCT; Lipopolysaccharide: LPS; phosphate buffered saline: PBS; 4-aminobenzoic acid hydrazide: 4ABAH

Table 7: Morphometry of Atherosclerotic Plaques in the BCT of Mice Determined by the Frozen Cross-Sections that Contained the Maximal Plaque Size in a Blinded Manner.

Cross-sectional Parameter	LPS+PBS (N=11)	LPS+4ABAH (N=13)	P value
Cap-plaque thickness ratio (%)	12 ± 7	22 ± 13*	0.032
Cap thickness (μm)	27 ± 11	48 ± 30†	0.043
Necrotic core / Plaque (%)	37.7 ± 14.6	31.4 ± 15.6*	0.319
Plaque size $\times 10^3$ (μm^2)	123 ± 74	108 ± 52†‡	0.566

The data are shown as mean ± standard deviation.

* Distribution was normal and unpaired student T test was performed

†Distribution was not normal and Mann-Whitney U test was performed

‡ The comparisons across the groups were performed with the parameter normalized by perimeter of EEL.

Brachiocephalic trunk: BCT; External elastic lamina: EEL; Lipopolysaccharide: LPS; Phosphate buffered saline: PBS; 4-aminobenzoic acid hydrazide: 4-ABAH

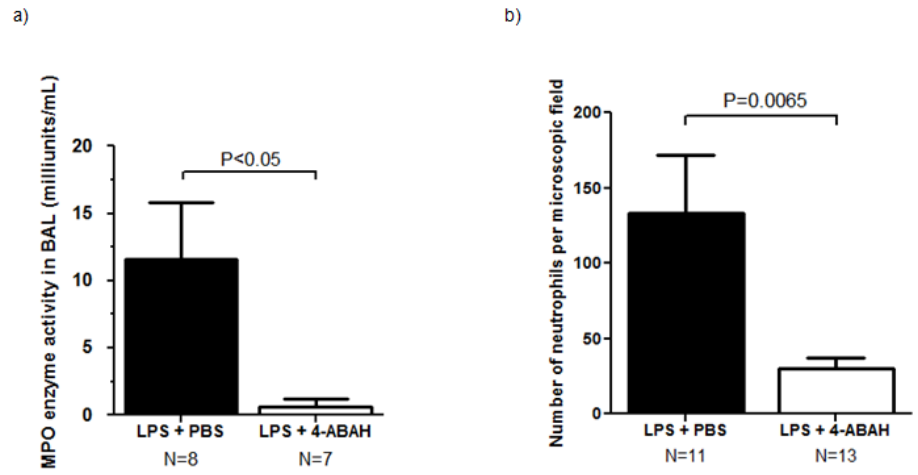

Figure 43: MPO Inhibition Reduced Neutrophil Infiltration into the Lungs.

a) MPO enzymatic activity in the bronchoalveolar lavage (BAL) of LPS-exposed mice treated with the MPO enzymatic inhibitor, 4-ABAH and PBS. LPS-exposed mice treated of 4-ABAH showed significantly less MPO activity in their BAL compared to LPS-exposed mice treated with PBS. b) Neutrophil counts in BAL was significantly lower in LPS-exposed mice treated of 4-ABAH compared to PBS.

5.3.3 Depletion of Circulating Neutrophil Prevented MPO Accumulation in the Plaques of LPS-exposed Mice

As previously described, MPO protein was detected in the necrotic core and was three times more abundant in the LPS 24h group than in the saline 24h group ($P<0.005$). MPO+ cells appeared firstly in the plaque edges beginning at 4 hours following LPS lung challenge and progressively accumulated in the core region over time. In LPS-ND mice, depletion of circulating neutrophils led to the abolition of MPO positivity in the plaques (<1% MPO positivity in LPS-ND 24h versus 6% in LPS-Ctrl 24h, $p= 0.03$). There were significantly higher levels of MPO signal detected in the center of atherosclerotic plaques 24 hours versus 4 hours post-instillation of LPS. However, depletion of circulating neutrophils in LPS-exposed mice

using anti-Ly6G antibodies significantly reduced the localization and accumulation of MPO in these plaques [Figure 44].

In wild-type mice exposed to LPS, the plasma MPO level was elevated starting at 4 hours post intratracheal LPS instillation [Figure 45]. The MPO level in the BAL fluid also became detectable 4 hours following LPS lung exposure and dramatically increased by 24 hours following LPS exposure [Figure 46].

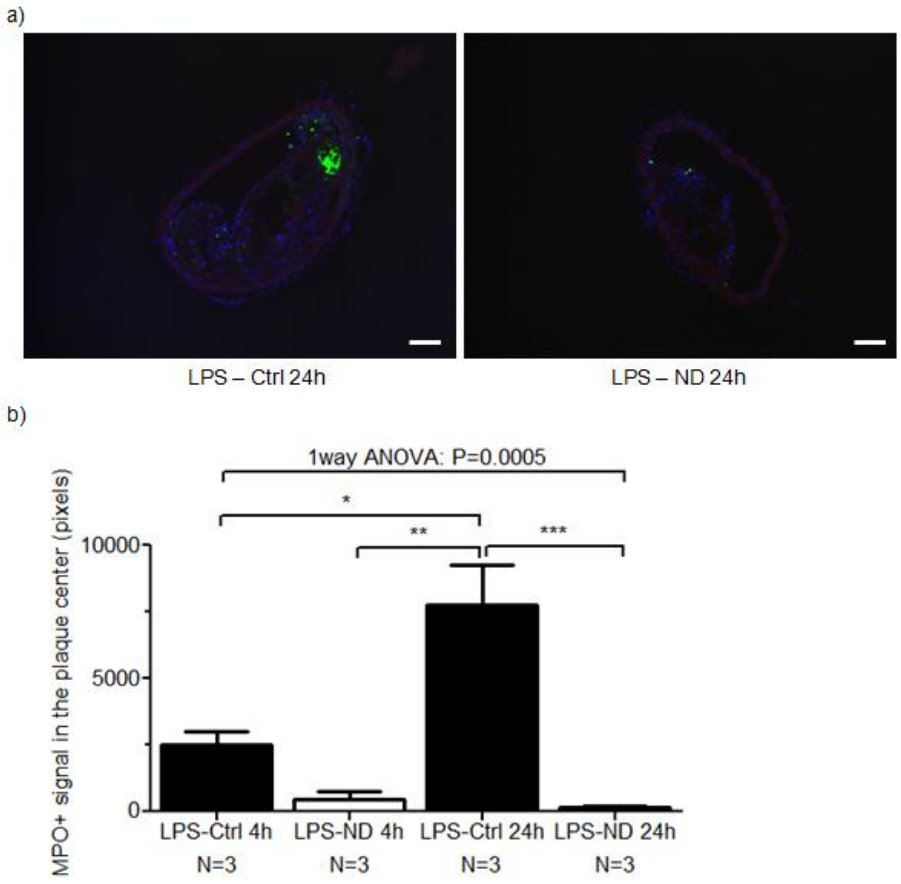

Figure 44: Neutrophil Depletion Reduced MPO Signals in the Atherosclerotic Plaques.

a) The 2D presentation of MPO Immunofluorescent stained atherosclerotic plaques in the BCT of LPS-exposed mice injected with neutrophil-depletion antibodies (LPS-ND; left) and that of LPS-exposed mice injected with control IgG antibodies (LPS-Ctrl; right). b) 2D quantitation of MPO in the atherosclerotic plaques in the early (4h) and later (24h) stages in the LPS-exposed mice injected with the antibodies. LPS-exposed mice injected with neutrophil depletion antibodies demonstrated significantly less MPO signals in their atherosclerotic in different stages, while LPS-exposed mice injected with control IgG antibodies demonstrated increased MPO signals in the later stage. Error bars represent SE.

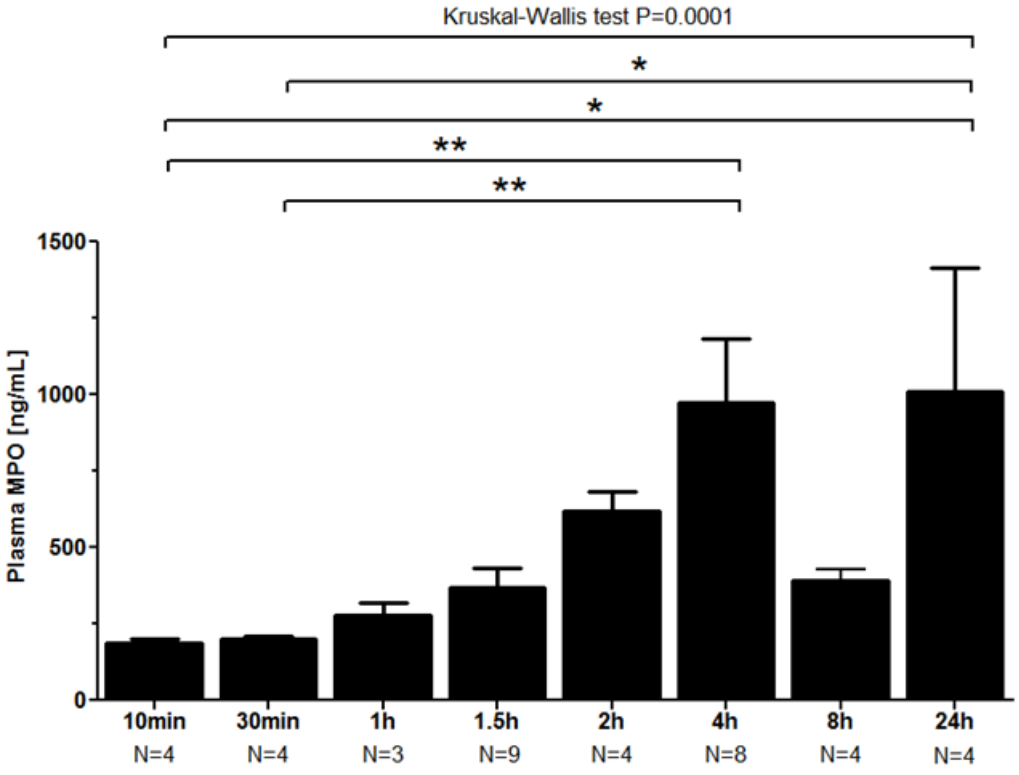

Figure 45: Dynamic Changes of Plasma MPO Level in the Wild-Type Mice after Intratracheal LPS Exposure.

Plasma MPO became detectable 1 hour after LPS instillation and increased significantly at 4 hours and 24 hours post LPS instillation. Error bars represent SE.

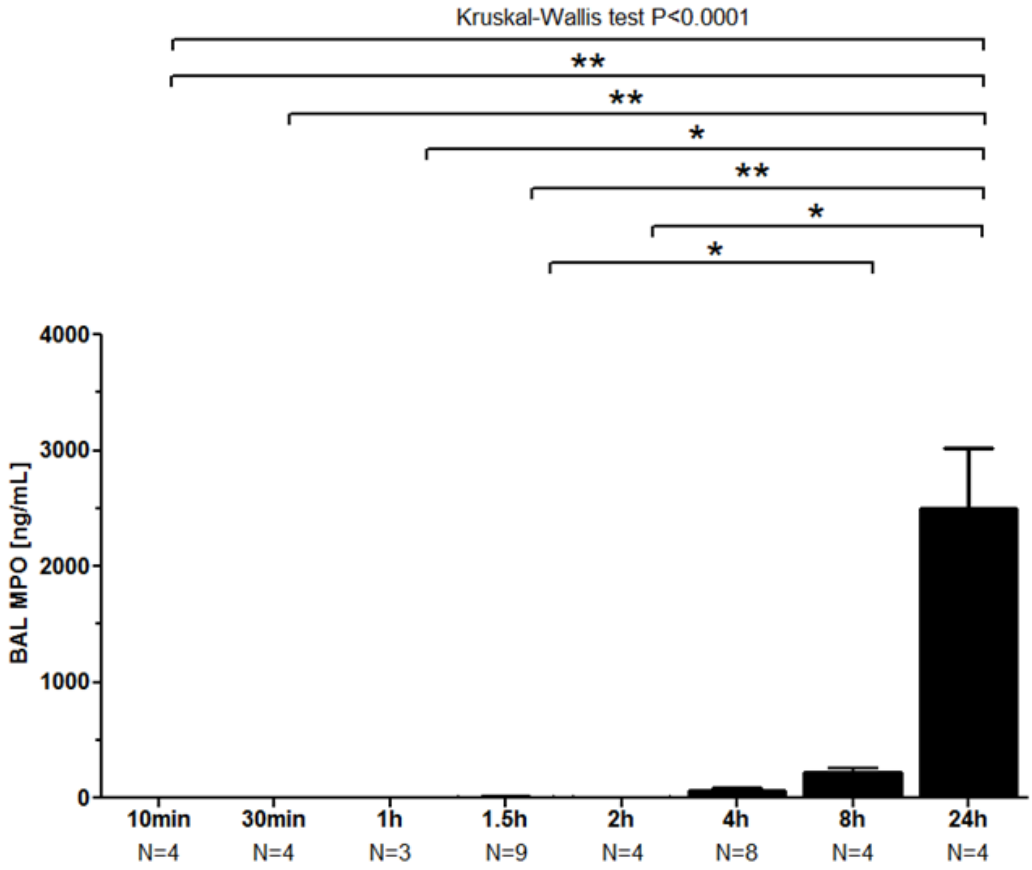

Figure 46: Dynamic Changes of MPO Level in Bronchoalveolar Lavage (BAL) of Wild-type Mice after Intratracheal LPS Exposure.

MPO level in BAL became detectable 4 hours after LPS instillation and increased significantly at 8 hours and 24 hours post LPS instillation. Error bars represented SE.

5.4 Discussions

We have previously reported the effects of LPS lung exposure on acute plaque rupture using this mouse model. However, the molecular mechanisms contributing to plaque rupture were not investigated. In the present study, the most important and novel findings were that there was heavy accumulation of MPO throughout atherosclerotic plaques (but most notably at the site of plaque rupture) acutely following lung injury induced by LPS, and that enzymatic inhibition of MPO using 4-ABAH mitigated the transition of stable plaques to vulnerable ones following LPS exposure. This effect was mediated by the attenuation of MPO/HOCl-mediated oxidation. We also found that depletion of circulating neutrophils prevented the accumulation of MPO in plaques, implicating neutrophils as the predominant source of MPO in this model. Furthermore, we used high resolution ex vivo OPT to detect plaque rupture and the distribution of MPO in addition to the traditional immunohistological evaluation to strengthen this study. Since treatments with 4-ABAH prevented plaque rupture and resulted in a more stable plaque phenotype, our data implicates a causal role of MPO in inducing plaque vulnerability. Together these data suggest that MPO might be a promising therapeutic target to prevent acute CV events related to lung inflammation.

Clinically, it is now well established that circulating MPO levels are associated with acute CV events among patients who present to emergency departments with chest pain (143, 145, 147, 148, 162, 163, 170, 173). In these and other studies, plasma MPO levels predicted the presence of plaque erosions, and importantly, the prognosis of patients who presented to hospitals with unstable angina (144, 146). Patients with elevated plasma levels of MPO at hospital presentation have two to three times the risk of death or nonfatal MI within the next 6 months compared to

patients who have low MPO levels (independent of other well-established risk factors for CVD, such as age, sex, and diabetes) (143, 144, 146). A genetic study also showed that individuals with partial or total deficiency of MPO were protected against CVD (148). Consistent with this observation, irradiated atherogenic mice that were repopulated with macrophages containing the human MPO gene developed atherosclerosis at a rate that was two times faster than control mice repopulated with wild-type mouse bone marrow (142). Although the role of MPO in atherogenesis had been previously shown, the pathological role of MPO in plaque rupture had not yet been investigated experimentally. In a previous study, we found that circulating neutrophils contributed to plaque destabilization related to LPS-induced lung inflammation in mice, confirming the concept of widespread neutrophilic inflammation during acute CV events (133). It is postulated that during CV events, neutrophils are activated and recruited to the coronary arteries (and other vessels containing atheroma) where they release their contents of azurophilic (primary) granules, amplifying the original inflammatory signal (133, 139, 140, 142-148, 161-164, 170, 173-178). Based on this concept, we hypothesized that MPO could be localized to atherosclerotic plaques following LPS lung exposure, and that MPO-mediated oxidation would be a contributor to plaque vulnerability. In this study we observed that MPO, stored in the primary granules of neutrophils, is accumulated in atherosclerotic plaque following LPS lung exposure and is a molecular contributor to plaque vulnerability.

Studies have shown that MPO is the most abundant protein in neutrophils, accounting for up to 5% of their dry mass (136). In humans, it is also present in monocytes at lower levels. The ability of monocytes to produce this protein decreases during maturation into tissue macrophages. In humans, MPO can be found in atherosclerotic plaques, especially at the site of plaque rupture

(135, 137-140, 142, 144, 161, 176, 177). Pathologic studies have shown that MPO and MPO-modified proteins are co-localized to the subendothelium of vulnerable plaques at the sites of plaque fissures, as well as to superficial erosions in patients who experienced sudden death from an acute CV event (144). During an inflammatory episode, several possible mechanisms related to the MPO pathway might cause acute plaque destabilization and rupture [Figure 47]. First, MPO could be released at vascular tissue and it could utilize chloride as a co-substrate in a reaction with hydrogen peroxide (H_2O_2). This reaction will generate chlorinating oxidants such as hypochlorous acid (HOCl), which could modify DNA, proteins, and lipids. (175) Second, the vascular endothelium is another important and vulnerable target of MPO. MPO could catalytically consume nitric oxide (NO) to generate NO-derived oxidants, such as ONOO- and lead to vessel damage and endothelial dysfunction (177). Third, at high concentrations, MPO can also promote endothelial cell apoptosis by down-regulating Bcl-2, thereby activating cytochrome c release (179). The loss of endothelial cells and smooth muscle cells in turn can lead to the thinning of the fibrous cap, the development of superficial erosions on the plaque, and in certain cases plaque fissuring and rupture (177). Fourth, MPO could also facilitate plaque rupture by activating metalloproteinases (MMPs). Studies have shown that MPO/ HOCl are able to activate MMPs by oxygenating the cysteine switch domain of these enzymes (176). Upon activation, MMPs can degrade extra-cellular matrix (collagen and elastin), damage cap structure, and injure the endothelium (176, 179, 180). Past studies have shown that over-expression of the auto-activating form of MMP-9 in mouse macrophages, which enhance elastin degradation, can significantly increase the risk of plaque disruption of advanced atherosclerotic lesions in ApoE KO mice (76). Administration of a selective MMP-12 (metalloelastase) inhibitor by implanting an osmotic minipump subcutaneously also retards atherosclerotic plaque development in ApoE

KO mice (181). It is well-established that mice with dysfunctional and fragmented elastin develop vulnerable plaques that lead to MI, stroke, and sudden death. However, inhibitors targeting MMPs triggers a serious side effect (musculoskeletal syndrome) and the results of clinical trials have been disappointing due to low-specificity (182). Treatment targeting the MPO enzymatic pathway that regulates downstream selective groups of MMPs during inflammatory episodes might be an alternative route to reduce CV burden. We had previously reported the observation of MMP-9 at the site of the plaque disruption in this model [Figure 24]. Future studies that investigate the interaction between MPO and selective MMPs in causing plaque rupture would map out more detailed mechanisms of plaque destabilization and give insight into the generation of selective inhibitors targeting specific pathways (178).

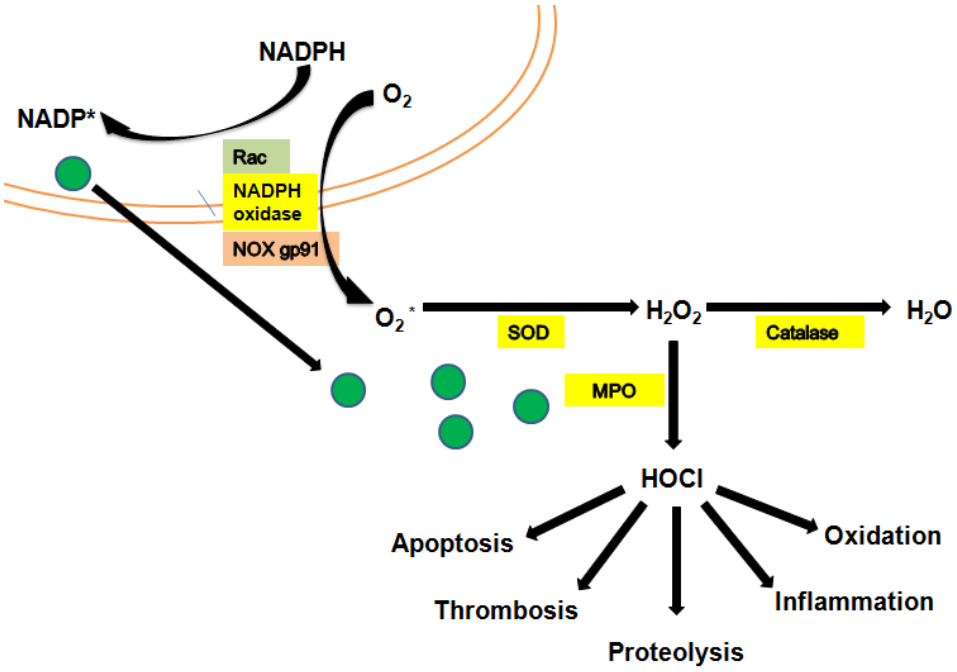

Figure 47: Postulated MPO and HOCl Mediated Effect that Cause Plaque Destabilization.

Future studies using different specific inhibitors or conditional gene knockout mice could be carried out to investigate the mechanisms of plaque destabilization of MPO dependent pathway.

There were several limitations to this study. First, 4-ABAH is a safe and potent MPO inhibitor for animal research but might be potentially toxic to humans at higher doses. Therefore, other MPO specific inhibitors suitable for human usage will be needed for future translational studies (126, 183). Second, it is well known that when 4-ABAH interacts with MPO, MPO can bind and oxidize 4-ABAH to a radical form. This compound then reduces the heme component of MPO to its ferrous intermediate to cause irreversible MPO enzymatic inactivation (in the presence of oxygen) (126, 171, 184). Since post-treatment of 4-ABAH prevented plaque rupture and resulted in a more stable plaque phenotype, our data implicates a causal role of MPO in inducing plaque vulnerability. 4-ABAH is highly selective for MPO over other heme-peroxidases and has shown high selectivity to MPO during LPS-induced lung inflammation in mice (126), but it may still have unknown off-target effects in humans.

A third limitation to our study is that we did not use ApoE and MPO double knockout mice to confirm our findings. While these mice are viable and can be generated, they have several concerns that make them unsuitable for this study. First, the MPO is an important developmental gene and as such these mice demonstrate certain innate developmental impairments, and harbor other genetic and epigenetic effects that would complicate the phenotype (185-188). Second, studies showed that knocking out the MPO gene altered the progression of atherosclerosis and yielded conflicting plaque phenotypes. Therefore, the plaques that developed after WD would be inconsistent and difficult to characterize (141, 189). This in turn may lead to different developmental stages of atherosclerotic plaques between MPO knockout mice and control mice, before induction of acute lung inflammation. Therefore, the resulting interpretation would be

affected by developmental factors, but not LPS-induced inflammation alone. Third, experimental models to investigate the role of MPO in the pathogenesis of CV events have been hampered by some major differences in the way in which MPO is regulated in mice compared to humans. For instance, in humans, it is known that foamy macrophages in atherosclerotic lesions are regulated by peroxisome proliferator-activated receptor γ (PPARγ), a transcription factor that is involved in inflammatory responses and scavenger receptor expression. When human macrophages are treated with PPARγ ligands, MPO expression is up-regulated by ~20-fold. Conversely, in mice, the MPO gene lacks the PPARγ binding site. Because low density lipoprotein (LDL) upregulates PPARγ, the lack of responsiveness of MPO to PPARγ in mice may in part explain the absence of MPO in the atherosclerotic lesions of experimental models of atherosclerosis (141, 190).

Other groups successfully used transgenic mice that are made to express human MPO (e.g. −463G/A alleles) and found that these mice demonstrate increased burden of atherosclerosis, along with heavy deposition of MPO in the plaques (141, 142). Nevertheless, their result can only explain the role of MPO in plaque progression at early stage. Only comparing the atheroma developmental stage between mice that express human MPO and control mice could not address the effect of acute localization of MPO from neutrophils in causing acute plaque rupture during an acute inflammatory episode and would underestimate the potential value of targeting the MPO/HOCl pathway as a therapeutic target for acute CV events. Therefore, we chose to use a simple animal model with the capability of inducing MPO in response to episodes of lung inflammation (to mimic observations in humans) and demonstrated the subsequent spontaneous plaque rupture, without transgenic modifications, or surgical induction of plaque vulnerability to test our hypothesis. This model is physiologically and clinically relevant because it is well-

established that acute LPS-induced lung inflammation up-regulates MPO in mice (126), and acute respiratory infection in humans is known as a trigger for acute CVD (90, 92-94, 97). Taking into account the limitations mentioned above, our study demonstrated that MPO is localized in the vulnerable atherosclerotic plaques following LPS lung exposure. Furthermore, we showed that MPO enzymatic inhibition could reduce plaque vulnerability related to LPS lung exposure.

5.5 Conclusion

In conclusion, our data are consistent with the reported human data in the literature. Although the causes of plaque vulnerability and acute CVDs are likely multi-factorial, our results suggest that MPO/HOCl might be one of the key pathways that not only chronically promotes plaque vulnerability, but under certain acute inflammatory episodes, would promote plaque erosion and rupture that results in athero-thrombotic complications. Treatments targeting the MPO/HOCl pathway could be beneficial in some groups of patients that have a high risk of CVD with high MPO activity in their plasma and atherosclerotic plaques. New diagnostic techniques for MPO activity measurement and CV imaging would be important in monitoring and treating acute CVDs related to lung inflammation. The detailed molecular mechanisms of plaque rupture and erosion should be further elucidated in the future by generating properly-validated gene knockout animals and therapeutically screening specific molecular inhibitors using proper plaque rupture models.

Chapter 6: Conclusion

In this research, we successfully established a novel mouse model of plaque vulnerability by intratracheal LPS administration, which mimics the observation in humans that acute respiratory tract infection and inflammation can increase the risk of MI and stroke. By using this model, we successfully validated the role of neutrophils and MPO in the process of atherosclerotic plaque destabilization under the context of lung inflammatory. Furthermore, we combined the 3D whole-mount MPO immunofluorescent staining and optical projection tomography to strengthen the traditional 2D histological approaches and eliminated the concerns of artifact and plaque disruption due to histological processing. This animal model and subsequent evidence generated in these studies may lead to future investigations that would ultimately result in better understanding of the molecule mechanisms of plaque rupture and erosion and facilitate the identification of therapeutic targets to ease the serious acute CV events.

In Chapter 1, we reviewed the motivation for this research and discussed the importance of this study in filling the current knowledge gap in plaque vulnerability research based upon important human and animal data in the literature. In Chapter 2, we provided our experimental approaches for validating our working hypothesis that lung exposure to LPS would cause acute atherosclerotic plaque destabilization in mice. Furthermore, neutrophils and MPO might be important cellular and molecular contributors to this process, respectively. In Chapter 3, we established a robust and minimally invasive animal model of plaque vulnerability by intratracheal LPS administration. Through careful 2D and 3D evaluation of the atherosclerotic plaques, we found that a single intratracheal administration of LPS aerosol particles into mouse lungs caused the stable atheromatous plaques to become vulnerable within 24 hours of exposure,

demonstrating the feature of intraplaque hemorrhage and thrombus. At 8 hours post-instillation, plaques vulnerability signals including hemorrhage and thrombus formation could be detected and quantified by high resolution OPT. However, administration of the same dose of LPS intraperitoneally failed to induce these acute changes, despite causing greater rises in serum LPS levels and more end-organ damage in the liver and kidneys. These findings highlight the tight connectivity of acute lung inflammation and plaque destabilization and rupture. As 100% of total cardiac output flows through the lungs, the inflammatory condition of the lung could amplify the inflammation downstream in the arteries (as the inflammatory cells in the lungs could amplify local inflammatory processes and make them into an intense systemic inflammation). These results are consistent with clinical observations in humans (90-98, 148, 174, 175, 191). Importantly, we provided the first experimental evidence of the comparison of intratracheal versus intraperitoneal LPS administration in causing acute plaque vulnerability in mice. Our results showed that systemic inflammatory response induced by lung injury may be unique with regard to its downstream effect on blood vessels. This concept needs further evaluation.

In chapter 4, we showed that the lung inflammation and plaque vulnerability induced by intratracheal LPS challenge can be attenuated by the depletion of circulating neutrophils using the specific anti-Ly6g antibodies. This revealed the important role of circulating neutrophils as a major cellular link between acute lung inflammation and acute plaque destabilization. It is generally believed that systemic neutrophilic inflammations are important in the cause of plaque vulnerability (25, 133, 139, 140, 161, 163-165, 167, 174, 179, 192-197) and this study has provided important *in vivo* experimental validation. In parts, data in Chapter 3 and 4 has been published (132).

In Chapter 5, we reported the development of 3D whole-mount immunofluorescent staining combined with OPT for 3D detection of MPO in the atherosclerotic plaques. We found there was a rapid and heavy accumulation of MPO throughout atherosclerotic plaques (but most notably at the site of plaque rupture) within 8 hours following intratracheal LPS instillation. Moreover, enzymatic inhibition of MPO using 4-ABAH mitigated the transition of stable plaques to vulnerable ones following LPS exposure. This effect was mediated by the attenuation of MPO/HOCl related oxidation. We also found that depletion of circulating neutrophils prevented the accumulation of MPO in plaques, implicating neutrophils as the predominant source of MPO in this model. This study provided the first *in vivo* experimental evidence that supported the casual-effect role of MPO in acute plaque destabilization.

Our results are consistent with concept of widespread neutrophilic inflammation during acute CV events (133). It is postulated that during CV events, neutrophils are activated and recruited to the coronary arteries (and other vessels containing atheroma) where they release their contents of azurophilic (primary) granules, amplifying the original inflammatory signal. Based on this concept, we hypothesized that neutrophils and MPO could be localized to atherosclerotic plaques following LPS induced lung inflammation, and that MPO-mediated oxidation would be an important contributor to plaque vulnerability. In this study, we successfully observed that MPO, stored in the primary granules of neutrophils, is accumulated in atherosclerotic plaque following LPS lung exposure and is a molecular contributor to plaque destabilization [Figure 48].

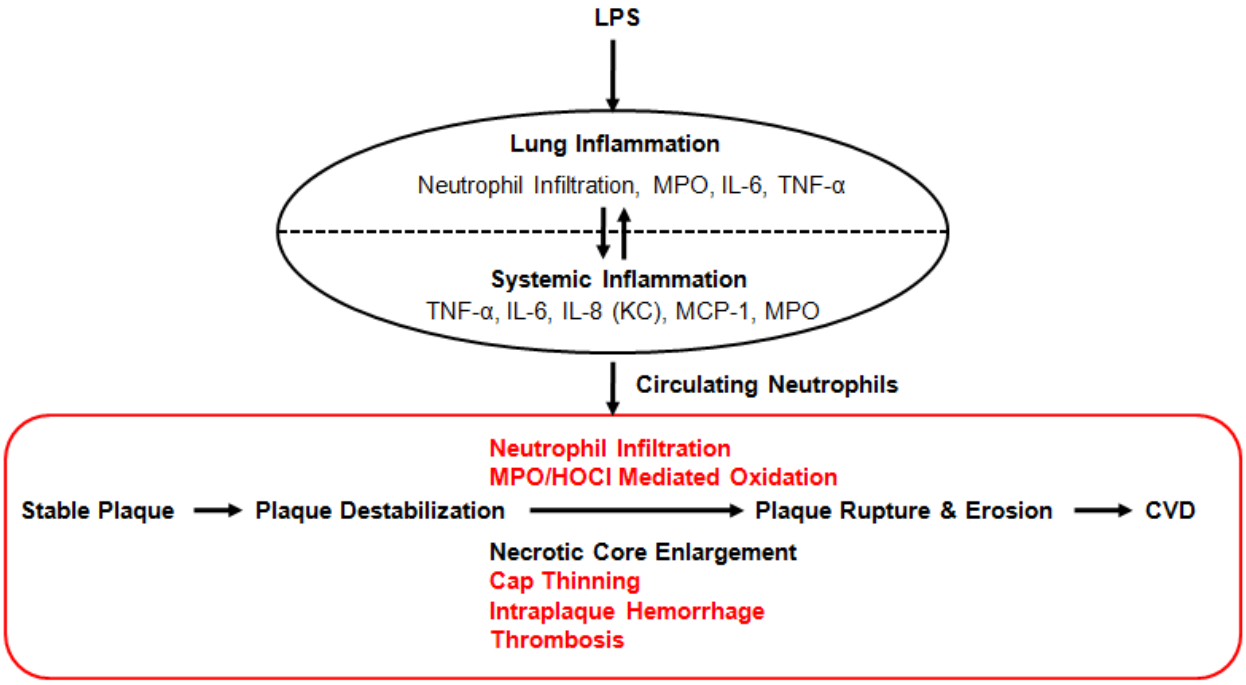

Figure 48: Conceptual Diagram of Plaque Destabilization Induced by LPS Lung Exposure.

We recognize several limitations to this study. First, we have used LPS as a convenient trigger to induce lung injury and inflammation, simulating an acute lung infection with gram negative bacteria. Future studies should explore more common human pathogens, such as respiratory viruses or bacteria that would enhance the application and generalizability of this model to clinical conditions. However, the trade-off could be a more complicated model of lung inflammation and host responses that may be difficult to fully characterize. Second, in this model we showed that circulating neutrophils contribute to the LPS-induced acute destabilization and rupture of plaques. However, it should be noted that we did not identify the mediators responsible for the activation and recruitment of neutrophils into the plaques following LPS stimulation. Further research will be required to unravel the molecular underpinnings of this process. Third, 4-ABAH is a safe and potent MPO inhibitor for animal research, but might be

potentially toxic to humans at higher doses. Therefore, other MPO specific inhibitors suitable for human usage will be needed for future translational studies (183). Fourth, although 4-ABAH is highly selective for MPO over other heme-peroxidases and has shown high selectivity to MPO during LPS-induced lung inflammation in mice (126), we cannot eliminate the possible off-target effects. Fifth, we did not use ApoE and MPO double knockout mice to confirm our findings. While these mice are viable and can be generated, they have several critical concerns regarding developmental abnormality and controversial plaque phenotypes that make them unsuitable for this study (141, 188-190). For future study, generation of conditional MPO KO mice using Cre-Lox or CRISPR/Cas9 technologies along with GFP tagged MPO would upgrade the research to the next phase. Lastly, we did not investigate the interactions between MPO and various MMPs (or other mediators) in atherosclerotic plaques, which required development of multiple specific inhibitors and generation of gene knockout models beyond the purview of this study. Further investigations would be required to understand these detail mechanisms.

Overall, our model is consistent with the human data reported in the literature (90-98, 148, 174, 175, 191). Although the causes of plaque vulnerability and acute CVD are likely multi-factorial (69, 198, 199), our results suggest that neutrophils and MPO/HOCl might be one of the key pathways that not only chronically promote plaque vulnerability, but under certain acute inflammatory episodes, would promote plaque erosion and rupture that results in athero-thrombotic complications. Treatments targeting the MPO/HOCl pathway could be beneficial in some groups of patients that have a high risk of CVD with high MPO activity in their plasma and atherosclerotic plaques. New diagnostic techniques for MPO activity measurement and CV imaging would be important in monitoring and treating acute CVDs related to lung

inflammation. The detailed molecular mechanisms of plaque rupture and erosion should be further elucidated in the future by generating properly-validated gene knockout animals and therapeutically screening specific molecular inhibitors using proper plaque rupture models.

Bibliography

1. Mendis S, Davis S, Norrving B. Organizational update: the world health organization global status report on noncommunicable diseases 2014; one more landmark step in the combat against stroke and vascular disease. Stroke. 2015;46(5):e121-2.

2. Lim SS, Gaziano TA, Gakidou E, Reddy KS, Farzadfar F, Lozano R, et al. Prevention of cardiovascular disease in high-risk individuals in low-income and middle-income countries: health effects and costs. Lancet. 2007;370(9604):2054-62.

3. Smith SC, Jr., Collins A, Ferrari R, Holmes DR, Jr., Logstrup S, McGhie DV, et al. Our time: a call to save preventable death from cardiovascular disease (heart disease and stroke). J Am Coll Cardiol. 2012;60(22):2343-8.

4. Mozaffarian D, Benjamin EJ, Go AS, Arnett DK, Blaha MJ, Cushman M, et al. Heart disease and stroke statistics--2015 update: a report from the American Heart Association. Circulation. 2015;131(4):e29-322.

5. Ordunez P, Prieto-Lara E, Pinheiro Gawryszewski V, Hennis AJ, Cooper RS. Premature Mortality from Cardiovascular Disease in the Americas - Will the Goal of a Decline of "25% by 2025" be Met? PLoS One. 2015;10(10):e0141685.

6. Ross R, Harker L. Hyperlipidemia and atherosclerosis. Science. 1976;193(4258):1094-100.

7. Libby P. Inflammation in atherosclerosis. Nature. 2002;420(6917):868-74.

8. Duewell P, Kono H, Rayner KJ, Sirois CM, Vladimer G, Bauernfeind FG, et al. NLRP3 inflammasomes are required for atherogenesis and activated by cholesterol crystals. Nature. 2010;464(7293):1357-61.

9. Libby P, Warner SJ, Friedman GB. Interleukin 1: a mitogen for human vascular smooth muscle cells that induces the release of growth-inhibitory prostanoids. J Clin Invest. 1988;81(2):487-98.

10. Loppnow H, Libby P. Proliferating or interleukin 1-activated human vascular smooth muscle cells secrete copious interleukin 6. J Clin Invest. 1990;85(3):731-8.

11. Saren P, Welgus HG, Kovanen PT. TNF-alpha and IL-1beta selectively induce expression of 92-kDa gelatinase by human macrophages. J Immunol. 1996;157(9):4159-65.

12. Hermansson A, Johansson DK, Ketelhuth DF, Andersson J, Zhou X, Hansson GK. Immunotherapy with tolerogenic apolipoprotein B-100-loaded dendritic cells attenuates atherosclerosis in hypercholesterolemic mice. Circulation. 2011;123(10):1083-91.

13. Hermansson A, Ketelhuth DF, Strodthoff D, Wurm M, Hansson EM, Nicoletti A, et al. Inhibition of T cell response to native low-density lipoprotein reduces atherosclerosis. J Exp Med. 2010;207(5):1081-93.

14. Stemme S, Faber B, Holm J, Wiklund O, Witztum JL, Hansson GK. T lymphocytes from human atherosclerotic plaques recognize oxidized low density lipoprotein. Proc Natl Acad Sci U S A. 1995;92(9):3893-7.

15. Frostegard J, Ulfgren AK, Nyberg P, Hedin U, Swedenborg J, Andersson U, et al. Cytokine expression in advanced human atherosclerotic plaques: dominance of pro-inflammatory (Th1) and macrophage-stimulating cytokines. Atherosclerosis. 1999;145(1):33-43.

16. Amento EP, Ehsani N, Palmer H, Libby P. Cytokines and growth factors positively and negatively regulate interstitial collagen gene expression in human vascular smooth muscle cells. Arterioscler Thromb. 1991;11(5):1223-30.

17. Hansson GK, Hellstrand M, Rymo L, Rubbia L, Gabbiani G. Interferon gamma inhibits both proliferation and expression of differentiation-specific alpha-smooth muscle actin in arterial smooth muscle cells. J Exp Med. 1989;170(5):1595-608.

18. Choi JH, Cheong C, Dandamudi DB, Park CG, Rodriguez A, Mehandru S, et al. Flt3 signaling-dependent dendritic cells protect against atherosclerosis. Immunity. 2011;35(5):819-31.

19. Subramanian M, Thorp E, Hansson GK, Tabas I. Treg-mediated suppression of atherosclerosis requires MYD88 signaling in DCs. J Clin Invest. 2013;123(1):179-88.

20. Kaartinen M, Penttila A, Kovanen PT. Mast cells of two types differing in neutral protease composition in the human aortic intima. Demonstration of tryptase- and tryptase/chymase-containing mast cells in normal intimas, fatty streaks, and the shoulder region of atheromas. Arterioscler Thromb. 1994;14(6):966-72.

21. Myoishi M, Hao H, Minamino T, Watanabe K, Nishihira K, Hatakeyama K, et al. Increased endoplasmic reticulum stress in atherosclerotic plaques associated with acute coronary syndrome. Circulation. 2007;116(11):1226-33.

22. Libby P, Tabas I, Fredman G, Fisher EA. Inflammation and its resolution as determinants of acute coronary syndromes. Circ Res. 2014;114(12):1867-79.

23. Thorp E, Cui D, Schrijvers DM, Kuriakose G, Tabas I. Mertk receptor mutation reduces efferocytosis efficiency and promotes apoptotic cell accumulation and plaque necrosis in atherosclerotic lesions of apoe-/- mice. Arterioscler Thromb Vasc Biol. 2008;28(8):1421-8.

24. Tabas I. Consequences and therapeutic implications of macrophage apoptosis in atherosclerosis: the importance of lesion stage and phagocytic efficiency. Arterioscler Thromb Vasc Biol. 2005;25(11):2255-64.

25. Serhan CN, Fredman G, Yang R, Karamnov S, Belayev LS, Bazan NG, et al. Novel proresolving aspirin-triggered DHA pathway. Chem Biol. 2011;18(8):976-87.

26. Ait-Oufella H, Pouresmail V, Simon T, Blanc-Brude O, Kinugawa K, Merval R, et al. Defective mer receptor tyrosine kinase signaling in bone marrow cells promotes apoptotic cell accumulation and accelerates atherosclerosis. Arterioscler Thromb Vasc Biol. 2008;28(8):1429-31.

27. Zheng Y, Gardner SE, Clarke MC. Cell death, damage-associated molecular patterns, and sterile inflammation in cardiovascular disease. Arterioscler Thromb Vasc Biol. 2011;31(12):2781-6.

28. Lin J, Li H, Yang M, Ren J, Huang Z, Han F, et al. A role of RIP3-mediated macrophage necrosis in atherosclerosis development. Cell Rep. 2013;3(1):200-10.

29. Kiousis DE, Rubinigg SF, Auer M, Holzapfel GA. A methodology to analyze changes in lipid core and calcification onto fibrous cap vulnerability: the human atherosclerotic carotid bifurcation as an illustratory example. J Biomech Eng. 2009;131(12):121002.

30. Stary HC, Chandler AB, Glagov S, Guyton JR, Insull W, Jr., Rosenfeld ME, et al. A definition of initial, fatty streak, and intermediate lesions of atherosclerosis. A report from the Committee on Vascular Lesions of the Council on Arteriosclerosis, American Heart Association. Arterioscler Thromb. 1994;14(5):840-56.

31. Stary HC, Chandler AB, Dinsmore RE, Fuster V, Glagov S, Insull W, Jr., et al. A definition of advanced types of atherosclerotic lesions and a histological classification of atherosclerosis. A report from the Committee on Vascular Lesions of the Council on Arteriosclerosis, American Heart Association. Arterioscler Thromb Vasc Biol. 1995;15(9):1512-31.

32. Virmani R, Kolodgie FD, Burke AP, Farb A, Schwartz SM. Lessons from sudden coronary death: a comprehensive morphological classification scheme for atherosclerotic lesions. Arterioscler Thromb Vasc Biol. 2000;20(5):1262-75.

33. Cai JM, Hatsukami TS, Ferguson MS, Small R, Polissar NL, Yuan C. Classification of human carotid atherosclerotic lesions with in vivo multicontrast magnetic resonance imaging. Circulation. 2002;106(11):1368-73.

34. Sanz J, Fayad ZA. Imaging of atherosclerotic cardiovascular disease. Nature. 2008;451(7181):953-7.

35. Schaar JA, Muller JE, Falk E, Virmani R, Fuster V, Serruys PW, et al. Terminology for high-risk and vulnerable coronary artery plaques. Report of a meeting on the vulnerable plaque, June 17 and 18, 2003, Santorini, Greece. Eur Heart J. 2004;25(12):1077-82.

36. Virmani R, Burke AP, Farb A, Kolodgie FD. Pathology of the vulnerable plaque. J Am Coll Cardiol. 2006;47(8 Suppl):C13-8.

37. Finn AV, Nakano M, Narula J, Kolodgie FD, Virmani R. Concept of vulnerable/unstable plaque. Arterioscler Thromb Vasc Biol. 2010;30(7):1282-92.

38. Davies MJ, Thomas A. Thrombosis and acute coronary-artery lesions in sudden cardiac ischemic death. N Engl J Med. 1984;310(18):1137-40.

39. Farb A, Burke AP, Tang AL, Liang TY, Mannan P, Smialek J, et al. Coronary plaque erosion without rupture into a lipid core. A frequent cause of coronary thrombosis in sudden coronary death. Circulation. 1996;93(7):1354-63.

40. Hansson GK, Libby P, Tabas I. Inflammation and plaque vulnerability. J Intern Med. 2015;278(5):483-93.

41. Spagnoli LG, Bonanno E, Sangiorgi G, Mauriello A. Role of inflammation in atherosclerosis. J Nucl Med. 2007;48(11):1800-15.

42. Davies MJ, Thomas AC. Plaque fissuring--the cause of acute myocardial infarction, sudden ischaemic death, and crescendo angina. Br Heart J. 1985;53(4):363-73.

43. Falk E. Morphologic features of unstable atherothrombotic plaques underlying acute coronary syndromes. Am J Cardiol. 1989;63(10):114e-20e.

44. Hong MK, Mintz GS, Lee CW, Kim YH, Lee SW, Song JM, et al. Comparison of coronary plaque rupture between stable angina and acute myocardial infarction: a three-vessel intravascular ultrasound study in 235 patients. Circulation. 2004;110(8):928-33.

45. Rosa GM, Bauckneht M, Masoero G, Mach F, Quercioli A, Seitun S, et al. The vulnerable coronary plaque: update on imaging technologies. Thromb Haemost. 2013;110(4):706-22.

46. Gutierrez-Chico JL, Alegria-Barrero E, Teijeiro-Mestre R, Chan PH, Tsujioka H, de Silva R, et al. Optical coherence tomography: from research to practice. Eur Heart J Cardiovasc Imaging. 2012;13(5):370-84.

47. Pedrigi RM, de Silva R, Bovens SM, Mehta VV, Petretto E, Krams R. Thin-cap fibroatheroma rupture is associated with a fine interplay of shear and wall stress. Arterioscler Thromb Vasc Biol. 2014;34(10):2224-31.

48. Newby AC. Metalloproteinases promote plaque rupture and myocardial infarction: A persuasive concept waiting for clinical translation. Matrix Biol. 2015;44-46:157-66.

49. Vilahur G, Padro T, Badimon L. Atherosclerosis and thrombosis: insights from large animal models. J Biomed Biotechnol. 2011;2011:907575.

50. Kita T, Brown MS, Watanabe Y, Goldstein JL. Deficiency of low density lipoprotein receptors in liver and adrenal gland of the WHHL rabbit, an animal model of familial hypercholesterolemia. Proc Natl Acad Sci U S A. 1981;78(4):2268-72.

51. Ishibashi S, Brown MS, Goldstein JL, Gerard RD, Hammer RE, Herz J. Hypercholesterolemia in low density lipoprotein receptor knockout mice and its reversal by adenovirus-mediated gene delivery. J Clin Invest. 1993;92(2):883-93.

52. Maeda N. Development of apolipoprotein E-deficient mice. Arterioscler Thromb Vasc Biol. 2011;31(9):1957-62.

53. Rekhter MD, Hicks GW, Brammer DW, Work CW, Kim JS, Gordon D, et al. Animal model that mimics atherosclerotic plaque rupture. Circ Res. 1998;83(7):705-13.

54. Rekhter MD. How to evaluate plaque vulnerability in animal models of atherosclerosis? Cardiovasc Res. 2002;54(1):36-41.

55. Matoba T, Sato K, Egashira K. Mouse models of plaque rupture. Curr Opin Lipidol. 2013;24(5):419-25.

56. Rosenfeld ME, Polinsky P, Virmani R, Kauser K, Rubanyi G, Schwartz SM. Advanced atherosclerotic lesions in the innominate artery of the ApoE knockout mouse. Arterioscler Thromb Vasc Biol. 2000;20(12):2587-92.

57. Johnson JL, Jackson CL. Atherosclerotic plaque rupture in the apolipoprotein E knockout mouse. Atherosclerosis. 2001;154(2):399-406.

58. Schwartz SM, Galis ZS, Rosenfeld ME, Falk E. Plaque rupture in humans and mice. Arterioscler Thromb Vasc Biol. 2007;27(4):705-13.

59. Reddick RL, Zhang SH, Maeda N. Aortic atherosclerotic plaque injury in apolipoprotein E deficient mice. Atherosclerosis. 1998;140(2):297-305.

60. Sasaki T, Kuzuya M, Nakamura K, Cheng XW, Shibata T, Sato K, et al. A simple method of plaque rupture induction in apolipoprotein E-deficient mice. Arterioscler Thromb Vasc Biol. 2006;26(6):1304-9.

61. Rekhter MD, Hicks GW, Brammer DW, Hallak H, Kindt E, Chen J, et al. Hypercholesterolemia causes mechanical weakening of rabbit atheroma : local collagen loss as a prerequisite of plaque rupture. Circ Res. 2000;86(1):101-8.

62. von der Thusen JH, van Vlijmen BJ, Hoeben RC, Kockx MM, Havekes LM, van Berkel TJ, et al. Induction of atherosclerotic plaque rupture in apolipoprotein E-/- mice after adenovirus-mediated transfer of p53. Circulation. 2002;105(17):2064-70.

63. Eitzman DT, Westrick RJ, Xu Z, Tyson J, Ginsburg D. Hyperlipidemia promotes thrombosis after injury to atherosclerotic vessels in apolipoprotein E-deficient mice. Arterioscler Thromb Vasc Biol. 2000;20(7):1831-4.

64. Sun X, Cao W, Cui J, Wang L, Ma L, Wang T, et al. An animal model of atherosclerotic plaque disruption and thrombosis in rabbit using pharmacological triggering to plaques induced by perivascular collar placement. Cardiovasc Pathol. 2013;22(4):264-9.

65. Nakamura M, Abe S, Kinukawa N. Aortic medial necrosis with or without thrombosis in rabbits treated with Russell's viper venom and angiotensin II. Atherosclerosis. 1997;128(2):149-56.

66. Constantinides P, Chakravarti RN. Rabbit arterial thrombosis production by systemic procedures. Arch Pathol. 1961;72:197-208.

67. Caligiuri G, Levy B, Pernow J, Thoren P, Hansson GK. Myocardial infarction mediated by endothelin receptor signaling in hypercholesterolemic mice. Proc Natl Acad Sci U S A. 1999;96(12):6920-4.

68. Roth L, Rombouts M, Schrijvers DM, Lemmens K, De Keulenaer GW, Martinet W, et al. Chronic intermittent mental stress promotes atherosclerotic plaque vulnerability, myocardial infarction and sudden death in mice. Atherosclerosis. 2015;242(1):288-94.

69. Ni M, Wang Y, Zhang M, Zhang PF, Ding SF, Liu CX, et al. Atherosclerotic plaque disruption induced by stress and lipopolysaccharide in apolipoprotein E knockout mice. Am J Physiol Heart Circ Physiol. 2009;296(5):H1598-606.

70. Prescott MF, McBride CH, Hasler-Rapacz J, Von Linden J, Rapacz J. Development of complex atherosclerotic lesions in pigs with inherited hyper-LDL cholesterolemia bearing mutant alleles for apolipoprotein B. Am J Pathol. 1991;139(1):139-47.

71. Shi ZS, Feng L, He X, Ishii A, Goldstine J, Vinters HV, et al. Vulnerable plaque in a Swine model of carotid atherosclerosis. AJNR Am J Neuroradiol. 2009;30(3):469-72.

72. Brown AJ, Teng Z, Evans PC, Gillard JH, Samady H, Bennett MR. Role of biomechanical forces in the natural history of coronary atherosclerosis. Nat Rev Cardiol. 2016;13(4):210-20.

73. Cheng C, Tempel D, van Haperen R, van der Baan A, Grosveld F, Daemen MJ, et al. Atherosclerotic lesion size and vulnerability are determined by patterns of fluid shear stress. Circulation. 2006;113(23):2744-53.

74. Cheng C, Tempel D, van Haperen R, de Boer HC, Segers D, Huisman M, et al. Shear stress-induced changes in atherosclerotic plaque composition are modulated by chemokines. J Clin Invest. 2007;117(3):616-26.

75. Cheng C, Tempel D, van Haperen R, van Damme L, Algur M, Krams R, et al. Activation of MMP8 and MMP13 by angiotensin II correlates to severe intra-plaque hemorrhages and

collagen breakdown in atherosclerotic lesions with a vulnerable phenotype. Atherosclerosis. 2009;204(1):26-33.

76. Gough PJ, Gomez IG, Wille PT, Raines EW. Macrophage expression of active MMP-9 induces acute plaque disruption in apoE-deficient mice. J Clin Invest. 2006;116(1):59-69.

77. Van Herck JL, De Meyer GR, Martinet W, Van Hove CE, Foubert K, Theunis MH, et al. Impaired fibrillin-1 function promotes features of plaque instability in apolipoprotein E-deficient mice. Circulation. 2009;120(24):2478-87.

78. Van der Donckt C, Van Herck JL, Schrijvers DM, Vanhoutte G, Verhoye M, Blockx I, et al. Elastin fragmentation in atherosclerotic mice leads to intraplaque neovascularization, plaque rupture, myocardial infarction, stroke, and sudden death. Eur Heart J. 2015;36(17):1049-58.

79. Sachs UJ, Nieswandt B. In vivo thrombus formation in murine models. Circ Res. 2007;100(7):979-91.

80. Bond AR, Jackson CL. The fat-fed apolipoprotein E knockout mouse brachiocephalic artery in the study of atherosclerotic plaque rupture. J Biomed Biotechnol. 2011;2011:379069.

81. Van Eeden S, Leipsic J, Paul Man SF, Sin DD. The relationship between lung inflammation and cardiovascular disease. Am J Respir Crit Care Med. 2012;186(1):11-6.

82. Hernandez Garduno E. Tuberculosis and acute coronary syndrome. Int J Tuberc Lung Dis. 2014;18(2):250.

83. Man SF, Van Eeden S, Sin DD. Vascular risk in chronic obstructive pulmonary disease: role of inflammation and other mediators. Can J Cardiol. 2012;28(6):653-61.

84. Sin DD, Man SF. Chronic obstructive pulmonary disease as a risk factor for cardiovascular morbidity and mortality. Proc Am Thorac Soc. 2005;2(1):8-11.

85. Sin DD, Wu L, Man SF. The relationship between reduced lung function and cardiovascular mortality: a population-based study and a systematic review of the literature. Chest. 2005;127(6):1952-9.

86. Soriano JB, Rigo F, Guerrero D, Yanez A, Forteza JF, Frontera G, et al. High prevalence of undiagnosed airflow limitation in patients with cardiovascular disease. Chest. 2010;137(2):333-40.

87. Suda K, Tsuruta M, Eom J, Or C, Mui T, Jaw JE, et al. Acute lung injury induces cardiovascular dysfunction: effects of IL-6 and budesonide/formoterol. Am J Respir Cell Mol Biol. 2011;45(3):510-6.

88. Suda K, Eom J, Jaw JE, Mui T, Bai N, Or C, et al. Endotoxin-induced cardiovascular dysfunction in mice: effect of simvastatin. J Appl Physiol (1985). 2011;111(4):1118-24.

89. Suwa T, Hogg JC, Quinlan KB, Ohgami A, Vincent R, van Eeden SF. Particulate air pollution induces progression of atherosclerosis. J Am Coll Cardiol. 2002;39(6):935-42.

90. Clayton TC, Capps NE, Stephens NG, Wedzicha JA, Meade TW. Recent respiratory infection and the risk of myocardial infarction. Heart. 91. England2005. p. 1601-2.

91. Corrales-Medina VF, Serpa J, Rueda AM, Giordano TP, Bozkurt B, Madjid M, et al. Acute bacterial pneumonia is associated with the occurrence of acute coronary syndromes. Medicine (Baltimore). 2009;88(3):154-9.

92. Harskamp RE, van Ginkel MW. Acute respiratory tract infections: a potential trigger for the acute coronary syndrome. Ann Med. 2008;40(2):121-8.

93. Koskela RS, Mutanen P, Sorsa JA, Klockars M. Respiratory disease and cardiovascular morbidity. Occup Environ Med. 2005;62(9):650-5.

94. Kuanprasert S, Apichartpikul N, Chuenkitmongkol S, Wiangosot W, Topaiboon P, Sukonthasarn A. Evidence of influenza or influenza-like-illness preceding acute coronary syndrome. Southeast Asian J Trop Med Public Health. 2008;39(6):1040-4.

95. Phrommintikul A, Kuanprasert S, Wongcharoen W, Kanjanavanit R, Chaiwarith R, Sukonthasarn A. Influenza vaccination reduces cardiovascular events in patients with acute coronary syndrome. Eur Heart J. 2011;32(14):1730-5.

96. Ramirez J, Aliberti S, Mirsaeidi M, Peyrani P, Filardo G, Amir A, et al. Acute myocardial infarction in hospitalized patients with community-acquired pneumonia. Clin Infect Dis. 2008;47(2):182-7.

97. Smeeth L, Thomas SL, Hall AJ, Hubbard R, Farrington P, Vallance P. Risk of myocardial infarction and stroke after acute infection or vaccination. N Engl J Med. 2004;351(25):2611-8.

98. Udell JA, Zawi R, Bhatt DL, Keshtkar-Jahromi M, Gaughran F, Phrommintikul A, et al. Association between influenza vaccination and cardiovascular outcomes in high-risk patients: a meta-analysis. Jama. 2013;310(16):1711-20.

99. Hansson GK. Inflammation, atherosclerosis, and coronary artery disease. N Engl J Med. 2005;352(16):1685-95.

100. Anthonisen NR, Connett JE, Kiley JP, Altose MD, Bailey WC, Buist AS, et al. Effects of smoking intervention and the use of an inhaled anticholinergic bronchodilator on the rate of decline of FEV1. The Lung Health Study. Jama. 1994;272(19):1497-505.

101. Pope CA, 3rd, Muhlestein JB, May HT, Renlund DG, Anderson JL, Horne BD. Ischemic heart disease events triggered by short-term exposure to fine particulate air pollution. Circulation. 2006;114(23):2443-8.

102. Simkhovich BZ, Kleinman MT, Kloner RA. Particulate air pollution and coronary heart disease. Curr Opin Cardiol. 2009;24(6):604-9.

103. Pope CA, 3rd, Ezzati M, Dockery DW. Fine-particulate air pollution and life expectancy in the United States. N Engl J Med. 2009;360(4):376-86.

104. Humair JP, Garin N, Gerstel E, Carballo S, Carballo D, Keller PF, et al. Acute respiratory and cardiovascular admissions after a public smoking ban in Geneva, Switzerland. PLoS One. 2014;9(3):e90417.

105. Wang CC, Peng CL, Wang GJ, Sung FC, Kao CH. Pneumococcal pneumonia and the risk of acute coronary syndrome: a population-based cohort study. Int J Cardiol. 2013;168(4):4480-1.

106. Hole DJ, Watt GC, Davey-Smith G, Hart CL, Gillis CR, Hawthorne VM. Impaired lung function and mortality risk in men and women: findings from the Renfrew and Paisley prospective population study. Bmj. 1996;313(7059):711-5; discussion 5-6.

107. Toren K, Bergdahl IA, Nilsson T, Jarvholm B. Occupational exposure to particulate air pollution and mortality due to ischaemic heart disease and cerebrovascular disease. Occup Environ Med. 2007;64(8):515-9.

108. Brunekreef B, Beelen R, Hoek G, Schouten L, Bausch-Goldbohm S, Fischer P, et al. Effects of long-term exposure to traffic-related air pollution on respiratory and cardiovascular mortality in the Netherlands: the NLCS-AIR study. Res Rep Health Eff Inst. 2009(139):5-71; discussion 3-89.

109. Pesonen E, Tiirola T, Andsberg E, Jauhiainen M, Paldanius M, Persson K, et al. Serum chlamydial lipopolysaccharide as a prognostic factor for a new cardiovascular event. Heart Lung. 2009;38(3):176-81.

110. Pope CA, 3rd, Burnett RT, Thurston GD, Thun MJ, Calle EE, Krewski D, et al. Cardiovascular mortality and long-term exposure to particulate air pollution: epidemiological evidence of general pathophysiological pathways of disease. Circulation. 2004;109(1):71-7.

111. Gairola CG, Drawdy ML, Block AE, Daugherty A. Sidestream cigarette smoke accelerates atherogenesis in apolipoprotein E-/- mice. Atherosclerosis. 2001;156(1):49-55.

112. Ngeh J, Goodbourn C. Chlamydia pneumoniae, Mycoplasma pneumoniae, and Legionella pneumophila in elderly patients with stroke (C-PEPS, M-PEPS, L-PEPS): a case-control study on the infectious burden of atypical respiratory pathogens in elderly patients with acute cerebrovascular disease. Stroke. 2005;36(2):259-65.

113. Ashkenazi H, Rudensky B, Paz E, Raveh D, Balkin JA, Tzivoni D, et al. Incidence of immunoglobulin G antibodies to Chlamydia pneumoniae in acute myocardial infarction patients. Isr Med Assoc J. 2001;3(11):818-21.

114. Iriz E, Cirak MY, Engin ED, Zor MH, Erer D, Imren Y, et al. Effects of atypical pneumonia agents on progression of atherosclerosis and acute coronary syndrome. Acta Cardiol. 2007;62(6):593-8.

115. Azambuja MI, Duncan BB. Similarities in mortality patterns from influenza in the first half of the 20th century and the rise and fall of ischemic heart disease in the United States: a new hypothesis concerning the coronary heart disease epidemic. Cad Saude Publica. 2002;18(3):557-66; discussion 67-77.

116. Modica A, Karlsson F, Mooe T. Platelet aggregation and aspirin non-responsiveness increase when an acute coronary syndrome is complicated by an infection. J Thromb Haemost. 2007;5(3):507-11.

117. Tsui KL, Leung TC, Yam LY, So LK, Poon E, Lung KC, et al. Coronary plaque instability in severe acute respiratory syndrome. Int J Cardiol. 99. Ireland2005. p. 471-2.

118. Puig-Barbera J, Diez-Domingo J, Varea AB, Chavarri GS, Rodrigo JA, Hoyos SP, et al. Effectiveness of MF59-adjuvanted subunit influenza vaccine in preventing hospitalisations for cardiovascular disease, cerebrovascular disease and pneumonia in the elderly. Vaccine. 2007;25(42):7313-21.

119. Meier CR, Jick SS, Derby LE, Vasilakis C, Jick H. Acute respiratory-tract infections and risk of first-time acute myocardial infarction. Lancet. 1998;351(9114):1467-71.

120. Sun Q, Wang A, Jin X, Natanzon A, Duquaine D, Brook RD, et al. Long-term air pollution exposure and acceleration of atherosclerosis and vascular inflammation in an animal model. Jama. 2005;294(23):3003-10.

121. Kido T, Tamagawa E, Bai N, Suda K, Yang HH, Li Y, et al. Particulate matter induces translocation of IL-6 from the lung to the systemic circulation. Am J Respir Cell Mol Biol. 2011;44(2):197-204.

122. Mutlu GM, Green D, Bellmeyer A, Baker CM, Burgess Z, Rajamannan N, et al. Ambient particulate matter accelerates coagulation via an IL-6-dependent pathway. J Clin Invest. 2007;117(10):2952-61.

123. Raetz CR, Whitfield C. Lipopolysaccharide endotoxins. Annu Rev Biochem. 2002;71:635-700.

124. Bryant CE, Spring DR, Gangloff M, Gay NJ. The molecular basis of the host response to lipopolysaccharide. Nat Rev Microbiol. 2010;8(1):8-14.

125. Togbe D, Schnyder-Candrian S, Schnyder B, Doz E, Noulin N, Janot L, et al. Toll-like receptor and tumour necrosis factor dependent endotoxin-induced acute lung injury. Int J Exp Pathol. 2007;88(6):387-91.

126. Zhang N, Francis KP, Prakash A, Ansaldi D. Enhanced detection of myeloperoxidase activity in deep tissues through luminescent excitation of near-infrared nanoparticles. Nat Med. 2013;19(4):500-5.

127. Eutamene H, Theodorou V, Schmidlin F, Tondereau V, Garcia-Villar R, Salvador-Cartier C, et al. LPS-induced lung inflammation is linked to increased epithelial permeability: role of MLCK. Eur Respir J. 2005;25(5):789-96.

128. Stolk J, Rudolphus A, Davies P, Osinga D, Dijkman JH, Agarwal L, et al. Induction of emphysema and bronchial mucus cell hyperplasia by intratracheal instillation of lipopolysaccharide in the hamster. J Pathol. 1992;167(3):349-56.

129. Kobayashi S, Fujinawa R, Ota F, Angata T, Ueno M, Maeno T, et al. A single dose of lipopolysaccharide into mice with emphysema mimics human chronic obstructive pulmonary disease exacerbation as assessed by micro-computed tomography. Am J Respir Cell Mol Biol. 2013;49(6):971-7.

130. Spond J, Billah MM, Chapman RW, Egan RW, Hey JA, House A, et al. The role of neutrophils in LPS-induced changes in pulmonary function in conscious rats. Pulm Pharmacol Ther. 2004;17(3):133-40.

131. Hardaker EL, Freeman MS, Dale N, Bahra P, Raza F, Banner KH, et al. Exposing rodents to a combination of tobacco smoke and lipopolysaccharide results in an exaggerated inflammatory response in the lung. Br J Pharmacol. 2010;160(8):1985-96.

132. Jaw JE, Tsuruta M, Oh Y, Schipilow J, Hirano Y, Ngan DA, et al. Lung exposure to lipopolysaccharide causes atherosclerotic plaque destabilisation. Eur Respir J. 2016.

133. Buffon A, Biasucci LM, Liuzzo G, D'Onofrio G, Crea F, Maseri A. Widespread coronary inflammation in unstable angina. N Engl J Med. 2002;347(1):5-12.

134. Lacy P. Mechanisms of degranulation in neutrophils. Allergy Asthma Clin Immunol. 2006;2(3):98-108.

135. Malle E, Waeg G, Schreiber R, Grone EF, Sattler W, Grone HJ. Immunohistochemical evidence for the myeloperoxidase/H2O2/halide system in human atherosclerotic lesions: colocalization of myeloperoxidase and hypochlorite-modified proteins. Eur J Biochem. 2000;267(14):4495-503.

136. Schultz J, Kaminker K. Myeloperoxidase of the leucocyte of normal human blood. I. Content and localization. Arch Biochem Biophys. 1962;96:465-7.

137. Daugherty A, Dunn JL, Rateri DL, Heinecke JW. Myeloperoxidase, a catalyst for lipoprotein oxidation, is expressed in human atherosclerotic lesions. J Clin Invest. 1994;94(1):437-44.

138. Sugiyama S, Okada Y, Sukhova GK, Virmani R, Heinecke JW, Libby P. Macrophage myeloperoxidase regulation by granulocyte macrophage colony-stimulating factor in human atherosclerosis and implications in acute coronary syndromes. Am J Pathol. 2001;158(3):879-91.

139. Naruko T, Ueda M, Haze K, van der Wal AC, van der Loos CM, Itoh A, et al. Neutrophil infiltration of culprit lesions in acute coronary syndromes. Circulation. 2002;106(23):2894-900.

140. Tavora FR, Ripple M, Li L, Burke AP. Monocytes and neutrophils expressing myeloperoxidase occur in fibrous caps and thrombi in unstable coronary plaques. BMC Cardiovasc Disord. 2009;9:27.

141. Castellani LW, Chang JJ, Wang X, Lusis AJ, Reynolds WF. Transgenic mice express human MPO -463G/A alleles at atherosclerotic lesions, developing hyperlipidemia and obesity in -463G males. J Lipid Res. 2006;47(7):1366-77.

142. McMillen TS, Heinecke JW, LeBoeuf RC. Expression of human myeloperoxidase by macrophages promotes atherosclerosis in mice. Circulation. 2005;111(21):2798-804.

143. Brennan ML, Penn MS, Van Lente F, Nambi V, Shishehbor MH, Aviles RJ, et al. Prognostic value of myeloperoxidase in patients with chest pain. N Engl J Med. 2003;349(17):1595-604.

144. Ferrante G, Nakano M, Prati F, Niccoli G, Mallus MT, Ramazzotti V, et al. High levels of systemic myeloperoxidase are associated with coronary plaque erosion in patients with acute coronary syndromes: a clinicopathological study. Circulation. 2010;122(24):2505-13.

145. Graner M, Tikkanen E, Rimpila O, Tikkanen H, Ripatti S, Lokki ML, et al. Diagnostic efficacy of myeloperoxidase to identify acute coronary syndrome in subjects with chest pain. Ann Med. 2013;45(4):322-7.

146. Baldus S, Heeschen C, Meinertz T, Zeiher AM, Eiserich JP, Munzel T, et al. Myeloperoxidase serum levels predict risk in patients with acute coronary syndromes. Circulation. 2003;108(12):1440-5.

147. Loria V, Dato I, Graziani F, Biasucci LM. Myeloperoxidase: a new biomarker of inflammation in ischemic heart disease and acute coronary syndromes. Mediators Inflamm. 2008;2008:135625.

148. Kutter D, Devaquet P, Vanderstocken G, Paulus JM, Marchal V, Gothot A. Consequences of total and subtotal myeloperoxidase deficiency: risk or benefit ? Acta Haematol. 2000;104(1):10-5.

149. Soehnlein O. Multiple roles for neutrophils in atherosclerosis. Circ Res. 2012;110(6):875-88.

150. Madjid M, Miller CC, Zarubaev VV, Marinich IG, Kiselev OI, Lobzin YV, et al. Influenza epidemics and acute respiratory disease activity are associated with a surge in autopsy-confirmed coronary heart disease death: results from 8 years of autopsies in 34,892 subjects. Eur Heart J. 2007;28(10):1205-10.

151. Arbustini E, Dal Bello B, Morbini P, Burke AP, Bocciarelli M, Specchia G, et al. Plaque erosion is a major substrate for coronary thrombosis in acute myocardial infarction. Heart. 1999;82(3):269-72.

152. Falk E. Plaque rupture with severe pre-existing stenosis precipitating coronary thrombosis. Characteristics of coronary atherosclerotic plaques underlying fatal occlusive thrombi. Br Heart J. 1983;50(2):127-34.

153. Johnson J, Carson K, Williams H, Karanam S, Newby A, Angelini G, et al. Plaque rupture after short periods of fat feeding in the apolipoprotein E-knockout mouse: model characterization and effects of pravastatin treatment. Circulation. 2005;111(11):1422-30.

154. Sharpe J, Ahlgren U, Perry P, Hill B, Ross A, Hecksher-Sorensen J, et al. Optical projection tomography as a tool for 3D microscopy and gene expression studies. Science. 2002;296(5567):541-5.

155. Kirkby NS, Low L, Seckl JR, Walker BR, Webb DJ, Hadoke PW. Quantitative 3-dimensional imaging of murine neointimal and atherosclerotic lesions by optical projection tomography. PLoS One. 2011;6(2):e16906.

156. Hu JH, Du L, Chu T, Otsuka G, Dronadula N, Jaffe M, et al. Overexpression of urokinase by plaque macrophages causes histological features of plaque rupture and increases vascular

matrix metalloproteinase activity in aged apolipoprotein e-null mice. Circulation. 2010;121(14):1637-44.

157. Sze MA, Tsuruta M, Yang SW, Oh Y, Man SF, Hogg JC, et al. Changes in the bacterial microbiota in gut, blood, and lungs following acute LPS instillation into mice lungs. PLoS One. 2014;9(10):e111228.

158. King BA, Kingma PS. Surfactant protein D deficiency increases lung injury during endotoxemia. Am J Respir Cell Mol Biol. 2011;44(5):709-15.

159. Chen YC, Bui AV, Diesch J, Manasseh R, Hausding C, Rivera J, et al. A novel mouse model of atherosclerotic plaque instability for drug testing and mechanistic/therapeutic discoveries using gene and microRNA expression profiling. Circ Res. 2013;113(3):252-65.

160. Silvestre-Roig C, de Winther MP, Weber C, Daemen MJ, Lutgens E, Soehnlein O. Atherosclerotic plaque destabilization: mechanisms, models, and therapeutic strategies. Circ Res. 2014;114(1):214-26.

161. Rudolph V, Steven D, Gehling UM, Goldmann B, Rudolph TK, Friedrichs K, et al. Coronary plaque injury triggers neutrophil activation in patients with coronary artery disease. Free Radic Biol Med. 2007;42(4):460-5.

162. Heslop CL, Frohlich JJ, Hill JS. Myeloperoxidase and C-reactive protein have combined utility for long-term prediction of cardiovascular mortality after coronary angiography. J Am Coll Cardiol. 2010;55(11):1102-9.

163. Zhang R, Brennan ML, Fu X, Aviles RJ, Pearce GL, Penn MS, et al. Association between myeloperoxidase levels and risk of coronary artery disease. Jama. 2001;286(17):2136-42.

164. van Leeuwen M, Gijbels MJ, Duijvestijn A, Smook M, van de Gaar MJ, Heeringa P, et al. Accumulation of myeloperoxidase-positive neutrophils in atherosclerotic lesions in LDLR-/- mice. Arterioscler Thromb Vasc Biol. 2008;28(1):84-9.

165. Zernecke A, Bot I, Djalali-Talab Y, Shagdarsuren E, Bidzhekov K, Meiler S, et al. Protective role of CXC receptor 4/CXC ligand 12 unveils the importance of neutrophils in atherosclerosis. Circ Res. 2008;102(2):209-17.

166. Daley JM, Thomay AA, Connolly MD, Reichner JS, Albina JE. Use of Ly6G-specific monoclonal antibody to deplete neutrophils in mice. J Leukoc Biol. 2008;83(1):64-70.

167. Ionita MG, van den Borne P, Catanzariti LM, Moll FL, de Vries JP, Pasterkamp G, et al. High neutrophil numbers in human carotid atherosclerotic plaques are associated with characteristics of rupture-prone lesions. Arterioscler Thromb Vasc Biol. 2010;30(9):1842-8.

168. Lozano R, Naghavi M, Foreman K, Lim S, Shibuya K, Aboyans V, et al. Global and regional mortality from 235 causes of death for 20 age groups in 1990 and 2010: a systematic analysis for the Global Burden of Disease Study 2010. Lancet. 2012;380(9859):2095-128.

169. Bentzon JF, Otsuka F, Virmani R, Falk E. Mechanisms of plaque formation and rupture. Circ Res. 2014;114(12):1852-66.

170. Klebanoff SJ. Myeloperoxidase: friend and foe. J Leukoc Biol. 2005;77(5):598-625.

171. Kettle AJ, Gedye CA, Winterbourn CC. Mechanism of inactivation of myeloperoxidase by 4-aminobenzoic acid hydrazide. Biochem J. 1997;321 (Pt 2):503-8.

172. Forghani R, Wojtkiewicz GR, Zhang Y, Seeburg D, Bautz BR, Pulli B, et al. Demyelinating diseases: myeloperoxidase as an imaging biomarker and therapeutic target. Radiology. 2012;263(2):451-60.

173. Liang J, Zheng Z, Wang M, Han L, Peng J, Liu Z, et al. Myeloperoxidase (MPO) and interleukin-17 (IL-17) plasma levels are increased in patients with acute coronary syndromes. J Int Med Res. 2009;37(3):862-6.

174. Alfakry H, Sinisalo J, Paju S, Nieminen MS, Valtonen V, Tervahartiala T, et al. The association of serum neutrophil markers and acute coronary syndrome. Scand J Immunol. 2012;76(2):181-7.

175. Eiserich JP, Baldus S, Brennan ML, Ma W, Zhang C, Tousson A, et al. Myeloperoxidase, a leukocyte-derived vascular NO oxidase. Science. 2002;296(5577):2391-4.

176. Fu X, Kassim SY, Parks WC, Heinecke JW. Hypochlorous acid oxygenates the cysteine switch domain of pro-matrilysin (MMP-7). A mechanism for matrix metalloproteinase activation and atherosclerotic plaque rupture by myeloperoxidase. J Biol Chem. 2001;276(44):41279-87.

177. Hazen SL. Myeloperoxidase and plaque vulnerability. Arterioscler Thromb Vasc Biol. 24. United States2004. p. 1143-6.

178. Malle E, Furtmuller PG, Sattler W, Obinger C. Myeloperoxidase: a target for new drug development? Br J Pharmacol. 2007;152(6):838-54.

179. Quillard T, Araujo HA, Franck G, Shvartz E, Sukhova G, Libby P. TLR2 and neutrophils potentiate endothelial stress, apoptosis and detachment: implications for superficial erosion. Eur Heart J. 2015;36(22):1394-404.

180. Weiss SJ, Peppin G, Ortiz X, Ragsdale C, Test ST. Oxidative autoactivation of latent collagenase by human neutrophils. Science. 1985;227(4688):747-9.

181. Johnson JL, Devel L, Czarny B, George SJ, Jackson CL, Rogakos V, et al. A selective matrix metalloproteinase-12 inhibitor retards atherosclerotic plaque development in apolipoprotein E-knockout mice. Arterioscler Thromb Vasc Biol. 2011;31(3):528-35.

182. Jacobsen JA, Major Jourden JL, Miller MT, Cohen SM. To bind zinc or not to bind zinc: an examination of innovative approaches to improved metalloproteinase inhibition. Biochim Biophys Acta. 2010;1803(1):72-94.

183. Churg A, Marshall CV, Sin DD, Bolton S, Zhou S, Thain K, et al. Late intervention with a myeloperoxidase inhibitor stops progression of experimental chronic obstructive pulmonary disease. Am J Respir Crit Care Med. 2012;185(1):34-43.

184. Arvadia P, Narwaley M, Whittal RM, Siraki AG. 4-Aminobenzoic acid hydrazide inhibition of microperoxidase-11: catalytic inhibition by reactive metabolites. Arch Biochem Biophys. 2011;515(1-2):120-6.

185. Rensen SS, Bieghs V, Xanthoulea S, Arfianti E, Bakker JA, Shiri-Sverdlov R, et al. Neutrophil-derived myeloperoxidase aggravates non-alcoholic steatohepatitis in low-density lipoprotein receptor-deficient mice. PLoS One. 2012;7(12):e52411.

186. Golubinskaya V, Brandt-Eliasson U, Gan LM, Kjerrulf M, Nilsson H. Endothelial function in a mouse model of myeloperoxidase deficiency. Biomed Res Int. 2014;2014:128046.

187. Takizawa S, Aratani Y, Fukuyama N, Maeda N, Hirabayashi H, Koyama H, et al. Deficiency of myeloperoxidase increases infarct volume and nitrotyrosine formation in mouse brain. J Cereb Blood Flow Metab. 2002;22(1):50-4.

188. Brennan M, Gaur A, Pahuja A, Lusis AJ, Reynolds WF. Mice lacking myeloperoxidase are more susceptible to experimental autoimmune encephalomyelitis. J Neuroimmunol. 2001;112(1-2):97-105.

189. Brennan ML, Anderson MM, Shih DM, Qu XD, Wang X, Mehta AC, et al. Increased atherosclerosis in myeloperoxidase-deficient mice. J Clin Invest. 2001;107(4):419-30.

190. Reynolds WF, Kumar AP, Piedrafita FJ. The human myeloperoxidase gene is regulated by LXR and PPARalpha ligands. Biochem Biophys Res Commun. 2006;349(2):846-54.

191. Wang SS, Hu SW, Zhang QH, Xia AX, Jiang ZX, Chen XM. Mesenchymal Stem Cells Stabilize Atherosclerotic Vulnerable Plaque by Anti-Inflammatory Properties. PLoS One. 2015;10(8):e0136026.

192. Ozturk S, Erdem A, Ozlu MF, Ayhan S, Erdem K, Ozyasar M, et al. Assessment of the neutrophil to lymphocyte ratio in young patients with acute coronary syndromes. Turk Kardiyol Dern Ars. 2013;41(4):284-9.

193. Tamhane UU, Aneja S, Montgomery D, Rogers EK, Eagle KA, Gurm HS. Association between admission neutrophil to lymphocyte ratio and outcomes in patients with acute coronary syndrome. Am J Cardiol. 2008;102(6):653-7.

194. Tuomainen AM, Kormi I, Havulinna AS, Tervahartiala T, Salomaa V, Sorsa T, et al. Serum tissue-degrading proteinases and incident cardiovascular disease events. Eur J Prev Cardiol. 2014;21(7):806-12.

195. Uygur F, Tanriverdi H, Aktop Z, Erboy F, Altinsoy B, Damar M, et al. The neutrophil-to-lymphocyte ratio in patients with obstructive sleep apnoea syndrome and its relationship with cardiovascular disease. Heart Lung. 2016;45(2):121-5.

196. Yilmaz M, Tenekecioglu E, Arslan B, Bekler A, Ozluk OA, Karaagac K, et al. White Blood Cell Subtypes and Neutrophil-Lymphocyte Ratio in Prediction of Coronary Thrombus Formation in Non-ST-Segment Elevated Acute Coronary Syndrome. Clin Appl Thromb Hemost. 2015;21(5):446-52.

197. Yu C, Chen M, Chen Z, Lu G. Predictive and prognostic value of admission neutrophil-to-lymphocyte ratio in patients with CHD. Herz. 2016.

198. B OH, Bosch JA, Carroll D, Hemming K, Pilz S, Loerbroks A, et al. Evidence of a synergistic association between heart rate, inflammation, and cardiovascular mortality in patients undergoing coronary angiography. Eur Heart J. 2013;34(12):932-41.

199. Thondapu V, Bourantas CV, Foin N, Jang IK, Serruys PW, Barlis P. Biomechanical stress in coronary atherosclerosis: emerging insights from computational modelling. Eur Heart J. 2016.

Appendix

Video Demonstration

Video 1 — 3D presentation of mouse aortic arch containing brachiocephalic trunk (BCT) from a LPS-exposed mouse: Blood (red color) was auto-fluorescent 10 times higher than the vessel wall (blue color). Blood clot in LPS mice was associated with shoulders of ruptured plaque in BCT. Online Link: https://app.box.com/s/ujbf9s9du2p6vxrrb1ygosg48zkemhwy

Video 2 — 3D presentation of mouse aortic arch and brachiocephalic trunk (BCT) from a saline-exposed mouse: No blood clot or intraplaque hemorrhage was observed in the atheroma of BCT. Online Link: https://app.box.com/s/27dphowyvh9xb3a17kunm2oel7nc1ee9

Video 3 — 3D presentation of aortic arch containing brachiocephalic trunk (BCT) from another LPS-exposed mouse that displayed intraplaque hemorrhage (red color) inside atheroma.

Online Link: https://app.box.com/s/puq08ehvcw74disuqs9kc8g9ns9npqwe

Video 4 — 3D presentation of aortic arch containing brachiocephalic trunk (BCT) from a different LPS-exposed mouse: Blood clots (color red) localized in the plaque shoulders at the proximal end of BCT and extended into the aortic arch.

Online: Link: https://app.box.com/s/gcs2sx5d14w4bpz4uz38fwis5ymdrby1

Video 5 — 3D presentation of brachiocephalic trunk (BCT) from LPS-exposed mice treated with neutrophil-specific antibodies (LPS-ND, left) and control antibodies (LPS-Ctrl, right): Blood clots (color red) localized at the plaque shoulders of BCT in the LPS-Ctrl group but not in the LPS-ND group. Online Link: https://app.box.com/s/ww9x8uz0p5zonjs5obkmd52zhxyas4wv

Video 6 — Three-dimensional (3D) demonstration of brachiocephalic trunk (BCT) from saline-exposed mice (left) and LPS-exposed mice (Right): Blood clots were detected in the BCTs of LPS-exposed mice by optical projection tomography (OPT) but not in those of saline-exposed mice. Online Link: https://app.box.com/s/sjpv5k962evhj6bbd8n1z4069xm57ywu

Video 7 — Three-dimensional (3D) demonstration of sectioned brachiocephalic trunk (BCT) from saline-exposed mice (left) and LPS-exposed mice (Right): Intraplaque hemorrhages were detected in the BCTs of LPS-exposed mice by optical projection tomography (OPT) but not in those of saline-exposed mice.
Online Link: https://app.box.com/s/gh9afv6krqi5azcdes3f205kv2ef97a5

Video 8 — Three-dimensional (3D) demonstration of whole-mount immunofluorescent stained Myeloperoxidase (MPO) in the brachiocephalic trunk (BCT) of LPS-exposed mice: A thrombus (white) was attached to the plaque in the BCT (gray) of a LPS-exposed mouse and MPO (green) was found mainly localized at the site of thrombosis.
Online Link: https://app.box.com/s/ig7bqbczgdwmh6wfpparb97bho4en39o

Video 9 — Three-dimensional (3D) demonstration of whole-mount immunofluorescent stained Myeloperoxidase (MPO) in the brachiocephalic trunk (BCT) of a saline-exposed mouse: No thrombus (white) was observed in the BCT (gray) and low MPO (green) was found in the BCT.

Online Link: https://app.box.com/s/rpudybi94wrao4ypq39k6sctdvtht5cj